5-2018

Investigating the Roles of Master Cell Cycle Regulators during Cytokinesis and Embryonic Development in *Caenorhabditis elegans*

Xiaofei Bai
University of Tennessee, xbai5@vols.utk.edu

To the Graduate Council:

I am submitting herewith a dissertation written by Xiaofei Bai entitled "Investigating the Roles of Master Cell Cycle Regulators during Cytokinesis and Embryonic Development in *Caenorhabditis elegans*." I have examined the final electronic copy of this dissertation for form and content and recommend that it be accepted in partial fulfillment of the requirements for the degree of Doctor of Philosophy, with a major in Biochemistry and Cellular and Molecular Biology.

Joshua N. Bembenek, Major Professor

We have read this dissertation and recommend its acceptance:

Mariano Labrador, Jaan Mannik, Bruce D. McKee, Andreas Nebenführ

Accepted for the Council:

Dixie L. Thompson

Vice Provost and Dean of the Graduate School

(Original signatures are on file with official student records.)

Investigating the Roles of Master Cell Cycle Regulators during Cytokinesis and Embryonic Development in *Caenorhabditis elegans*

A Dissertation Presented for the

Doctor of Philosophy

Degree

The University of Tennessee, Knoxville

Xiaofei Bai

May 2018

ACKNOWLEDGMENTS

ABSTRACT

Faithful cell division is required to maintain ploidy and generate daughter cells with necessary genetic components for life. During mitosis, dividing cells face the challenge of coordinating multiple processes to ensure that nascent daughter cells inherit an exact copy of the parent cell's genetic identity to maintain viability. To ensure the proper execution of cell division, multiple core cell cycle proteins, such as Aurora B kinase and separase, are involved in regulating chromosome segregation, cytokinesis and abscission. Interestingly, fundamental roles for these core cell cycle proteins are being characterized in this coordination. Separase regulates chromosome segregation and vesicle trafficking during meiotic and mitotic divisions. Aurora B kinase is well characterized to eliminate incorrect attachments of kinetochore with centromere through its phosphorylation. These faultless attachments initiate a series of signaling pathways to activate separase and promote chromosome segregation. Additionally, Aurora B kinase also phosphorylates centralspindlin to complete cytokinesis and midbody formation. The collection of work presented here addresses the role of these two master cell cycle regulators in cytokinesis, abscission, and cellular events during later morphogenesis. Chapter I outlines the contribution of separase to cytokinesis, highlight how the protease activity of separase regulates exocytosis in anaphase, and suggesting that an unknown substrate is involved in separase's regulation of exocytosis. Chapter II elucidates how programmed cytokinesis in different tissues contributes to later cellular events during morphogenesis and uncovers the novel migration pattern of midbody to apical surface. Finally, in Chapter III, we present several live imaging methods for observing *C. elegans* embryogenesis which were applied for this study. Collectively, the

work presented here addresses the roles of these master cell cycle regulators in exocytosis, cytokinesis, abscission, and later developmental events, which is critical to understand how failure of cell division promote tumorigenesis and aneuploidy. Finally, our study may provide insightful ideas to generate clinical technologies to cure human infertility, cancer and other genetic diseases.

TABLE OF CONTENTS

LIST OF FIGURES

LIST OF ATTACHMENTS

File 1: Chromosome segregation during mitosis..................................Bai Movie S1.mov

File 2: Chromosome segregation during meiosis I..............................Bai Movie S2.mov

File 3: SEP-1^{PD}::GFP does not inhibit centriole disengagement...........Bai Movie S3.mov

File 4: Cytokinesis failure of SEP-1^{PD}::GFP is synergistically enhanced by *syx-4(RNAi)*...Bai Movie S4.mov

File 5: Depletion of t-SNARE *syx-4* caused cytokinesis failure in heterozygous SEP-1^{PD}::GFP/-; RAB11::mCherry expression embryos..............................Bai Movie S5.mov

File 6: SEP-1^{PD}::GFP/- affects RAB-11 trafficking during cytokinesis....Bai Movie S6.mov

File 7: Separase localization during cortical granule exocytosis……....Bai Movie S7.mov

File 8: SEP-1^{PD}::GFP delays completion of CGE………………………..Bai Movie S8.mov

File 9: Separase associates with plasma membrane after CGE…..…….Bai Movie S9.mov

File 10: Separase colocalizes to cortical granules with RAB-11……......Bai Movie S10.mov

File 11: Cytokinesis in the first two mitotic divisions...……….…....Bai Movie S11.mov

File 12: Cytokinesis in the intestine epithelia………………….....Bai Movie S12.mov

File 13: High temporal resolution of cytokinesis in the intestine epithelia…………………………………………………..………..Bai Movie S13.mov

File 14: Cytokinesis in the intestine epithelia with lattice light sheet microscopy ………………………………………………………...Bai Movie S14.mov

File 15: Cytokinesis in E16 to E20 cell division…………………….....Bai Movie S15.mov

File 16: Cytokinesis in the pharynx from ventral view…..…………....Bai Movie S16.mov

File 17: Cytokinesis in the pharynx from dorsal view …………..…....Bai Movie S17.mov

File 18: Cytokinesis in the pharynx with lattice light sheet microscopy……………………………………………………….………Bai Movie S18.mov

INTRODUCTION

Faithful cell division occurs as a result of spatiotemporally-specific cell cycle events including error-free chromosome segregation and cytoplasmic division or cytokinesis. Many cell cycle regulators are dedicated to controlling progression from chromosome segregation to cytoplasmic division to abscission, which physically separates the daughter cells. Here we discuss current knowledge of several important cell cycle regulation mechanisms. Specifically, those that involve the cysteine protease separase and serine/threonine kinase Aurora B, which coordinate several aspects of cell division to ensure the inheritance of the necessary constituents by each daughter cell and the execution of the final abscission. Finally, this study sheds light on the newly emerging role of cytokinesis in regulating development, as well as the cellular mechanism of Aurora B kinase in regulating post-mitotic tissue development.

A Journey through Eukaryotic Cell Division

Cellular division is a multi-phase process that is necessary for growth, reproduction and ultimately the survival of the organism. During M phase, accurate chromosome segregation requires successful separation of sister chromatids that are produced during S-phase. Before chromosome segregation, it is essential that sister chromatids become attached to the microtubule spindle apparatus by kinetochores in a bipolar fashion (Lara-Gonzalez et al., 2012). The control mechanism to prevent incorrect bipolar attachment named Spindle Assembly Checkpoint (SAC) is activated to inhibit the metaphase-to-anaphase transition (Carmena et al., 2012; Lara-Gonzalez et al.,

2012). Correction of the erroneous chromosome-microtubule attachments is mediated by the phosphorylation of Aurora B kinase substrates at the kinetochores. The phosphorylation facilitates the destabilization of incorrect kinetochores-microtubule attachments. Interestingly, Aurora B kinase requires three other proteins, such as scaffold protein INCENP, and two non-enzymatic subunits Survivin and Borealin, to form into hetero-tetrameric complexes called Chromosomal Passenger Complex (CPC). The CPC complex localized at the inner centromere and continually detects and corrects kinetochore-microtubule attachment errors (Carmena et al., 2015; Ruchaud et al., 2007; Munoz-Barrera and Monje-Casas, 2014; Pinsky et al., 2006; Welburn et al., 2010).

Once all chromosomes have their kinetochores attached to the spindle apparatus properly, the metaphase-anaphase transition is triggered. The Mitotic Checkpoint Complex (MCC) is liberated during the metaphase-anaphase transition, which activates an E3 ubiquitin-protein ligase called the Anaphase-Promoting Complex/Cyclosome (APC/C). Once activated, the APC/C can lead to securin, the separase inhibition chaperone, degradation through ubiquitination. The sudden destruction of securin frees separase to cleave the cohesin subunit SCC-1 (also known as Mcd1/Rad 21) and promotes sister chromatid separation (Hauf et al., 2001; Lara-Gonzalez et al., 2012; Nasmyth and Haering, 2009). Simultaneously, activation of the APC/C also promotes the degradation of cyclin B1 and inactivates Cdk1, leading to mitotic exit (Herzog et al., 2009).

After chromosome segregation, cytokinesis begins with the formation of the central spindle and equatorial contractile ring between the separating chromosomes (Glotzer, 2009). In early anaphase, the mitotic kinase Cdk-1/cyclin B phosphorylates MKLP1 subunits and activates the heterotetrameric centralspindlin complex, which contains two subunits (kinesin-6 MKLP1/ZEN-4 and GTPase-activating protein CYK-4), to promote central spindle formation (Mishima et al., 2004). With the inactivation of Cdk1, Aurora B kinase relocates from centromeres to the spindle center to stabilize the central spindle and control its length by phosphorylating multiple kinesins, such as KIF2A and KIF4A (Gruneberg et al., 2004; Uehara et al., 2013).

Additionally, the actomyosin ring generates contractile force and initiates cleavage furrow ingression. A subcellular structure called the midbody forms at the end of the furrowing, which connects the nascent daughter cells and orchestrates abscission. The midbody is remodeled from the bundled central spindle microtubule. A large number of contractile ring and central spindle proteins are required to regulate midbody formation (D'Avino and Capalbo, 2016; Green et al., 2012). One group of central spindle proteins, including centralspindlin and Ect2, are transported from microtubules to the midbody ring, where they localize with Anillin, RhoA and other proteins (Green et al., 2012). Another group of central spindle proteins, including Aurora B and MKLP2, colocalizes with midbody microtubules in the region called the midbody flank at the outer edges of the midbody (Green et al., 2012; Hu et al., 2012). Inactivation of the Plk1 and Aurora B kinases leads to abscission through the recruitment and activation of the ESCRT components (Green et al., 2013; Green et al., 2012; Mierzwa and Gerlich, 2014).

3

Cytokinesis also requires cell shape remodeling, which causes a dramatic reduction of plasma membrane surface area. Rapid recovery of the daughter cell plasma membrane surface area is led by vesicle-mediated membrane transportation and subsequent vesicle fusion that targets plasma membranes (Boucrot and Kirchhausen, 2007; Schiel and Prekeris, 2013). Inhibition of vesicle secretory and protein transport to the plasma membrane impairs cytokinesis in *C. elegans* (Skop et al., 2001; Skop et al., 2004). Additionally, vesicle transportation also delivers numerous regulator proteins to the cleavage furrow to reconstruct the cytoskeleton and nascent plasma membrane, which are required for successful abscission (Skop et al., 2001). The small GTPase RAB (Ras-related proteins in brain) family is well characterized as molecular switches in regulating endosome vesicle trafficking and controlling cytokinesis (Stenmark, 2009). RAB-11 is a well-defined RAB GTPase that promotes endosomal vesicle docking on the target membrane (Campa and Hirsch, 2017; Welz et al., 2014). Other factors, such as the t-SNARE syntaxin, v-SNARE, and the exocyst complex execute vesicle tethering and fusion to complete cytokinesis (Malsam et al., 2008; Wickner and Schekman, 2008).

Separase has a Myriad of Roles during the Cell Cycle

Separase is a cell cycle component evolutionarily conserved from yeast to mammalian cells (Hauf et al., 2001; Uhlmann et al., 2000; Waizenegger et al., 2002). The canonical function of separase is to regulate chromosome segregation. The mechanism by which separase controls meiotic and mitotic chromosome segregation is well known (Siomos et al., 2001; Uhlmann et al., 2000). Separase is a multiple-motif protein, which contains

protease domain at the C-terminus, and an extended helical repeat domain at N-terminus (Boland et al., 2017). In addition to mediating canonical cohesin proteolysis at metaphase-anaphase transition, separase is also necessary for other cell cycle events. For example, separase cleaves spindle associated protein Slk19 to control stabilization of the anaphase spindle in *Saccharomyces cerevisiae* (Sullivan et al., 2004; Sullivan et al., 2001). Additionally, the protease activity of separase is required to cleave the pericentriolar material proteins for disengagement and duplication of centrioles in mammalian cells(Lee and Rhee, 2012; Matsuo et al., 2012). Intriguingly, separase also cleaves itself at multiple adjacent sites. The auto-cleaved fragments maintain catalytic activity, which controls the following cell cycle progression (Papi et al., 2005; Zou et al., 2002). All of the characterized separase substrates share a consensus recognition motif SxD/ExxR. In addition to its roles as a protease, several non-proteolytic functions of separase have been identified. Separase regulate Cdc14 early anaphase release (FEAR) pathway to initiate mitotic exit in budding yeast(Stegmeier et al., 2002). Separase is also identified to bind and inhibit CDK-1 through an uncharacterized region outside the protease domain (Gorr et al., 2005; Gorr et al., 2006). Other non-proteolytic functions of separase have been identified, such as control of mitotic exit, polar body extrusion, and dynamics of the anaphase spindle (Kudo et al., 2006; Lu and Cross, 2009; Sullivan and Uhlmann, 2003).

We utilized the powerful model system *Caenorhabditis elegans* to address fundamental cell cycle events during meiosis and mitosis. Our previous studies have identified that separase directly regulates vesicle trafficking in anaphase to promote cortical granule

5

exocytosis during meiotic anaphase I and mitotic cytokinesis (Bembenek et al., 2007; Bembenek et al., 2010). In *C. elegans*, cortical granules are secreted during meiotic anaphase I and exocytosed at plasma membrane to promote eggshell formation. This prevents polyspermy and provides protection to other environmental stresses after fertilization (Bembenek et al., 2007; Richie et al., 2011). Interestingly, separase localizes to cortical granules and is required for their exocytosis in anaphase (Bembenek et al., 2007). Core component of exocytosis machinery, RAB-11, is also required for cortical granule exocytosis in *C. elegans*. However, RAB-11 appears on cortical granules prior to separase localization, which suggests an temporal recruitment of regulators to the vesicles before exocytosis occurs (Kimura and Kimura, 2012; Sato et al., 2008). Additionally, our previous studies found that depletion of separase led to increased and persistent accumulation of RAB-11 positive vesicles at the ingressing furrow and midbody, consistent with a function of separase in promoting exocytosis at the plasma membrane (Bembenek et al., 2010). In addition to mediating substrate proteolysis, three different hypermorphic alleles at the non-proteolytic domain of separase cause defects in cortical granule exocytosis and cytokinesis, but minimal disruption of chromosome segregation (Richie et al., 2011). However, the mechanism by which separase mediates exocytosis and membrane trafficking in anaphase, such as proteolytic vs. non-proteolytic functions, has not been fully characterized. To investigate whether the protease activity of separase is involved in exocytosis, we generated a separase mutant by mutagenizing the conserved catalytic activity residue cysteine to serine, which was denominated as protease dead separase (SEP-1^{PD}::GFP) mutant. Interestingly, in Chapter I, we show that chromosome segregation, vesicle exocytosis,

6

and RAB-11 positive vesicle trafficking were impaired in SEP-1^{PD}::GFP mutant. Cohesin

SCC-1 depletion substantially rescues chromosome bridging in the SEP-1^{PD}::GFP

mutant, consistent with our hypothesis that SEP-1^{PD}::GFP may disrupt chromosome

segregation and cytokinesis by preventing substrate cleavage (Bai and Bembenek,

2017b). In conclusion, this study indicates that separase may cleave an unknown

substrate to promote exocytosis during CGE and cytokinesis, similar to its function

during chromosome segregation. Therefore, separase coordinates chromosome

segregation with vesicle trafficking events to promote cell division, although the details

of many aspects of separase's regulatory mechanism remain unanswered.

Aurora B Kinase Performs Multiple Roles during Cell Division

Aurora B kinase is a serine/threonine protein kinase coordinates chromosomal and

cytoskeletal events, such as kinetochore-microtubule attachment, kinetochore

assembly, sister chromatid biorientation, and segregation (Archambault and Carmena,

2012; Krenn and Musacchio, 2015; Lampson and Cheeseman, 2011). The activation of

Aurora B kinase in coordinating cellular events requires three additional regulatory

proteins to form the Chromosomal Passenger Complex (CPC) (Carmena et al., 2012).

The CPC localized at chromosome region during early mitosis to regulate chromosomal

events, then it was transferred to the central spindle and the midbody during late

mitosis, where it regulates anaphase spindle stabilization, construction of the contractile

ring and drives abscission. During the formation of central spindle, Aurora B

phosphorylates the serine at the MKLP-1/ZEN-4 C-terminal tail, which prevents MKLP-

1/ZEN-4 from binding to the centralspindlin clustering inhibitor 14-3-3 protein and

promotes centralspindlin assembly into clustered oligomers to bundle central spindle

microtubules, thereby stabilizing the central spindle (Basant et al., 2015; Hutterer et al.,

2009; Zhao and Fang, 2005). Interestingly, the phosphorylation of KIF4A by Aurora B

kinase also suppresses microtubule dynamics and the growth of the central spindle and

the midbody (Bastos et al., 2014). Additionally, Aurora B phosphorylates the

centralspindlin component MgcRacGAP, which indirectly regulates the small GTPase

RhoA to govern contractile ring maturation (Ban et al., 2004). Aurora B also

phosphorylates a number of cytoskeletal regulators to lead constriction of the contractile

ring and control cell shape during cytokinesis (Ferreira et al., 2013; Floyd et al., 2013;

Goto et al., 2003; Kettenbach et al., 2011). Before cell abscission, Aurora B kinase acts

as a negative regulator to delay abscission in presence of lagging chromatin at

cleavage furrow (Bembenek et al., 2013; Steigemann et al., 2009). During abscission,

Aurora B acts independent of the CPC complex and phosphorylates ESCRT-III protein

Snf7 (CHMP4) to preclude formation of ESCRT-III filaments and complete abscission

(Capalbo et al., 2012; Carlton et al., 2012; Manic et al., 2017; Steigemann et al., 2009).

Execution of Cell Division Spatiotemporally Regulates Tissue Development

Cytokinesis is the last step of cell division and required for cell proliferation. The

mechanisms governing cytokinesis are well characterized in one-cell model systems

such as yeast, in mammalian cultured cells and early zygotic cell division in *C. elegans*

(D'Avino et al., 2015). Successful execution of cytokinesis relies on assembly and

constriction of the actomyosin contractile ring, precise deposition of new plasma

membrane in a spatiotemporal manner, as well as the coordination between cell

polarization and mitotic spindle orientation (D'Avino et al., 2015; Green et al., 2012; Pollard, 2017). Remarkably, in addition to the canonical function of maintaining cell proliferation, successful cytokinesis is also important for developmental regulation in eukaryotic organisms (Chen et al., 2013; Herszterg et al., 2014; Li, 2007). A much appreciated regulation of cytokinesis during development is asymmetric cell division in multiple epithelial/ neuroepithelial tissues. Any disruption of cytokinesis in these asymmetric divisions caused a variety of defects during lumenogensis (Herszterg et al., 2013; Herszterg et al., 2014; Jaffe et al., 2008; Lujan et al., 2016; Morais-de-Sa and Sunkel, 2013; Zheng et al., 2010). Previous studies suggested that constriction of contractile ring during cytokinesis may provide mechanical tension to control adhesion and mechnotransduction between neighbor cells, which help tissue stabilization during development (Herszterg et al., 2014). Intriguingly, the midbody is consistently positioned and formed at the apical part after furrowing during asymmetric division, which is a primary observed feature of cytokinesis during epithelia development (Herszterg et al., 2014). Therefore, execution of cytokinesis may directly regulate tissue morphogenesis by providing mechanical tension or position the midbody to further orchestrate developmental events. To fully understand the role of cytokinesis during development, further studies on the proper execution of cytokinesis in different tissues and cell types is needed.

Midbody is Not Cellular Junk, but a Regulator of Developmental Events

A commonly observed function of furrow symmetry in epithelial tissues is to control the positioning of midbody at the apical interface. It is still unknown what the functional role

of the midbody is at this position and if it is indeed linked to epithelial morphogenesis. We do know that the canonical function of the midbody is to recruit and orchestrate a large amount of proteins during the execution of abscission (Chen et al., 2009; Green et al., 2012; Skop et al., 2004). These midbody proteins have been categorized into microtubule-associated proteins, actin-associated proteins, membrane trafficking proteins, and a large number of kinases and phosphatases (Skop et al., 2004). The midbodies also contain different regions including the midbody ring and the midbody central core, which have been characterized by the presence of an electron-dense material (Konig et al., 2017; Mullins and Biesele, 1977). Another region is called the midbody flank, which is a tightly-packed and microtubule-based structure. A group of central spindle proteins, including Aurora B kinase, colocalizes with the midbody flank region (Dionne et al., 2015; Green et al., 2012). Generally, the midbody forms between daughter cells and is abscised after cell division (Dionne et al., 2015; Schiel et al., 2011; Schiel and Prekeris, 2013). Post abscission, the midbody is observed to be engulfed and inherited by one of the daughter cells post-asymmetric abscission. However, other studies in cancer and stem cells show that the midbody can also travel to non-parent cells or persist extracellularly after symmetric abscission, suggesting that it may carry or transport signals between cells (Crowell et al., 2014). Consistent with this idea, a number of other post-abscission functions of midbody have been elucidated from recent studies. Midbody can also travel to non-parent cells in different systems after abscission, which suggests that the midbody may deliver signals during tissue development (Crowell et al., 2014; Dubreuil et al., 2007; Kuo et al., 2011). Further studies in MDCK cells revealed more clearly the role of the midbody during apical

polarization and lumenogenesis. Apical membrane markers are delivered to the

midbody through membrane trafficking during cytokinesis and establish an apical

surface between two daughter cells (Schluter et al., 2009). Consistent with this idea, the

midbody defines the site of polarization for dendrite extension in *Drosophila* neurons

(Pollarolo et al., 2011). The midbody is also required for a polarizing cue in C. elegans

embryos, which is necessary for dorsoventral axis formation (Singh and Pohl, 2014).

Interestingly, the midbody also regulates cilium formation in MDCK cells (Bernabe-

Rubio et al., 2016). Although the midbody regulates pattern formation in various tissues,

precise mechanism of the midbody in regulating these processes is largely unknown.

In order to further understand patterns of cytokinesis during development as well as the

functions of the midbody, we investigated cell divisions using the *C. elegans* embryonic

invariant lineage in Chapter II. The digestive tract of *C. elegans* consists of the pharynx,

intestinal tubes, and valve, all of which are linked and developed from a well-defined

lineage of cells. These tissue-specific cell divisions have been spatiotemporally

characterized based on the invariant embryonic lineage (the pharynx containing 80

cells, the valve containing 6 cells, and the intestine containing 20 cells) (Asan et al.,

2016; Mango, 2007; Sulston et al., 1983). To obtain high-quality images of these

complex structures, we developed several live imaging methods using the lattice light

sheet microscope and high-resolution confocal microscope, which are described in

Chapter III. The observations from the light sheet microscope provide us with

impressive details of cell division and midbody formation, which uncovered a highly

stereotyped midbody inheritance pattern and reproducible variations of furrow symmetry

during early cell divisions (Chen et al., 2014). During tissue morphogenesis, we observed an unexpected pattern of cytokinesis and striking midbody migration events in the developing intestine, pharynx, and neuronal sensory. Interestingly, the midbody flank marker Aurora B kinase AIR-2 migrates with midbodies and remains at apical surfaces in several tissues, while other midbody ring markers, including kinesin-6 ZEN-4 and non-muscle myosin NMY-2, are internalized into the cytosol. Given the observation of this novel cytokinesis pattern and the localization of AIR-2 to apical structures, we also tested whether inactivation of midbody components proteins during development would have an effect on epithelial morphogenesis. Indeed, inactivation of temperature-sensitive midbody proteins during morphogenesis disrupted the formation of these tissues. Therefore, cytokinesis may play an instrumental role during development, similar to the way spindle orientation and other features of cell division are known to contribute.

Taken collectively, these findings suggest that cytokinesis is critical to faithful cell division. There are various cell cycle regulators playing roles in governing cytokinesis and the final abscission process, such as separase and Aurora B kinase. Additionally, our findings shed light on a novel pattern of midbody movement to apical surfaces after cell division, strengthening the role of cytokinesis in developmental events. However, despite our studies and other previous work that provides high-throughput data to uncover the mechanism of cytokinesis in multicellular tissues and investigates the potential role of the midbody in apical polarization and lumenogenesis, many questions remain unanswered. The collection of work provided here addresses a number of

questions regarding cytokinesis, abscission, and membrane trafficking in an organism at the one-cell stage and in the multicellular tissues of *C. elegans*, consisting of (1) protease activity of separase orchestrating cytokinesis through cleavage of a unknown substrate during exocytosis, which provides some clues for identifying separase's substrate; (2) illustrating some variations of cytokinesis in the C. elegans embryonic lineage, including highly reproducible patterns of furrow symmetry, microtubule disassembly, etc.; (3) showing a striking midbody inheritance pattern in multiple tissues and suggesting that the midbody may contribute to apical surface construction; (4) showing the localization of Aurora B kinase AIR-2 at multiple apical surfaces post-mitosis. Inactivation of AIR-2 impairs morphogenesis in several tissues, which implies that AIR-2 may have a post-mitotic role in the formation of tissues; (5) our live imaging approaches, including light sheet microscopy, provide incredible details of cell division, allowing us to observe the process of embryogenesis in C. elegans. Collectively, this study highlights how some conserved regulators are critical to the proper execution of cell division as well as the regulation of later tissue development, ultimately ensuring organismal viability.

CHAPTER 1

Protease Dead Separase Inhibits Chromosome Segregation and RAB-11 Positive Vesicle Trafficking

This chapter contains one published manuscript (Bai and Bembenek, 2017b).

My contribution included: (1) designing experiments, (2) performing experiments, (3) collecting data and data analysis, (4) creating figures and writing the manuscript, (5) addressing the reviewers' comments and writing the rebuttal to the editor. Dr. Joshua N. Bembenek assisted with (1), (4) and (5). Only small revisions to the original figures have been made for the purposes of this dissertation.

Abstract

Separase cleaves cohesin to allow chromosome segregation. Separase also regulates cortical granule exocytosis and vesicle trafficking during cytokinesis, both of which involve RAB-11. We investigated whether separase regulates exocytosis through a proteolytic or non-proteolytic mechanism. In *C. elegans*, protease-dead separase (SEP-1^{PD}::GFP) is dominant negative. Consistent with its role in cohesin cleavage, SEP-1^{PD}::GFP causes chromosome segregation defects. As expected, partial depletion of cohesin rescues this defect, confirming that SEP-1^{PD}::GFP acts through a substrate-trapping mechanism. SEP-1^{PD}::GFP causes cytokinetic defects that is synergistically exacerbated by depletion of the t-SNARE SYX-4. Furthermore, SEP-1^{PD}::GFP delays furrow ingression, causes an accumulation of RAB-11 vesicles at the cleavage furrow site and delays the exocytosis of cortical granules during anaphase I. Depletion of *syx-4* further enhanced RAB-11::mCherry and SEP-1^{PD}::GFP plasma membrane accumulation during cytokinesis, while depletion of cohesin had no effect. In contrast, centriole disengagement appears normal in SEP-1^{PD}::GFP embryos, indicating that chromosome segregation and vesicle trafficking are more sensitive to inhibition by the

inactive protease. These findings suggest that separase cleaves an unknown substrate to promote the exocytosis of RAB-11 vesicles and paves the way for biochemical identification of substrates.

Introduction

Faithful cell division depends on coordinated regulation of chromosome segregation and cytokinesis. Chromosome segregation requires equal partitioning of sister chromatids that are duplicated and linked together by cohesin during mitotic S-phase (Onn et al., 2008). At the onset of anaphase, the kleisin subunit of cohesin, SCC-1, is cleaved by the caspase-like cysteine protease separase, allowing sister chromatid separation (Hauf et al., 2001). Separase is a large protease with two sub-domains, the pseudo-protease domain (PPD) and active protease domain (APD) as well as an extended helical repeat region in the N-terminus (Boland et al., 2017; Lin et al., 2016; Luo and Tong, 2017; Viadiu et al., 2005; Winter et al., 2015). The canonical role of separase is to cleave SCC-1, which allows chromosome segregation during mitotic and meiotic anaphase in all eukaryotic organisms studied to date (Uhlmann et al., 2000). The proteolytic function of separase is required for several other cell cycle events in anaphase. In budding yeast, separase cleaves the kinetochore and spindle associated protein Slk19, which stabilizes the anaphase spindle (Sullivan et al., 2004; Sullivan et al., 2001). Additionally, separase cleaves the pericentriolar material proteins kendrin and pericentrin B to regulate centriole licensing in mammalian cells (Lee and Rhee, 2012; Matsuo et al., 2012). Interestingly, separase cleaves itself at multiple adjacent sites (Stemmann et al., 2001; Waizenegger et al., 2002; Zou et al., 2002). The auto-cleaved fragments still

maintain catalytic activity, and self-cleavage plays important roles in controlling cell cycle progression, separase activity and chromosome segregation (Holland et al., 2007; Papi et al., 2005). These proteolytic functions stress the importance of identifying the distinct roles of separase and its substrates in both meiosis and mitosis.

In addition to its roles as a protease, several non-proteolytic functions of separase have been identified. At anaphase onset, separase-dependent activation of the Cdc14 early anaphase release (FEAR) pathway initiates mitotic exit in budding yeast (Stegmeier et al., 2002). A protease dead separase mutant is still sufficient to initiate mitotic exit but cannot promote cohesin cleavage and spindle elongation (Sullivan and Uhlmann, 2003). Interestingly, Cdc14 has been shown to promote cytokinesis by regulating ER to bud neck trafficking of chitin synthase and directly dephosphorylating several bud neck targets (Chin et al., 2012; Jakobsen et al., 2013; Kuilman et al., 2015; Miller et al., 2015; Palani et al., 2012). Separase is also known to bind and inhibit CDK-1 in mammalian cells through an unstructured region between the catalytic and N-terminal domain (Gorr et al., 2005; Gorr et al., 2006; Hellmuth et al., 2015; Viadiu et al., 2005). Consistent with this, several studies have shown that expression of catalytically inactive separase can rescue multiple aspects of separase function (Gorr et al., 2006; Kudo et al., 2006). In oocytes, expression of inactive separase can rescue polar body extrusion, a highly asymmetric form of cytokinesis, after knockdown of endogenous separase (Kudo et al., 2006). These earlier studies would suggest the hypothesis that protease dead separase might be capable of promoting the cytokinetic functions of separase. However, our unexpected observation that protease dead separase is dominant negative in *C.*

17

elegans suggests that it interferes with endogenous separase function (Mitchell et al., 2014). This provides a novel opportunity to investigate the cellular functions that are affected by protease dead separase.

Caenorhabditis elegans is a powerful model system for addressing fundamental cell cycle events. Oocytes mature and undergo fertilization every 25 minutes, then complete meiosis and initiate the mitotic cell divisions within an hour *in utero*, all of which can be imaged with relative ease (McCarter et al., 1999). In *C. elegans*, separase performs multiple functions during the oocyte-to-embryo transition in the first meiotic division and the mitotic metaphase-to-anaphase transition. Separase is essential for homologous chromosome disjunction through cleaving meiosis-specific kleisin subunit Rec8 (Siomos et al., 2001). During anaphase I, separase cleaves the CENP-A related protein, CPAR-1, which may regulate the metaphase-anaphase transition in *C. elegans* (Monen et al., 2015). Separase is involved in centriole disengagement during male spermatocyte meiosis (Schvarzstein et al., 2013) and regulates the separation and duplication of sperm-derived centrioles in embryos at the meiosis-mitosis transition (Cabral et al., 2013). During mitosis, separase cleaves the mitotic cohesin kleisin subunit SCC-1 to promote chromosome segregation (Mito et al., 2003; Siomos et al., 2001). Whether *C. elegans* separase has the same conserved non-proteolytic functions such as CDK-1 inhibition is unknown, as is whether other protease dead separase mutants are dominant negative in other systems.

Our previous studies have defined an essential function for separase in the regulation of vesicle exocytosis during anaphase. Separase inactivation causes eggshell defects and cytokinesis failures, both of which are due to defects in vesicle trafficking. During anaphase I, separase localizes to cortical granules and is required for their exocytosis, which is necessary for eggshell formation (Bembenek et al., 2007). Simultaneously, separase localizes to the base of the polar body and is required for successful cytokinesis during polar body extrusion (PBE). RAB-11, a small GTPase that regulates trafficking at recycling endosomes and is essential for cytokinesis in several systems, is also found on cortical granules and the base of the polar body and is required for both events in anaphase I (Sato et al., 2008). Further study indicated that separase is also required for cytokinesis during mitosis (Bembenek et al., 2010). Interestingly, depletion of separase in *C. elegans* with RNAi enhanced the accumulation of RAB-11 positive vesicles at the ingressing furrow and midbody, suggesting a role of separase in exocytosis during cytokinesis (Bembenek et al., 2010). Furthermore, the role of separase in exocytosis is independent of its function in chromosome segregation as a unique hypomorphic mutant that maps to the N-terminal domain promotes mostly normal chromosome segregation, while cortical granule exocytosis (CGE) and cytokinesis remain severely affected (Bembenek et al., 2007; Bembenek et al., 2010). These studies demonstrate that CGE is under the control of the same cellular machinery that regulates membrane trafficking during polar body extrusion and mitotic cytokinesis. Separase has been also found in plant and mammalian systems to regulate membrane trafficking (Bacac et al., 2011; Moschou et al., 2014), suggesting that separase may have a conserved function in regulating membrane trafficking.

19

There are many open questions about the exact mechanism of how separase regulates RAB-11 vesicle exocytosis. Previous studies in mouse oocytes suggest that separase has a non-proteolytic role in polar body extrusion, and thus possibly in vesicle trafficking (Kudo et al., 2006). However, we recently reported the unexpected observation that SEP-1^{PD}::GFP is dominant negative in *C. elegans* (Mitchell et al., 2014). Here, we investigated cellular phenotypes to understand what processes are impaired by SEP-1^{PD}::GFP in *C. elegans* and whether vesicle trafficking is affected. We used high-resolution confocal microscopy to observe SEP-1^{PD}::GFP phenotypes during meiosis I and mitotic cytokinesis. We show that SEP-1^{PD}::GFP impairs both chromosome segregation and RAB-11 vesicle trafficking, but does not impact centriole disengagement. Depletion of the substrate, cohesin *scc-1*, substantially rescues chromosome bridging during anaphase in SEP-1^{PD}::GFP embryos, consistent with the hypothesis that SEP-1^{PD}::GFP prevents substrate cleavage. SEP-1^{PD}::GFP also impairs vesicle exocytosis and genetically interacts with vesicle fusion machinery. Therefore, separase may also cleave a substrate to promote exocytosis during CGE and cytokinesis.

Results

SEP-1^{PD}::GFP Inhibits Chromosome Separation

To investigate the proteolytic functions of separase in C. elegans, we used the pie-1 promoter for germline expression of a protease-dead separase (C1040S) fused to GFP (SEP-1^{PD}::GFP) (Bembenek et al., 2010; Mitchell et al., 2014). We have devised two methods to propagate animals carrying the dominant negative protease dead separase

and have applied them to characterize the phenotype caused by stable expression of protease-dead separase (Mitchell et al., 2014). Depending on the experimental setup and desired genotype, our conditions lead to SEP-1^{PD}::GFP expression from either one or two copies of the transgene in a wild type background with endogenous separase expression. We also characterized multiple independently generated homozygous SEP-1^{PD}::GFP transgenic lines obtained by microparticle bombardment to identify the most reproducibly behaved lines. Two lines (WH520 and WH524) behave as chromosomal-integrated alleles with consistent expression of the protease-dead separase that lead to consistent phenotypes, while other lines were less consistent (Fig. A1). We used WH520 to characterize cellular phenotypes, which has nearly 100% embryo lethality after 5 generations off GFP RNAi (which we will call homozygous SEP-1^{PD}::GFP) and about 70% lethality in F2 embryos using the backcross propagation strategy (labeled as SEP-1^{PD}::GFP/+) (Fig. A1 B). In contrast, expression of SEP-1^{WT}::GFP causes no lethality and can fully rescue mutant separase embryos (Bembenek et al., 2010; Mitchell et al., 2014). Therefore, expression of SEP-1^{PD}::GFP in the wild type background with endogenous separase consistently causes embryo lethality.

Separase is well known to cleave cohesin to allow chromosome segregation. We hypothesized that SEP-1^{PD}::GFP is dominant negative in part because it may bind cohesin but would be unable to cleave it, thus preventing endogenous separase from cleaving cohesin and inhibiting chromosome separation. Separase has several conserved substrates that are found in *C. elegans* and mammalian cells, including cohesin. Prior to anaphase onset, SEP-1^{WT}::GFP and SEP-1^{PD}::GFP show identical

localization patterns and both show equivalent localization to chromosomes (Bembenek et al., 2010). However, in mitotic anaphase, when separase becomes catalytically active and would bind to substrates, SEP-1^{PD}::GFP displays ectopic localization at centrioles and the central spindle where known substrates are cleaved by separase in other systems (Bembenek et al., 2010), consistent with the hypothesis that it has enhanced association with substrates. In order to investigate the effects of SEP-1^{PD}::GFP on chromosome segregation, we compared embryos expressing H2B::mCherry to label the chromosome and homozygous SEP-1^{PD}::GFP or SEP-1^{WT}::GFP. We defined anaphase onset as the time point when the width of the chromosome signal increases due to spindle forces pulling sister chromatids apart, which always occurs very quickly after chromosome alignment on the metaphase plate in both SEP-1^{PD}::GFP and SEP-1^{WT}::GFP. Consistent with our hypothesis, chromosome segregation during the first mitotic anaphase was significantly delayed in homozygous SEP-1^{PD}::GFP compared to SEP-1^{WT}::GFP embryos (Fig. 1.1 A-L). To ensure cell cycle timing was not dramatically altered, we quantified the time from nuclear envelop breakdown (NEBD) to furrow ingression in homozygous SEP-1^{PD}::GFP embryos and did not observe a significant delay of global cell cycle events as compared with SEP-1^{WT}::GFP (Fig. A1 C-H, p=0.54, t-test).

Quantification of the distance that chromosomes separate after mitotic anaphase onset showed on average a 3.7 micron lag in separation over time in embryos expressing homozygous SEP-1^{PD}::GFP (Fig. 1.1 M). Homozygous SEP-1^{PD}::GFP embryos had some variation in the severity of segregation defects, from slight bridging (in 10/52 SEP-

1^{PD}::GFP embryos at 25 °C) to more severe bridging chromosomes (in 42/52 homozygous SEP-1^{PD}::GFP embryos at 25 °C) (Fig. 1.1 N), which was absent from WT (in 0/16 SEP-1^{WT}::GFP embryos at 25 °C). Interestingly, the delayed chromosome separation was more severe at 25 °C than at 20 °C (Fig. 1.1 N & Movie 1), which is likely due to higher transgene expression (fluorescence intensity in the cytoplasm is twofold higher at 25 °C as compared to 20 °C). We also investigated chromosome segregation during anaphase I of meiosis. Interestingly, homozygous SEP-1^{PD}::GFP embryos also displayed chromosome segregation defects during meiotic anaphase (Fig. 1.2 A-H). We measured the delay in separation over time and observed a less severe but significant delay in chromosome segregation (Fig. 1.2 I). In addition, the bridging defects were not as severe as observed in mitosis (bridge observed in 0/8 SEP-1^{WT}::GFP embryos at 25 °C; in 7/15 homozygous SEP-1^{PD}::GFP at 25 °C, Fig. 1.2 J & Movie 2). These data indicate that homozygous SEP-1^{PD}::GFP impairs chromosome segregation during both meiosis and mitosis, likely due to impaired cohesin cleavage.

If our hypothesis that cohesin cleavage is impaired by SEP-1PD::GFP is correct, we would expect that partial depletion of scc-1 by RNAi would alleviate the chromosome segregation defects. We carefully titrated the degree of RNAi depletion (feeding RNAi 24 hours at 20°C and 25 °C) to achieve a mild level of *scc-1* depletion to avoid causing
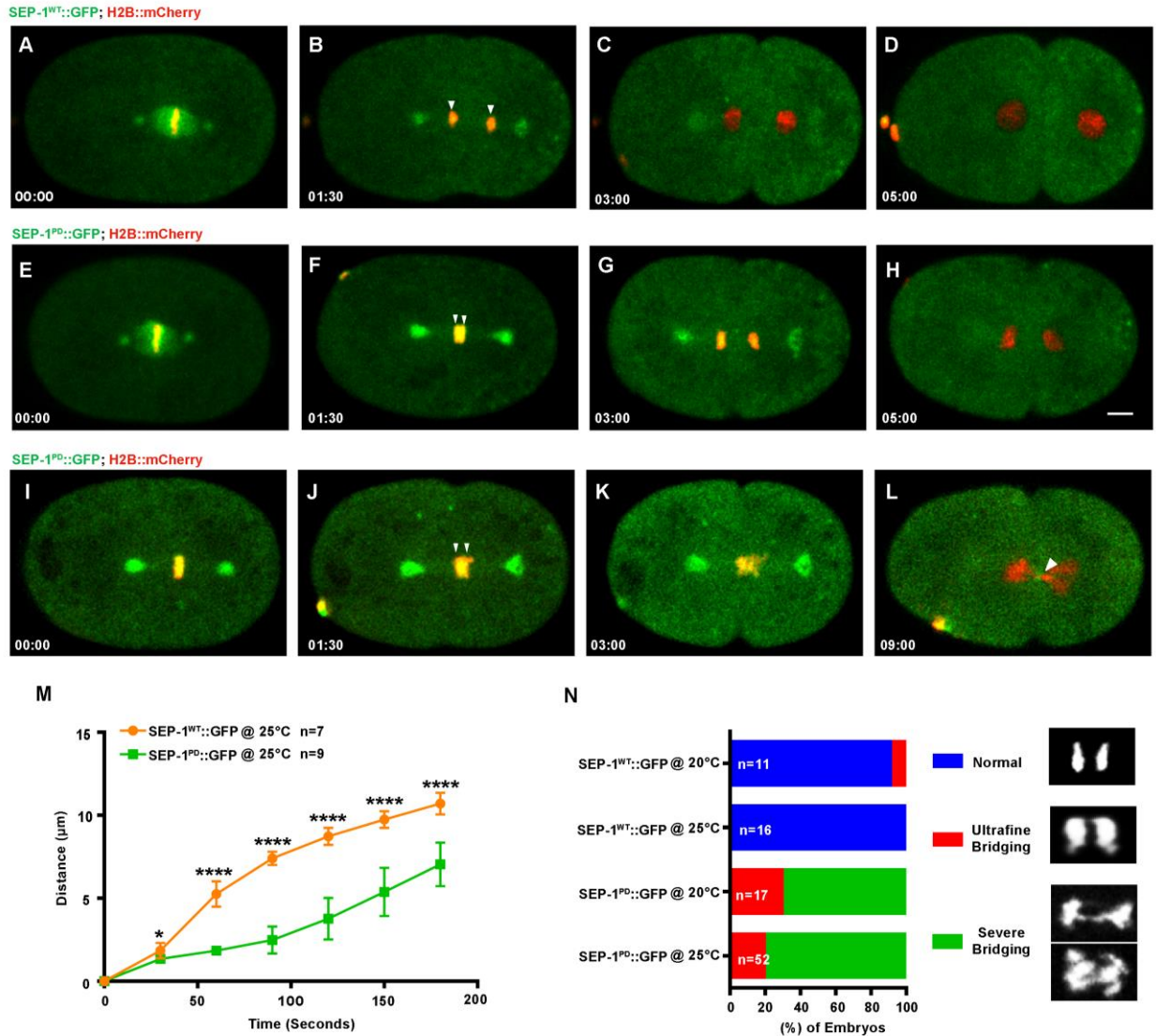
Figure 1. 1 SEP-1^{PD}::GFP causes chromosome segregation defects during mitosis.

Representative images of mitotic chromosome segregation in SEP-1^{WT}::GFP expressing embryos (A-D, green) or homozygous SEP-1^{PD}::GFP (green) embryos with slight bridging (E-H) and severe bridging (I-L) co-expressing H2B::mCherry (red). (M) Average distance between separating sister chromatids (as shown by arrowheads in B, F, J) during anaphase in SEP-1^{WT}::GFP (n=7) or SEP-1^{PD}::GFP (n=9) embryos from metaphase to late cytokinesis . (N) Percentage of embryos displaying normal chromosome separation (blue), slight bridging chromosomes (red) or severe chromosome bridges (green) during the first mitosis in embryos expressing either SEP-1^{WT}::GFP or SEP-1^{PD}::GFP at the temperature indicated (n= number of embryos imaged). Insert shows H2B::mCherry images scored as normal, slight bridging and severe bridging. Scale Bars, 10 μm. P-values: * =<0.05; ****=<0.0001 (t-test). Error bars indicated standard deviation of the mean.

24

severe chromosome segregation defects due to loss of cohesin (Mito et al., 2003). At both 20°C and 25 °C, *scc-1* RNAi causes only mild lethality in wild type (Fig. 1.3 A, B) but significantly rescues the homozygous SEP-1PD::GFP embryonic lethality from 100% down to 22% ± 10.34 at 25 °C (Fig. 1.3 B). Chromosome segregation defects were significantly alleviated after depletion of *scc-1* (RNAi) in homozygous SEP-1PD::GFP embryos (Fig. 1.3 C-F). Homozygous SEP-1PD::GFP depleted of scc-1 also had normal kinetics of chromosome segregation in anaphase (Fig. 1.3 G) and much less severe bridging defects (28/42 normal, 9/42 slightly bridging, 5/42 severe bridges, Fig. 1.3 H). Therefore, reducing the amount of cohesin largely rescues the chromosome segregation defects caused by expressing SEP-1PD::GFP together with endogenous separase in *C. elegans*. Presumably this is because there is less substrate that must be cleaved, reducing the amount of cohesin that endogenous separase must cleave in the presence of SEP-1PD::GFP to allow chromosome segregation. These substrate binding may not be necessary for localization. These findings suggest that SEP-1PD::GFP acts as a substrate trapping enzyme and inhibits cleavage of cohesin to impair chromosome segregation, as expected from the known functions of separase. Additionally, the data consistent with our hypothesis that SEP-1PD::GFP inhibits substrate cleavage, causing a dominant phenotype.
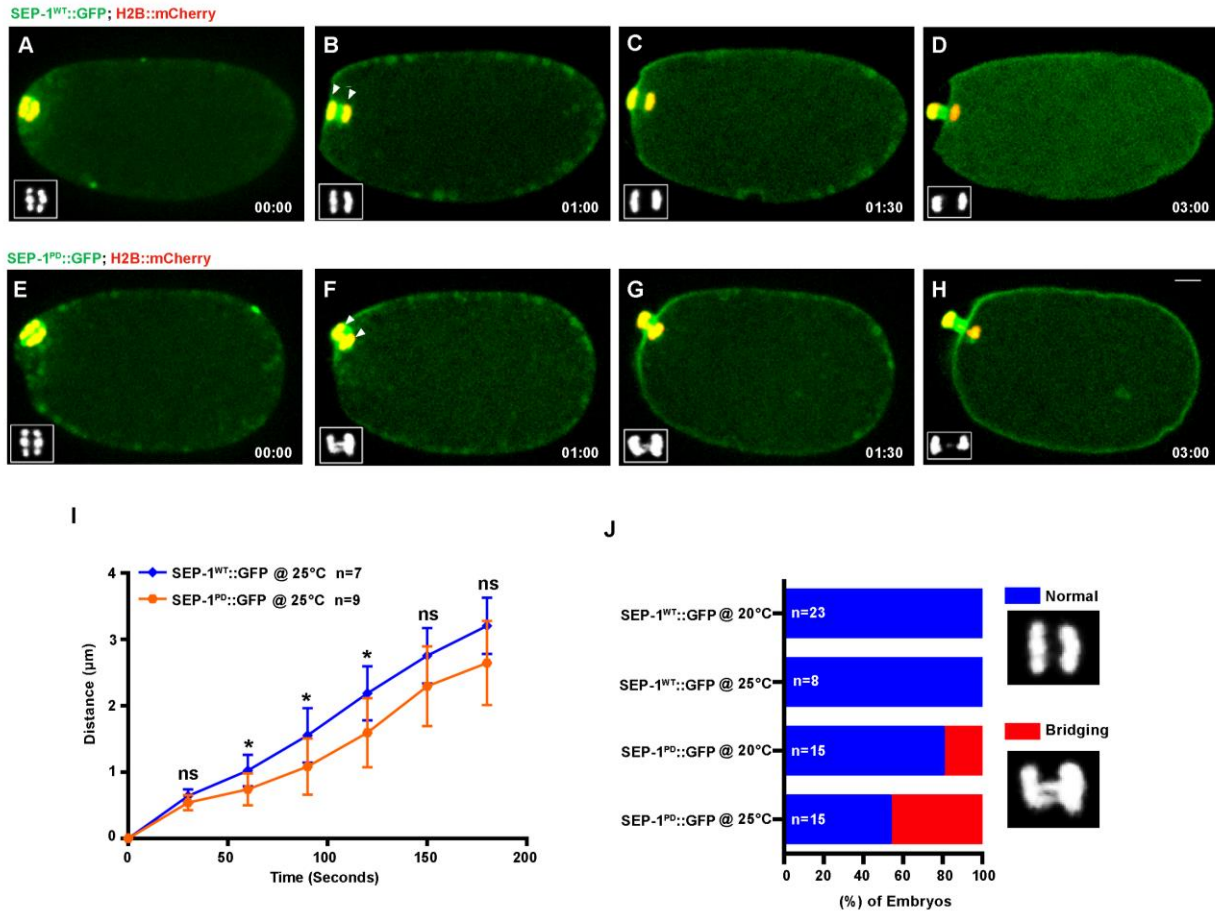
Figure 1. 2 SEP-1^{PD}::GFP causes chromosome segregation defects during meiosis I.

Representative images of meiotic chromosome segregation in SEP-1^{WT}::GFP (A-D, green) or homozygous SEP-1^{PD}::GFP expressing embryos (E-H, green) co-expressing H2B::mCherry (red). Lower left insets show H2B::mCherry. (I) Average distance between chromosomes (indicated by arrowheads in B, F) during anaphase in SEP-1^{WT}::GFP or homozygous SEP-1^{PD}::GFP. (J) Percentage of embryos displaying normal chromosome separation (blue), bridging chromosomes (red) during the anaphase I in embryos expressing either SEP-1^{WT}::GFP or homozygous SEP-1^{PD}::GFP (n= number of embryos imaged). Insets show examples scored as normal or bridging chromosomes during anaphase I. Scale Bars, 10 μm. P-values: * =<0.05; ns= not significant (t-test). Error bars indicated standard deviation of the mean.

Current studies indicate that separase cleaves substrates such as kendrin and cohesin to sever the physical link between centrioles (Matsuo et al., 2012; Schockel et al., 2011; Tsou and Stearns, 2006). We hypothesized that SEP-1^{PD}::GFP may bind to potential substrates at the centrosome, delaying their cleavage by endogenous separase and inhibiting centriole disengagement. In order to investigate the effects of SEP-1^{PD}::GFP on centriole disengagement, we compared embryos expressing SPD-2::mCherry (Peel et al., 2017) to label the centrioles and homozygous SEP-1^{PD}::GFP or SEP-1^{WT}::GFP (Fig. A2 A, B and Movie 3). We measured the signal intensity of separase in SEP-1^{PD}::GFP and SEP-1^{WT}::GFP expressing embryos at the onset of furrow ingression, which is about the time that centrioles disengage in the AB daughter cell. Interestingly, SEP-1^{PD}::GFP signal is significantly higher at the centriole and centrosome over time, relative to SEP-1^{WT}::GFP embryos (Fig. A2 C). However, we did not observe any significant delays in disengagement of daughter centrioles in SEP-1^{PD}::GFP embryos (Fig. A2 D). These data suggest that chromosome segregation is more sensitive to inhibition by the protease dead separase than centriole disengagement. Therefore, separase regulates multiple cell cycle events, which have different sensitivity to inhibition by protease dead separase.

SEP-1^{PD}::GFP expression impairs cytokinesis independent of cohesin

In addition to the canonical function of separase in chromosome segregation, separase is required for cytokinesis by regulating vesicle exocytosis (Bembenek et al., 2010). If separase has a substrate that it must cleave in order to promote vesicle exocytosis
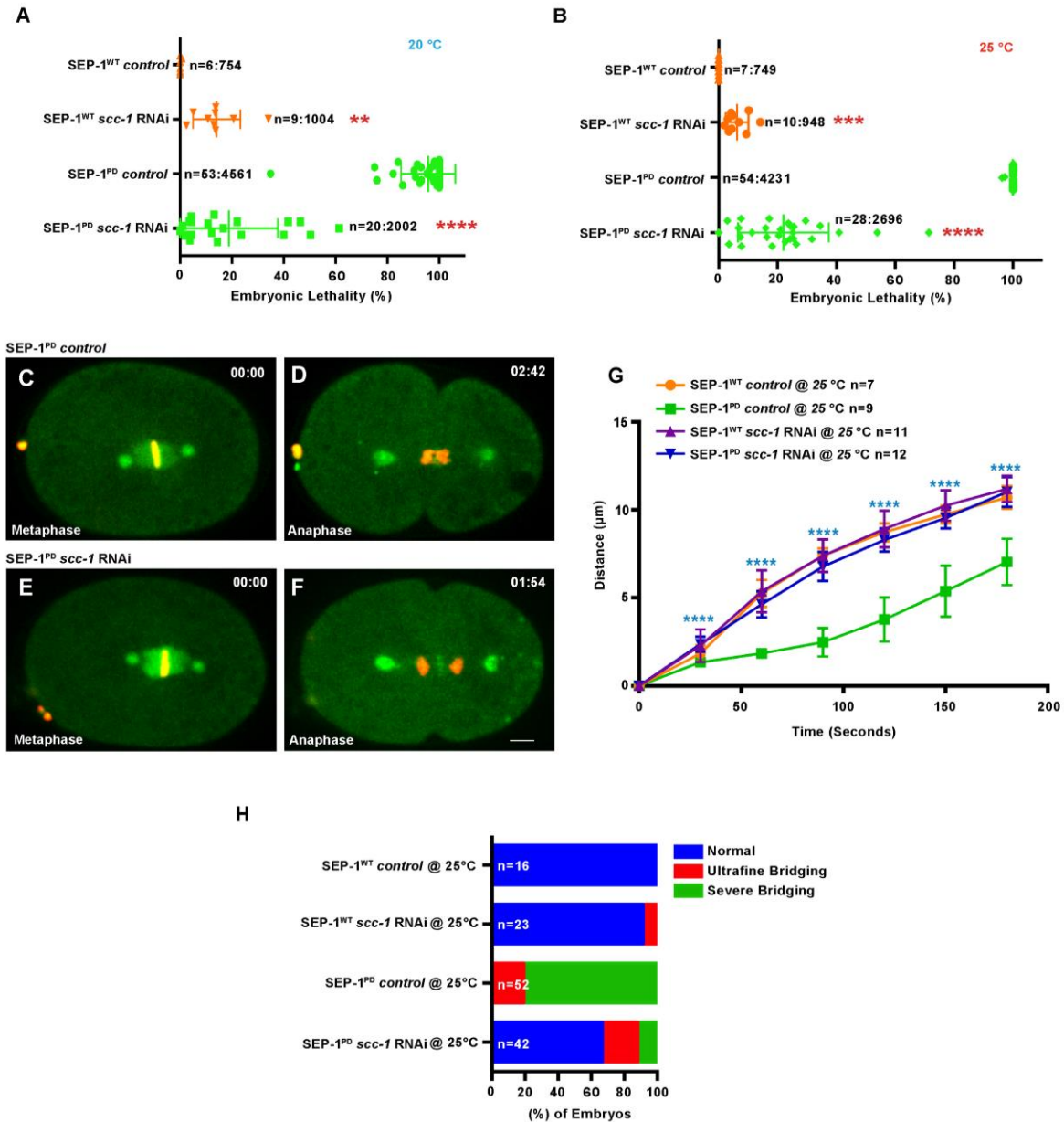
Figure 1. 3 Cohesin depletion rescues chromosome segregation defects caused by SEP-1^{PD}::GFP.

(A, B) Partial cohesin depletion significantly rescues the SEP-1^{PD}::GFP embryonic lethality at both 20°C and 25 °C (n=singled worm number: total embryo count). (C-F) Chromosome segregation defects were significantly alleviated after partial depletion of *scc-1* in homozygous SEP-1^{PD}::GFP (green) embryos (DNA in red). (G) Distance between separating sister chromatids during anaphase in SEP-1^{WT}::GFP or SEP-1^{PD}::GFP control or with *scc-1* (RNAi). (H) Percentage of embryos displaying normal chromosome separation (blue), slight bridging chromosomes (red) or severe chromosome bridges (green) during the first mitosis in embryos expressing SEP-1^{WT}::GFP or SEP-1^{PD}::GFP with and without *scc-1* (RNAi) treatment (n= number of embryos imaged). Scale Bars, 10 μm. P-values: ** =<0.01; ***=<0.001; ****=<0.0001 (*t*-test). Error bars indicated standard deviation of the mean.

28

during cytokinesis, we postulated that SEP-1^{PD}::GFP would inhibit this process similar to the way it impairs chromosome segregation. We tested whether homozygous SEP-1^{PD}::GFP embryos fail cytokinesis using live imaging. Interestingly, we found some homozygous SEP-1^{PD}::GFP embryos with multipolar spindles, indicative of cytokinesis failure, in one cell through two cell stages (in 2/52 homozygous SEP-1^{PD}::GFP embryos; 0/70 SEP-1^{WT}::GFP embryo; in 0/13 N2 at 25 °C. Fig. 1.4 A). Additionally, cytokinesis failures are sporadic and are often seen in older SEP-1^{PD}::GFP but not SEP-1^{WT}::GFP embryos, but are difficult to quantify accurately because cells that fail cytokinesis subsequently undergo multipolar division and cellularize. These data indicate that SEP-1^{PD}::GFP expression impairs cytokinesis, consistent with the hypothesis that it may inhibit cleavage of a substrate necessary for cytokinesis.

Next, we analyzed the rate of furrow ingression to determine if there are additional defects during cytokinesis despite the low rate of cytokinesis failure. We generated homozygous SEP-1^{PD}::GFP and SEP-1^{WT}::GFP lines expressing mCherry fused to the pleckstrin homology domain of phospholipase C-delta (PH::mCherry for short) to observe the plasma membrane during cytokinesis (Kachur et al., 2008). We imaged furrow ingression in a single focal plane of the central spindle and midbody. We found that furrow ingression rate in homozygous SEP-1^{PD}::GFP embryos was consistently slower compared with the SEP-1^{WT}::GFP and AIR-2::GFP control (0.14 µm/second, n=8 in homozygous SEP-1^{PD}::GFP; 0.17 µm/second ± 0.01 n=10 in SEP-1^{WT}::GFP, p=0.0004 (*t*-test), Fig. 1.4 B, D). We also measured the time from the initiation of furrow ingression until it completed, generating a smooth cell boundary. In SEP-1^{WT}::GFP

29
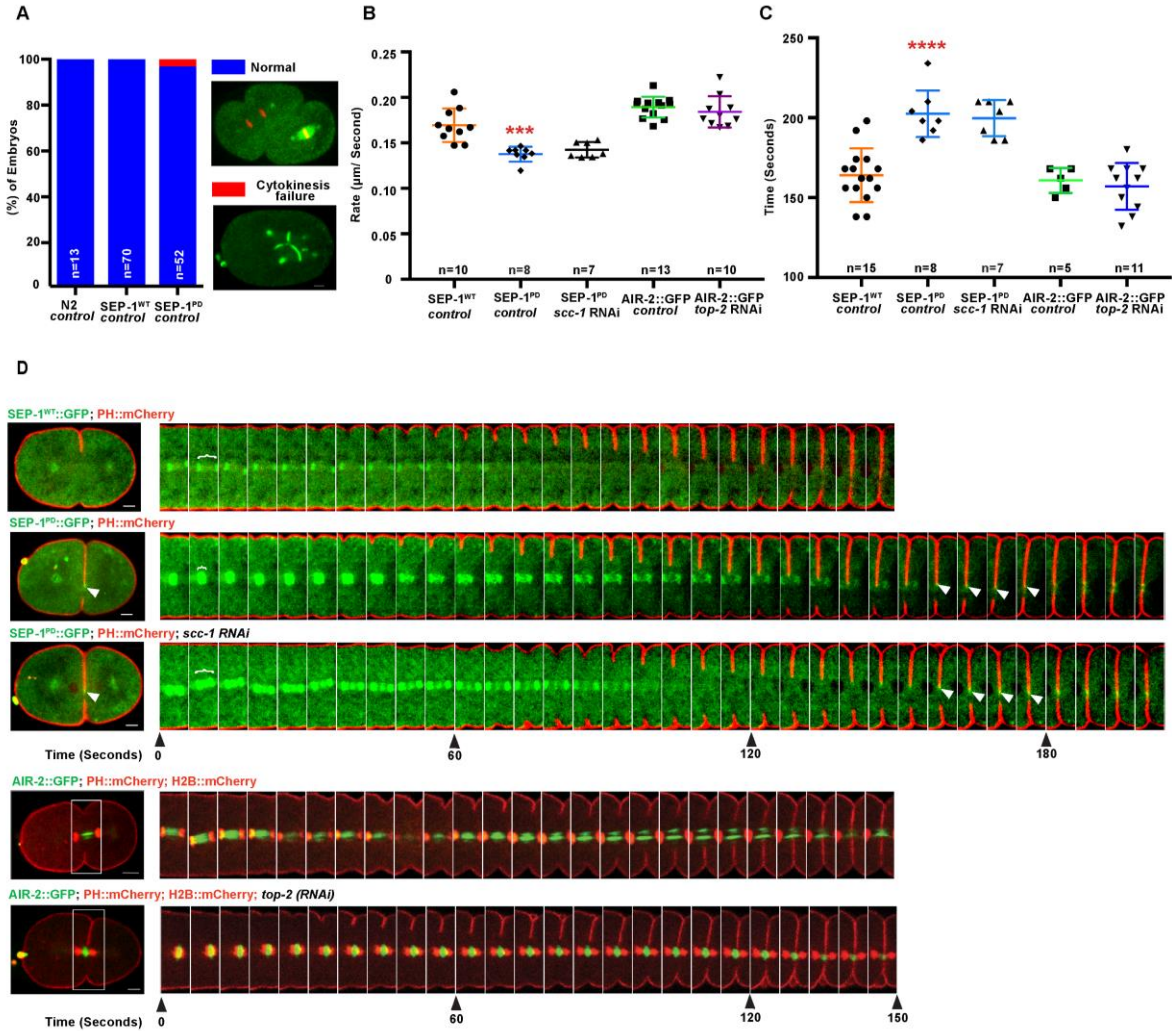
Figure 1. 4 SEP-1^{PD}::GFP causes cytokinesis defects.

(A) Percentage of embryos displaying normal cell division (blue) and cytokinesis failure (red) during first mitotic division in N2 wild type, SEP-1^{WT}::GFP or homozygous SEP-1^{PD}::GFP. Right panels show examples scored as normal or cytokinesis failure. (B) Quantification of the furrow ingression rate in different genotypes. Depletion of SCC-1 in SEP-1^{PD}::GFP embryos does not rescue the slower furrow ingression (p=0.29 (*t*-test), n= number of embryos imaged). (C) Quantification of the furrow ingression time in different conditions as indicated (n= number of embryos imaged). (D) Kymograph of the furrow region shows PH::mCherry (red) in SEP-1^{WT}::GFP, homozygous SEP-1^{PD}::GFP, SEP-1^{PD}::GFP; *scc-1(RNAi)* (time in seconds indicated below), or AIR-2::GFP (green) expressing PH::mCherry (red) and H2B::mCherry (red) with and without *top-2* (RNAi) during cytokinesis. Distance between separating sister chromatids at similar times after anaphase onset is indicated by brackets, furrow SEP-1^{PD}::GFP signal is indicated by arrowheads. Cohesin depletion rescues chromosome segregation, but not furrowing. The lower kymograph of an embryo treated with *top-2 (RNAi)* has chromatin in the path of the furrow without any change in furrow ingression. Scale Bars, 10 µm. Error bars indicated standard deviation of the mean. Each kymograph image is 6 seconds apart. P-values: ***=<0.001; ****=<0.0001 (*t*-test).

cells, this process took 164 seconds ± 4 (n=15, Fig. 1.4 C). Since SEP-1^{WT}::GFP does

not label the midbody, we also imaged the midbody maker AIR-2::GFP together with

PH::mCherry and found that our measurement of furrow completion timing was accurate

(161 seconds ± 4, n=5, p=0.69 (*t*-test), Fig. 1.4 C, D). SEP-1^{PD}::GFP, but not SEP-

1^{WT}::GFP, is often colocalized with the plasma membrane during furrowing and remains

at the midbody for an extended period of time, which could reflect enhanced association

with a membrane substrate (Fig. 1.4 D). In homozygous SEP-1^{PD}::GFP embryos,

cytokinesis completion was significantly delayed relative to wild type embryos (203

seconds ± 5; n=8, p<0.0001 (*t*-test), Fig. 1.4 C). Therefore, expression of dominant

negative SEP-1^{PD}::GFP specifically impairs furrow ingression and completion of

cytokinesis.

In several systems, lagging chromatin that becomes trapped in the midbody during

cytokinesis triggers an "abscission checkpoint" pathway to prevent cytokinesis failure

(Bembenek et al., 2013; Norden et al., 2006). In human cells, chromatin bridges induce

a delay in abscission but ultimately cells fail cytokinesis, which is observed when

cohesin cleavage is impaired (Hauf et al., 2001). However whether this is also due to

membrane trafficking defects is unknown. Several observations suggest that the

cytokinesis defects in SEP-1^{PD}::GFP embryos are different than those caused by other

chromosome bridging conditions. First, more penetrant cohesin *scc-1* RNAi causes

severe chromosome segregation defects but no cytokinesis defects, suggesting that

bridges resulting from the cohesin depletion do not cause cytokinesis failure in the

embryo (Mito et al., 2003). In addition, we previously demonstrated that many different

types of chromosome defects such as decondensation or catenation cause severe

bridging phenotypes but very rare cytokinesis failures due to the action of an abscission

checkpoint pathway in *C. elegans* (Bembenek et al., 2013; Bembenek et al., 2010).

Therefore, chromatin bridges do not cause cytokinesis defects in *C. elegans*, but elicit

the abscission checkpoint, which reduces the failure rate. Consistent with this, we

measured the furrow ingression rate in embryos with chromatin bridges after depletion

of *top-2* and observed normal ingression furrow rate (0.18 ± 0.01, n=10, p=0.40 (*t*-test),

Fig. 1.4 B), suggesting the abscission checkpoint does not affect the rate of furrowing

like SEP-1^{PD}::GFP. Reports in other systems have indicated that the abscission

checkpoint regulates other cytoskeletal regulators that function during cytokinesis

(Agromayor and Martin-Serrano, 2013). Therefore, the abscission checkpoint is likely

independent of separase-regulated cytokinesis events.

Cohesin is the critical target of separase in chromosome segregation and is also found

on the centrosome where it is cleaved during centriole licensing (Schockel et al., 2011).

A function for cohesin during cytokinesis has not been previously reported. If cohesin

were the relevant substrate involved in cytokinesis, even at a lower threshold, we would

expect its depletion to reduce the amount of substrate necessary to be cleaved and

alleviate the cytokinesis defects. However, while 70% of the SEP-1^{PD}::GFP embryos

treated with *scc-1(RNAi)* are rescued for the chromosome segregation defects (Fig. 1.3

H), they still show slow furrow ingression and delayed closure of the furrow (Fig. 1.4 C).

Partial depletion of *scc-1* rescues the chromosome segregation defects but did not

rescue the delay of furrow closure (200 seconds ± 4, n=7, p=0.69 (*t*-test), Fig. 1.4 C, D)

or the furrow ingression rate in homozygous SEP-1^{PD}::GFP embryos (0.14 µm/second

in homozygous SEP-1^{PD}::GFP *scc-1* RNAi; n=7, p=0.29 (*t*-test), Fig. 1.4 B).

Interestingly, we found that cohesin depletion leads to higher accumulation of SEP-

1^{PD}::GFP at the furrow and midbody in homozygous embryos (Fig. A3 A, B). This result

suggests that SEP-1^{PD}::GFP can compete with different substrates and when cohesin is

depleted, it is more free to interact with a putative unknown substrate at the furrow and

midbody. Therefore, the cytokinesis defects observed in embryos expressing SEP-

1^{PD}::GFP does not occur in other chromosome bridging conditions and is not rescued

by depletion of cohesin, suggesting that separase has a chromosome independent role

in cytokinesis.

We further investigated whether cohesin alleviates the cytokinesis defects caused by

inactivating separase. We depleted separase by RNAi with and without cohesin

depletion to determine whether cohesin depletion would impact the cytokinesis

phenotype. To obtain consistent phenotypes, we carefully titrated the degree of RNAi

depletion of cohesin and separase (feeding *scc-1* RNAi 24 hours and *sep-1* RNAi

together with *scc-1* RNAi for another 24 hours at 20°C). However, depletion of *scc-1* did

not affect the rate of cytokinesis failure after separase depletion (11/43 *sep-1 (RNAi),*

12/42 *sep-1; scc-1(RNAi),* Fig. A3 D). We also depleted *scc-1* in the hypomorphic

separase temperature sensitive mutant (feeding *scc-1* RNAi for 48 hours at 15 °C), *sep-*

1 (e2406) shifted to 25°C for 4-8 hours and saw no change in the rate of cytokinesis

failure (3/10 *control (RNAi); sep-1 (e2406)*, 4/15 *scc-1 (RNAi)*; *sep-1(e2406)*, Fig. A3 D).

Therefore, cohesin depletion does not affect the cytokinesis defects caused by

disrupting separase function in three different conditions, suggesting that separase has another substrate besides cohesin that it cleaves in order to promote cytokinesis.

SEP-1^{PD}::GFP genetically interacts with essential exocytosis machinery

Given that separase likely regulates cytokinesis by promoting RAB-11 vesicle exocytosis, we investigated whether SEP-1^{PD}::GFP interferes with exocytosis. We first tested whether there was a genetic interaction between SEP-1^{PD}::GFP and the t-SNARE *syx-4*. SYX-4 is a core part of the exocytosis fusion machinery and is localized to the plasma membrane where it is required for cytokinesis in *C. elegans* (Jantsch-Plunger and Glotzer, 1999)*. Therefore, we expected that combining SEP-1^{PD}::GFP expression and depletion of *syx-4* would greatly exacerbate the cytokinesis failure rate if they both inhibit exocytosis. *syx-4* RNAi is inefficient and causes highly variable phenotypes compared with other genes (Jantsch-Plunger and Glotzer, 1999). We carefully calibrated RNAi treatment and determined that 30-36 hours feeding *syx-4* RNAi was an optimal intermediate condition, which caused minimal eggshell permeability and cytokinesis defects in wild type embryos. Consistent with our hypothesis, 30-36 hours feeding *syx-4* RNAi synergistically enhanced embryonic cytokinesis defects in embryos expressing homozygous SEP-1^{PD}::GFP (in 15/21 cytokinesis failure, Fig. 1.5 B, C) as compared with wild type (in 0/23 SEP-1^{WT}::GFP embryos; in 2/30 N2 embryos, Fig. 1.5 A, C, Movie 4). Therefore, SEP-1^{PD}::GFP has a strong negative genetic interaction with *syx-4(RNAi),* consistent with the hypothesis that they both inhibit exocytosis during cytokinesis.
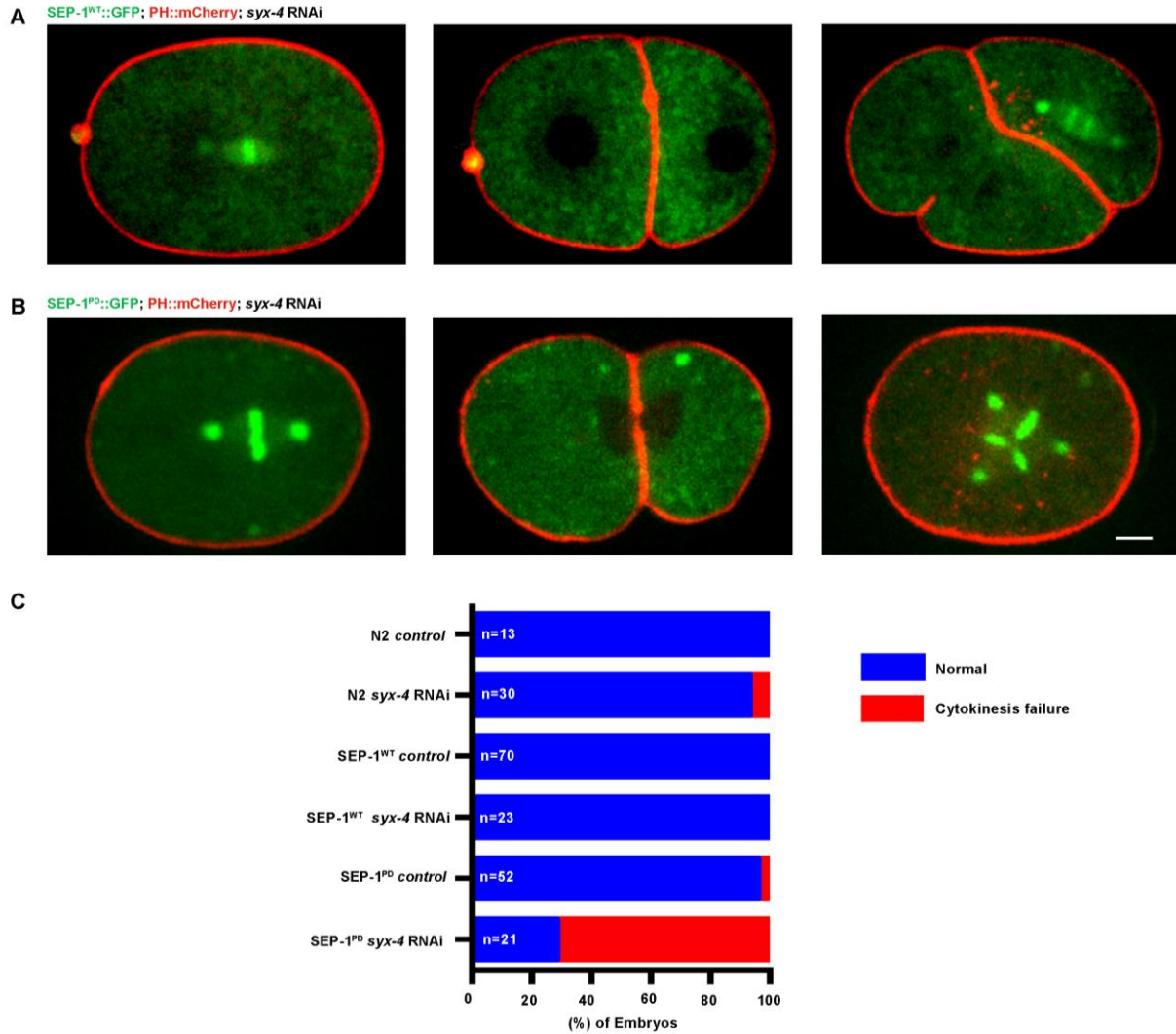
Figure 1. 5 SEP-1^{PD}::GFP was enhanced by t-SNARE syx-4 depletion.

(A) Representative images of mitotic cytokinesis in SEP-1^{WT}::GFP (A, green) or homozygous SEP-1^{PD}::GFP (B, green) embryos co-expressing PH::mCherry (red). (B) Representative images of mitotic cytokinesis failure in homozygous SEP-1^{PD}::GFP; PH::mCherry expressing embryos with *syx-4* (RNAi), resulting in a one cell embryo with a multi-polar spindle. (C) Percentage of embryos displaying normal cytokinesis (blue) or cytokinesis failure (red) in different conditions as indicated (n= number of embryos imaged). Scale Bars, 10 μm.

SEP-1PD::GFP inhibits RAB-11 positive vesicle trafficking during cytokinesis

We next wanted to investigate whether the cytokinesis defects caused by SEP-1PD::GFP expression were due to the inhibition of RAB-11 positive vesicle trafficking. Despite several attempts we were unable to generate viable lines homozygous for both SEP-1PD::GFP and RAB-11::mCherry, indicative of a negative genetic interaction. However, we could generate viable heterozygous SEP-1PD::GFP/+ and RAB-11::mCherry/+ F1 animals that reproducibly expressed both transgenes in order to film F2 embryos. Since the protein in newly fertilized F2 embryos is synthesized by the F1 maternal syncytial germline, each embryo will have the same cytoplasmic expression of SEP-1PD::GFP/+ and RAB-11::mCherry/+ despite having different genotypes. Although the cytokinesis phenotypes in SEP-1PD::GFP/+ expressing RAB-11::mCherry/+ are less severe than homozygous SEP-1PD::GFP, 30-36 hours feeding of *syx-4* RNAi substantially increased the rate of cytokinesis failures (0/30 *syx-4(RNAi)*; SEP-1WT::GFP, 0/15 SEP-1PD::GFP/+, 5/23 *syx-4(RNAi)*; SEP-1PD::GFP/+, Fig. 1.6 H and Movie 5). Mounting embryos on an agar pad or in hanging drop gave the same results after treating *syx-4* RNAi in SEP-1PD::GFP compared with SEP-1WT::GFP embryos, indicating that indirect effects from mounting were not an issue. Therefore, *syx-4* RNAi strongly exacerbates the cytokinesis defects in both heterozygous and homozygous SEP-1PD::GFP embryos, although the cytokinesis phenotypes are weaker in the heterozygous embryos.

Next, we imaged RAB-11 vesicle trafficking during cytokinesis in SEP-1WT::GFP and SEP-1PD::GFP/+ embryos. RAB-11 generates exocytic vesicles from a centrosomal

36

compartment of recycling endosomes, and remains associated with those vesicles as they are transported to and exocytosed at the plasma membrane (Albertson et al., 2005; Schiel et al., 2013; Skop et al., 2001). In SEP-1^{WT}::GFP and SEP-1^{PD}::GFP/+ embryos, RAB-11 is normally distributed at centrosomes and throughout the cytoplasm, indicating that early stages of vesicle trafficking are normal (Fig. 1.6 A, B). Interestingly, we found that the expression of SEP-1^{PD}::GFP/+ resulted in increased and persistent accumulation of RAB-11 vesicles at the cleavage furrow and midbody compared to SEP-1^{WT}::GFP expressing embryos, consistent with a defect in exocytosis at the plasma membrane (Fig. 1.6 A, B, G; Movie 6). The Golgi-associated GTPase, RAB-6, was shown to recruit separase to the cortical granule in *C. elegans* embryos (Kimura and Kimura, 2012). However, we did not observe the accumulation of RAB-6 at the ingressing furrow or midbody during cytokinesis in SEP-1^{PD}::GFP/+ expressing embryos (Fig. 1.6 E, F). Therefore, SEP-1^{PD}::GFP/+ interferes with RAB-11 trafficking during cytokinesis.

Given that SEP-1^{PD}::GFP expression combined with *syx-4* (RNAi) enhances cytokinesis failure (Fig. 1.6 H), we hypothesized that they both inhibit RAB-11 vesicle exocytosis. To examine this further, we examined whether RAB-11 trafficking was more defective in SEP-1^{PD}::GFP/+; *syx-4* (RNAi) embryos, which might explain the increased cytokinesis failure. We imaged RAB-11 vesicles in embryos expressing both RAB-11::mCherry and SEP-1^{PD}::GFP/+ with and without 30-36 hours feeding *syx-4* RNAi treatment. Depletion of *syx-4* caused a significantly higher accumulation of both RAB-11::mCherry and SEP-1^{PD}::GFP/+ at the ingressing furrow and midbody compared with untreated SEP-

Figure 1. 6 SEP-1^{PD}::GFP inhibits RAB-11 positive vesicle trafficking during cytokinesis.

(A, B) Representative images and kymograph of RAB-11::mCherry (red) trafficking to the furrow in SEP-1^{WT}::GFP (green) or heterozygous SEP-1^{PD}::GFP/+ (green). Arrowheads denote enhanced RAB-11::mCherry (grey) accumulation. (C, D) *syx-4* (RNAi) enhances RAB-11::mCherry (grey) in both SEP-1^{WT}::GFP and SEP-1^{PD}::GFP/+ at the furrow and midbody. (E) Kymograph of the furrow region showing that RAB-6::mCherry (red) and SEP-1^{WT}::GFP (green) do not accumulate in the furrow. (F) Accumulation of heterozygous SEP-1^{PD}::GFP/+ (green) is observed at the furrow and midbody, but not RAB-6::mCherry (red). (G) Quantification of separase and RAB-11 signals in the midbody during cytokinesis in different conditions as indicated. (H) The percentage of embryos displaying cytokinesis failure in heterozygous SEP-1^{PD}::GFP/+ (green) embryos expressing RAB-11::mCherry/+ (red) with indicated conditions. Scale Bars, 10 μm. P-values: * =<0.05; **=<0.01; ****=<0.0001 (*t*-test). Error bars indicated standard error of the mean. Each kymograph image is 6 seconds apart.

SEP-1^{WT}::GFP; RAB-11::mCherry; *control*

A

SEP-1^{PD}::GFP/- ; RAB-11::mCherry; *control*

B

SEP-1^{WT}::GFP; RAB-11::mCherry; *syx-4* RNAi

C

SEP-1^{PD}::GFP/- ; RAB-11::mCherry; *syx-4* RNAi

D

SEP-1^{WT}::GFP/-; RAB-6::mCherry

E

SEP-1^{PD}::GFP/-; RAB-6::mCherry

F

Time (Seconds)   0   30   60   90   120

G

SEP-1^{WT} *control*	n=12	
SEP-1^{WT} *syx-4*	n=17	
SEP-1^{WT} *scc-1*	n=5	
SEP-1^{PD} *control*	n=9	
SEP-1^{PD} *syx-4*	n=8	
SEP-1^{PD} *scc-1*	n=7	
SEP-1^{WT} *control*	n=12	
SEP-1^{WT} *syx-4*	n=17	
SEP-1^{WT} *scc-1*	n=5	
SEP-1^{PD} *control*	n=9	
SEP-1^{PD} *syx-4*	n=8	
SEP-1^{PD} *scc-1*	n=7	

Ratio (PM/Cytoplasm)

H

SEP-1^{WT}::GFP;RAB-11::mCherry F2
syx4 RNAi @ 25 °C   n=30

SEP-1^{PD}::GFP/-;RAB-11::mCherry F2
control @ 20 °C   n=32

SEP-1^{PD}::GFP/-;RAB-11::mCherry F2
control @ 25 °C   n=15

SEP-1^{PD}::GFP/-;RAB-11::mCherry F2
scc-1 RNAi @ 25 °C   n=13

SEP-1^{PD}::GFP/-;RAB-11::mCherry F2
syx-4 RNAi @ 25 °C   n=23

(%) of Embryos

Normal
Cytokinesis Failure

39

1[PD]::GFP/+ embryos (Fig. 1.6 B, D, G; Movie 6). Unfortunately we could not assay RAB-11 vesicle trafficking under the more severe condition of homozygous SEP-1[PD]::GFP; *syx-4* (RNAi) which has a much higher cytokinesis failure rate, but we expect that RAB-11 accumulation would be even greater. These data are consistent with the hypothesis that separase and RAB-11 are trafficked together on vesicles to the plasma membrane during cytokinesis, and that *syx-4(RNAi)* delays fusion of these vesicles. Finally, we examined whether cohesin would cause any change in RAB-11 vesicle trafficking. Given that partial depletion of *scc-1* does not significantly change the rate of furrow ingression in SEP-1[PD]::GFP embryos (Fig. 1.4 B), we expected RAB-11 trafficking would also not be affected. Indeed, depletion of SCC-1 did not alter the accumulation of RAB-11 vesicles at the furrow in SEP-1[PD]::GFP/+ embryos, but rescued the chromosome segregation defect (p=0.90, *t*-test, Fig. 1.6 G). Importantly, we previously demonstrated that depletion of *top-2*, which causes severe chromosome bridging and activates the abscission checkpoint response in *C. elegans*, does not have any impact on RAB-11 trafficking (Bembenek et al., 2013; Bembenek et al., 2010). Therefore, the response to chromosome bridging during cytokinesis does not explain the defects in RAB-11 trafficking in SEP-1[PD]::GFP embryos. These results suggest that separase regulates cytokinesis by hydrolyzing an unknown substrate to regulate RAB-11 vesicle trafficking.

SEP-1[PD]::GFP expression delays cortical granule exocytosis

Separase and RAB-11 both localize to cortical granules while SYX-4 localizes to the plasma membrane to promote their exocytosis during meiosis anaphase I (Bembenek et

al., 2007; Jantsch-Plunger and Glotzer, 1999; Sato et al., 2008). This is an excellent

cellular context to investigate exocytosis because separase can be observed directly on

these large 1μm vesicles, which release contents required for eggshell formation during

anaphase I. We investigated whether SEP-1^{PD}::GFP also impairs CGE similar to its

effects during cytokinesis. We analyzed whether embryos were permeable to dyes due

to disrupted eggshell formation from lack of CGE, but did not observe significant

permeability defects. This indicates that SEP-1^{PD}::GFP expression does not completely

inhibit CGE. To confirm localization, we filmed SEP-1^{PD}::GFP/+ embryos expressing the

cortical granule cargo, CPG-2::mCherry, during anaphase I. We observed that CGP-

2::mCherry localizes to cortical granules with both SEP-1^{WT}::GFP and SEP-1^{PD}::GFP/+

as expected (Fig. A4 and Movie 7). Interestingly, separase localizes to more vesicles

than those labeled by CPG-2::mCherry, indicating that this cargo is only packaged into

a subset of cortical granules (Fig. A4, Movie 7). This result is consistent with the

heterogeneity of the cortical granule vesicle population observed by transmission

electron microscope (Bembenek et al., 2007).

Next, we investigated whether CGE was delayed in homozygous SEP-1^{PD}::GFP

embryos relative to SEP-1^{WT}::GFP. We imaged anaphase I with H2B::mCherry and

SEP-1::GFP to observe both chromosomes and cortical granules and quantified the

time from anaphase onset until CGE completion during anaphase I. CGE was

significantly delayed in homozygous SEP-1^{PD}::GFP expressing embryos (198 seconds ±

8, n=8) compared with SEP-1^{WT}::GFP expressing embryos (136 seconds ± 5, n=7,

p<0.0001, t-test) at 25 °C (Fig. 1.7 A-G and Movie 8). In addition, we observed that
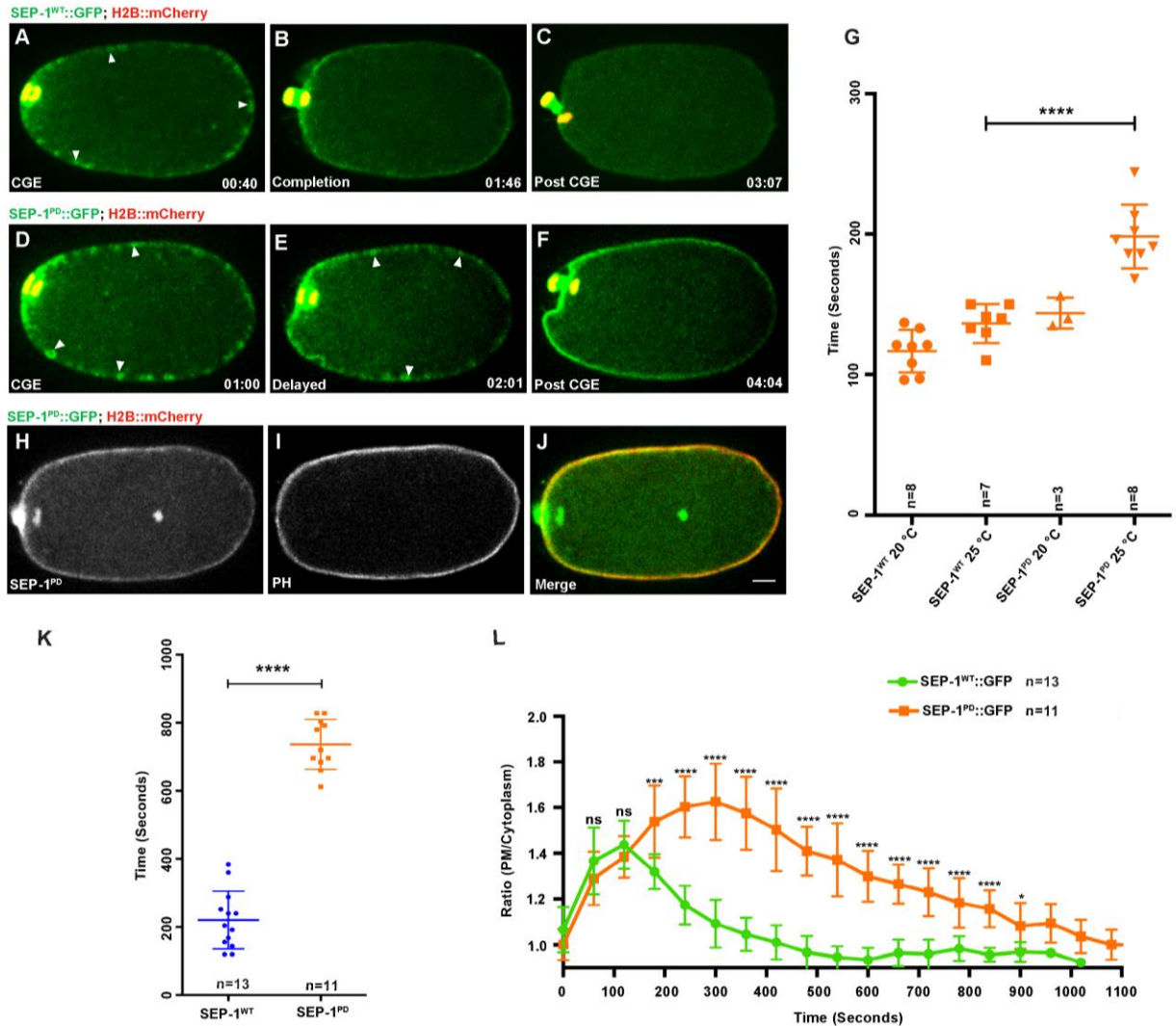
Figure 1. 7 SEP-1^{PD}::GFP expression delays cortical granule exocytosis.

(A-F) Representative images of separase localization during anaphase I. Localization of SEP-1^{WT}::GFP (A, green) and SEP-1^{PD}::GFP (D, green) to cortical granules indicated by white arrowheads (H2B::mCherry in red). CGE was delayed in homozygous SEP-1^{PD}::GFP (E) compared with SEP-1^{WT}::GFP (B) during late anaphase I. (F) SEP-1^{PD}::GFP associated with the cortex for a longer time after CGE compared with SEP-1^{WT}::GFP (C). (G) Quantification of anaphase onset to completion of CGE. SEP-1^{PD}::GFP embryos take longer to finish CGE than SEP-1^{WT}::GFP. (H-J) Colocalization of SEP-1^{PD}::GFP (green) with PH::Cherry (red) at the plasma membrane after CGE. (K) Average time that SEP-1^{WT}::GFP or SEP-1^{PD}::GFP remains associated with the plasma membrane after CGE. (L) Ratio of plasma membrane to cytoplasmic SEP-1^{PD}::GFP and SEP-1^{WT}::GFP after onset of anaphase I. Scale Bars, 10 μm. P-values: * =<0.05; ***=<0.001; ****=<0.0001; ns= not significant (t-test). Error bars indicated standard error of the mean.

SEP-1^{PD}::GFP remained associated with the plasma membrane for a longer time after

CGE (736 seconds ± 22, n=11) compared with SEP-1^{WT}::GFP (221 seconds ± 24, n=13,

p<0.0001, t-test) (Fig. 1.7 H-K & Movie 9). Quantification of the plasma membrane

localized signal shows that both SEP-1^{WT}::GFP and SEP-1^{PD}::GFP initially accumulate

on the membrane to similar amounts, but SEP-1^{PD}::GFP accumulates to a higher level

and remains associated with the membrane for substantially longer (Fig. 1.7 L). These

data are consistent with the hypothesis that SEP-1^{PD}::GFP may block cleavage of

putative substrate involved in exocytosis and that it may remain bound to a substrate

after exocytosis in the plasma membrane.

SEP-1^{PD}::GFP does not affect RAB-11 after cortical granule exocytosis

RAB-11 localizes to cortical granules and is required for CGE (Sato et al., 2008).

Therefore, we investigated whether SEP-1^{PD}::GFP affects the dynamics of RAB-11

during and after CGE. We filmed meiotic stage embryos expressing SEP-1::GFP/+ and

RAB-11::mCherry and observed that RAB-11::mCherry localizes to cortical granules

several minutes prior to anaphase (Sato et al., 2008), before either SEP-1^{WT}::GFP or

SEP-1^{PD}::GFP/+ localize to cortical granules (Fig. 1.8 A, D). Just after anaphase onset,

prior to exocytosis, both forms of separase fully co-localize with all RAB-11::mCherry

labeled cortical granules prior to exocytosis (Fig. 1.8 B, E, G-I). Therefore, RAB-11 and

separase are localized to the same population of CGs and are sequentially recruited to

cortical granules through an orderly process leading to exocytosis in anaphase I (Movie

9). After exocytosis, SEP-1^{PD}::GFP/+ associated with the plasma membrane for an

Figure 1. 8 SEP-1^{PD}::GFP does not affect RAB-11 after cortical granule exocytosis.

Representative images of meiosis I in embryos expressing separase (green) and RAB-11 (red). (A, D) RAB-11 localizes to cortical granules several minutes prior to anaphase, before either SEP-1^{WT}::GFP (B, green) or SEP-1^{PD}::GFP/+ (E, green) localize to cortical granules. SEP-1^{WT}::GFP (B, green) and SEP-1^{PD}::GFP (E, green) colocalize with RAB-11::mCherry (red) on the cortical granules in anaphase I. White arrowheads denote colocalization of separase and RAB-11 on cortical granules. (C, F) After exocytosis, SEP-1^{PD}::GFP/+ associated with the plasma membrane while SEP-1^{WT}::GFP and RAB-11::mCherry rapidly disappeared. (G-I) Surface plane of SEP-1^{WT}::GFP (G) and RAB-11::mCherry (H) clearly shows their colocalization (merge in I) on cortical granules. (J) Working model of separase function in exocytosis during cytokinesis. Separase cleaves cohesin kleisin subunit SCC-1 during mitotic anaphase and promotes chromosome segregation. In cytokinesis, separase colocalizes with RAB-11 vesicles. SNAREs including SYX-4 promote vesicle fusion with target membrane. Our results suggest that separase cleaves an unknown substrate to promote exocytosis. Scale Bars, 10 µm.

SEP-1^WT::GFP; RAB-11::mCherry

A — Metaphase
B — Anaphase
C — CGE Completion

SEP-1^PD::GFP/-; RAB-11::mCherry

D — Metaphase
E — Anaphase
F — CGE Completion

G — SEP-1^WT::GFP
H — RAB-11::mCherry
I — SEP-1^WT::GFP; RAB-11::mCherry

J

SCC-1 → Protease Activity / Cohesin Cleavage →

Target Membrane
Substrate X — RAB-11 — Separase — SNAREs
→ Protease Activity / Substrate X Cleavage →
Target Membrane
Cleaved Substrate X — RAB-11 — Separase — SNAREs

extended time while RAB-11::mCherry rapidly disappeared (Fig. 1.8 F and Movie 10). This result suggests that SEP-1^{PD}::GFP/+ does not require RAB-11 to remain associated with the plasma membrane, but might bind another unknown substrate. Therefore, RAB-11 and separase may function in parallel but independent pathways to promote exocytosis during anaphase.

Discussion

The mechanism by which separase regulates chromosome segregation is well known, while its function in exocytosis during CGE and cytokinesis needs to be elucidated. Here, we explore whether the proteolytic activity of separase is involved in its membrane trafficking roles. Utilizing our novel observation that protease dead separase is dominant negative, we provide data showing that it interferes with endogenous separase function during chromosome segregation and cytokinesis. Therefore, we hypothesize that separase uses its protease activity to cleave cohesin to allow chromosome segregation and to independently cleave multiple other substrates to promote several events during anaphase, including membrane trafficking during cytokinesis.

During chromosome segregation, the well-established function of separase is to cleave the cohesin subunit SCC-1 during mitosis. Consistent with the hypothesis that SEP-1^{PD}::GFP impairs substrate cleavage by the endogenous separase, we observe chromosome segregation defects in SEP-1^{PD}::GFP expressing embryos. Furthermore,

depletion of SCC-1 substantially recues mitotic chromosome segregation and embryo

lethality caused by SEP-1^{PD}::GFP. Previously, SCC-1 was not detected on

chromosomes after prophase, suggesting that separase may not cleave cohesin to

promote the metaphase to anaphase transition (Mito et al., 2003). However, our results

are consistent with the hypothesis that separase is required to cleave whatever

remaining cohesin is present on metaphase chromosomes for proper segregation to

occur at anaphase onset.

Whether separase has a substrate involved in exocytosis is unknown. However, we find

that the protease-dead separase causes cytokinesis failure and inhibits RAB-11 vesicle

exocytosis during mitotic cytokinesis. These data are consistent with a model whereby

separase cleaves a substrate to promote exocytosis (Fig. 1.8 J), similar to its function

during chromosome segregation. On its own, SEP-1^{PD}::GFP does not cause a severe

cytokinesis defect but synergistically inhibits cytokinesis when *syx-4* is depleted, while

chromosome segregation is more obviously defective. It is worth nothing that *C. elegans*

centromeres are holocentric (Albertson and Thomson, 1982), meaning that cohesin

must be cleaved along the entire chromosome instead of a point centromere as in other

organisms and thus chromosome segregation could be more sensitive to delayed

cohesin cleavage. We also did not observe significant defects in centriole

disengagement. Given that RAB-11 and endosomes have been observed at centrioles

in human cells (Hehnly et al., 2012), the enhanced centriole localization of SEP-

1^{PD}::GFP may be related to membrane trafficking functions as well as substrates

involved in disengagement. Therefore, separase likely cleaves substrates involved in

several different processes, but the effects imposed by SEP-1^{PD}::GFP vary in different events.

There are several possible explanations for these observations. The first is that our over-expression levels are not high enough to effectively block cleavage of a putative vesicle target, but is sufficient to inhibit chromosome segregation. This could be due to the affinity of separase toward different substrates. Alternatively, protease dead separase may bind to substrates and alter their function independently of cleavage, such as sequestering them from other interactions. Although the precise molecular effect of SEP-1^{PD}::GFP on substrates may be unclear, our results suggest that substrates are involved in various cellular functions of separase including exocytosis. While substrate cleavage may be involved in exocytosis, delayed cleavage may not be sufficient on its own to block exocytosis in the presence of all other factors that promote exocytosis. Consistent with this, depletion of separase does not completely block centriole separation and other factors minimize the resulting phenotypes (Cabral et al., 2013). Certainly the local environment at chromosomes, centrioles and vesicles is quite different. This could impact how stably separase can interact with substrates and thus how well SEP-1^{PD}::GFP can inhibit substrate cleavage. Indeed, separase catalytic activity toward cohesin is much greater in the presence of DNA (Sun et al., 2009), while the fluid environment of a membrane may not have the same effect. The finding that separase is dramatically stimulated by DNA suggests that both cohesin and separase associate with DNA, increasing the local concentration of both to promote catalysis. We did not observe any loss of separase localization to chromosomes after cohesin

depletion, suggesting separase localizes to chromosomes independently of the

substrate. In addition to substrate affinity, SEP-1^{PD}::GFP may displace endogenous

separase from chromosome more readily than it does in the membrane. Therefore,

there may also be differences in the relative amounts of transgenic SEP-1^{PD}::GFP to the

amount of endogenous separase at different cellular locations. The relative amounts of

endogenous vs. transgenic separase protein may also explain why we generally

observed less severe meiotic phenotypes vs. mitotic phenotypes. Future studies will be

required to resolve these issues.

While separase is a protease, critical non-proteolytic functions of separase are required

for mitotic exit. Previously, three *C. elegans* separase mutant alleles have been

identified, all of which map outside of the protease domain (Richie et al., 2011).

Interestingly, each of these mutants cause defects in cortical granule exocytosis and

mitotic cytokinesis failure, but minimal chromosome segregation defects (Richie et al.,

2011). Furthermore, these mutants are rescued by loss of phosphatase 5 (*pph-5*), which

might represent a signaling pathway that controls exocytosis (Richie et al., 2011). While

our results suggest that separase has a substrate involved in exocytosis, we cannot rule

out non-proteolytic functions that may also impact exocytosis. For example, Cdk5 is

involved in the regulation of synaptic vesicle exocytosis via phosphorylation of munc18

(Fletcher et al., 1999). Separase may regulate CDK or perhaps another signaling

pathway to control exocytosis. Ultimately, separase may have both proteolytic and non-

proteolytic functions that collaborate to promote exocytosis during anaphase. This might

be required to ensure that separase promotes exocytosis after a significant delay in

anaphase, which occurs during both meiosis and mitosis. Elucidating how the precise

control of separase function leads to exocytosis during anaphase will be an important

goal of future studies.

Our observations show that RAB-11 is recruited to cortical granules much earlier than

separase, which suggests an ordered recruitment of regulators to these vesicles prior to

their exocytosis in anaphase. Defining the pathway and signals that control the timing

sequence of this recruitment process will be important to better understand how the cell

cycle and potentially other pathways coordinate vesicle trafficking during cell division.

Whether the same process occurs during mitotic cytokinesis will require much better

imaging conditions since the individual vesicles are small and dynamic as they move

along the spindle. Interestingly, SEP-1^{PD}::GFP associates with plasma membrane for an

extended period of time after cortical granule exocytosis, however, RAB-11 does not.

This indicates that RAB-11 is not required for SEP-1^{PD}::GFP to remain associated with

the plasma membrane and may not be the substrate of the separase during exocytosis.

This result is consistent with previous observations that depletion of RAB-6, but not

RAB-11, prevents recruitment of separase to cortical granules (Kimura and Kimura,

2012). It is still possible that separase may cleave RAB-11 interacting proteins. This

could indicate that separase affects a different step in exocytosis than the membrane

docking and tethering functions mediated by RAB-11. For example, separase might

cleave a substrate that allows vesicles to move forward in the exocytosis pathway, i.e.,

moving from a docked to a primed state (Wickner and Schekman, 2008). The timing

when cortical granules undergo different steps of exocytosis in *C. elegans* is unknown,

but it is possible that the early steps are completed by the time that separase is completely transferred to vesicles in anaphase. Indeed, cortical granules in sea urchin have been shown to be in a "hemifusion" state and fertilization happens post anaphase in this organism (Wong et al., 2007). Separase may cleave RAB-11 interacting proteins, such as RAB-11 GEFs, to regulate RAB-11 activity during exocytosis (Sakaguchi et al., 2015). Another possibility is that separase cleaves an inhibitor of exocytosis, such as the complexin protein that prevents SNAREs from completing vesicle fusion prematurely (Tang et al., 2006). Identifying a putative vesicle target that separase cleaves to promote exocytosis is a primary pursuit for future investigation. This may provide novel mechanistic insights into how a protease can promote exocytosis, which may also be applicable to membrane trafficking events independent of the cell cycle.

Materials and Methods

C. elegans Strains

C. elegans strains were maintained with standard protocols, except for the modified procedures to maintain toxic transgenes (below). Strain information is listed in Table 1. Some strains used in this study were obtained from the Caenorhabditis Genetics Center (CGC). Strain RQ372 was gift from Dr. Risa Kitagawa. JAB18 was created by crossing WH520 males with OD56 hermaphrodites (Mitchell et al., 2014). JAB156 was generated by crossing WH520 males with EKM41 hermaphrodites, and subsequent generations were maintained on *gfp* RNAi. At F2 generation following the cross, L4 stage worms were singled from the original *gfp* RNAi feeding plates. We screened the F3 adults for

the presence of PH::mCherry transgenes by microscopy. Then approximately half of the PH::mCherry positive worms at L4 stage were moved to OP50 plates for 3-4 generations, and screened for the presence of both transgenes. The protocol was repeated until double homozygous transgenic lines were obtained, after which the line was maintained on *gfp* RNAi.

Propagation of the Protease Dead Separase Strains

We demonstrated that SEP-1[PD]::GFP expression is dominant negative (Mitchell et al., 2014). Using this mutant, we have devised two methods to propagate protease dead separase transgenic animals. One method is using SEP-1[PD]::GFP male worms to propagate the transgene by crossing with the *unc-119* mutant hermaphrodites. The *unc-119* mutant contains a paralysis selection marker due to a neural defect. Crossing the SEP-1[PD]::GFP transgene with an *unc-119* mutant rescues the movement defect of the F1 animals as the SEP-1[PD]::GFP construct contains wild type *unc-119*. The SEP-1[PD]::GFP transgene is driven by the *pie-1* promoter, which is only expressed in the female germline. Therefore, the SEP-1[PD]::GFP transgene can be propagated in male worms without deleterious effects and the hermaphrodite siblings can be assayed for phenotypes. This method reduces background mutations that might complicate phenotypic analysis and allows us to introduce the transgene into backgrounds that we cannot make homozygous. The second method is feeding *gfp* RNAi to eliminate SEP-1[PD]::GFP transgene expression. After animals are transferred from *gfp* RNAi food onto regular bacteria food for 5-6 generations, the inherited RNAi will be lost and transgene expression will occur again.

RNAi Treatment

The *gfp* and *syx-4* RNAi feeding constructs were previously described (Bembenek et al., 2010, Mitchell et al., 2014) and *scc-1* RNAi was obtained from the Ahringer library (Fraser et al., 2000). To silence the target genes, L4 hermaphrodites were picked onto lawns of IPTG-induced RNAi feeding bacteria. In order to provide the optimal RNAi effect for target genes silencing, RNAi cultures were grown till log phase. Then the log phase RNAi bacteria were spread on plates containing NGM agar with 1 mM IPTG and the plates were incubated at 15 °C for 24-48 hours to optimally induce the T7 promoter expression (Grishok et al., 2005). Worms were grown on RNAi plates at 20°C /25 °C for the amount of time indicated in the manuscript for different experiments.

Microscopy

For live imaging, young adult worms were dissected in M9 buffer and embryos were mounted on agar pads as previously described (Mitchell et al., 2014). For imaging of meiotic embryos, or potentially osmotic sensitive embryos, young adults were dissected and mounted in blastomere culture media by hanging drop to relieve mechanical and osmatic pressure (Edgar and Goldstein, 2012). Live cell imaging was performed on a spinning disk confocal system that uses a Nikon Eclipse inverted microscope with a 60 X 1.40NA objective, a CSU-22 spinning disc system and a Photometrics EM-CCD camera from Visitech International. Images were acquired by Metamorph (Molecular Devices) and analyzed by ImageJ/FIJI Bio-Formats plugins (National Institutes of Health) (Schindelin et al., 2012, Linkert et al., 2010).

53

Statistics

Quantification of SEP-1::GFP and RAB-11::mCherry at the midbody was performed in Image J by measuring the fluorescent intensity at the midbody in frames with the brightest signal shortly after furrow ingression was completed. Embryos were shifted to 25 °C to improve signal, but caused abnormal aggregates of RAB-11::mCherry in some embryos, which were not included in the analysis. To account for variations in imaging and z-depth, we calculated the ratio of the intensity at the midbody relative to cytoplasm. Cytoplasm signal was determined by averaging the intensities from three separate regions in the same image. Statistical significance was determined by p value from an unpaired two-tailed t-test. P-values: ns= not significant; * =<0.05; **=<0.01, *** =<0.001; ****=<0.0001. Each dataset was evaluated by both of the Shapiro-Wilk and Kolmogorov-Smirnov normality tests and all data follow normal distributions.

CHAPTER 2

Programmed Variations of Cytokinesis Contribute to Morphogenesis

in the *Caenorhabditis elegans* Embryo

This chapter will be submitted for publication:

Bai X., ….. 2018. The programmed Variations of Cytokinesis Contribute to Morphogenesis in the *C. elegans* Embryo.

Bai X. will be considered the first author. My contribution included: (1) designing experiments, (2) performing experiments, (3) collecting data and data analysis, (4) creating figures and writing the manuscript. Dr. Joshua N. Bembenek is assisting with (1), (4). Ryan Simmons, Dr. Bi-Chang Chen, Po-Yi Lee and Ben Nebenführ assisted with (2) and (3). Only small revisions to the original figures have been made for the purposes of this dissertation.

Abstract

Cytokinesis is the final step of cell division involving several regulated steps including cleavage furrow specification and ingression, midbody formation and abscission. While the basic mechanisms have been intensely studied, how various aspects of cytokinesis are regulated and deployed in different cell division contexts during development is not well understood. To address this, we investigated cytokinesis in the invariant lineage of the C. elegans embryo. We observed several markers that label the furrow, central spindle and different structures within the midbody. We show that several parameters of cytokinesis are reproducibly altered in different stages of the lineage. During the first two divisions, cells undergo consistent patterns of furrow ingression asymmetry and midbody inheritance, suggesting specific regulation of these events. A dramatic shift in

cytokinesis is observed in several tissues during morphogenesis. In two lumen-forming

tissues, the intestine and the pharynx, midbodies form after symmetric furrowing and

migrate across the cell to the nascent apical midline. This midbody migration event

coincides with previously characterized polarization events in these cells undergoing a

mesenchyme to epithelial transition. Interestingly, midbody ring components are

internalized, indicative of abscission completion, while other midbody components

including the Aurora B kinase remain on the apical surface for an extended period after

polarization. Finally, in cells that form amphid sensilla, we observe symmetrical

cytokinesis and a midbody migration event that leads to a focal aggregation of AIR-2

that coincides with apical surface markers. AIR-2 persists along the leading edge of

extending dendrite structures well after cytokinesis is complete. Inactivating temperature

sensitive cytokinesis mutants during morphogenesis causes defects in lumen formation

and defective dendrite formation. These data suggest that the proper execution of

cytokinesis, which shows surprising flexibility during development, and specific

cytokinetic regulators such as AIR-2, may regulate the final interphase architecture of a

terminally dividing cell during morphogenesis.

Introduction

Generation of a multicellular organism requires that carefully orchestrated cell division is

integrated properly into different developmental processes. Cell division is required not

only to generate new cells that organize into tissues, but also to dictate the size,

position and timing that daughter cells are generated. Several aspects of cell division,

including spindle orientation and division symmetry are well known instruments of developmental programs (Siller and Doe, 2009). Proper regulation of cytokinesis, the final stage of division when daughter cells separate from each other, has long been recognized as critical for the completion of cell division. Roles for cytokinesis in regulating developmental events are emerging, but are much less understood (Chen et al., 2013; Herszterg et al., 2013; Li, 2007). We sought to investigate cytokinesis using the well-defined divisions of the invariant *C. elegans* embryo lineage, which has been completely described (Sulston et al., 1983).

Cytokinesis is the final step of cell division and is normally a constitutive process defined by discrete steps that occur when cells exit mitosis (Oegema and Hyman, 2006). During cell division, signals from anaphase spindle initiate ingression of the cleavage furrow (Bringmann and Hyman, 2005), which constricts the plasma membrane into the spindle midzone and leads to formation of the midbody. The midbody is membrane channel connecting daughter cells containing the spindle midzone microtubules and a defined organization of more than one hundred proteins that collaborate to execute abscission, the final separation of daughter cells (Green et al., 2012; Hu et al., 2012; Skop et al., 2004). Many of the proteins that contribute to midbody formation and function have roles in the formation of the central spindle and the contractile ring (El Amine et al., 2013). In addition, vesicles are delivered to the midbody that contribute lipids as well as regulators of abscission (Schiel et al., 2013). Subsequently, the ESCRT machinery assembles, microtubules are cleared and membrane scission occurs (Guizetti et al., 2011; Schiel et al., 2011). Aurora B kinase is

required for the completion of cytokinesis, and also regulates the timing of abscission in response to chromatin bridges or developmental cues partly by regulating the ESCRT machinery (Carlton et al., 2012; Carmena et al., 2015; Mathieu et al., 2013; Norden et al., 2006; Steigemann et al., 2009). Substantial effort has been devoted to understanding factors that are required to assemble the midbody and the mechanisms of regulation and execution of abscission. In general, while mechanistic details are being elucidated, it is thought that these events occur through a standard, well-defined series of ordered events.

Exceptions to such a clear linear view of cytokinetic events have long been known, but are considered to be specialized cases. The most extreme examples are cells that do not complete cytokinesis altogether and become polyploid, such as liver or intestinal cells (Fox and Duronio, 2013; Hedgecock and White, 1985; Lacroix and Maddox, 2012). Another well-known example is found in several systems where germ cells do not complete abscission and remain connected through ring canals, which can allow flow of cytoplasm into germ cells (Greenbaum et al., 2007; Haglund et al., 2011; Hime et al., 1996; Maddox et al., 2005). Delayed abscission has also been observed in other cell types to keep daughter cells connected (McLean and Cooley, 2013; Zenker et al., 2017). Other variations of cytokinesis include re-positioning of the cleavage furrow during anaphase to change the size and fate of daughter cells (Ou et al., 2010). The symmetry of furrow ingression is important in established epithelial tissue where the furrow constricts toward the apical side of the cell and must occur while appropriate cellular contacts are preserved (Herszterg et al., 2014). In Zebrafish neuroepithelial

divisions, asymmetrical furrowing positions the midbody at the apical domain, which is inherited by the differentiating daughter (Paolini et al., 2015). Therefore, there are a number of ways the standard pattern of cytokinesis can be altered and more investigation is required to understand what is the functional purpose of these changes and how they are achieved.

Studies of abscission has driven renewed interest in the midbody that has led to insights into other functions it has in addition to abscission (Chen et al., 2013). In general, the midbody is cut off from each of the daughter cells that gave rise to it (Crowell et al., 2014; Konig et al., 2017). The midbody may then be engulfed by either cell or persist extracellularly, which can depend on cell type (Ettinger et al., 2011; Kuo et al., 2011; Salzmann et al., 2014). The midbody can also travel to non-parent cells, suggesting that it may carry or transport signals between cells (Crowell et al., 2014). Cancer cells or stem cells show distinct and consistent patterns of midbody inheritance (Kuo et al., 2011). In dividing neuroepithelial cells, a stem cell marker is concentrated at the midbody and released into the lumen of the neural tube, which might provide signals during neuronal development (Dubreuil et al., 2007). This has led to the hypothesis that the midbody provides cues that regulate cell fate, although a detailed mechanistic understanding of this has not been elucidated.

A more clearly defined function for the midbody has been uncovered in cells that undergo polarization events after the completion of cytokinesis. For example, marine

darby canine kidney (MDCK) cells can establish apical basal polarity and organize into

a simple epithelial lumen structure (Reinsch and Karsenti, 1994). Apical membrane

markers are first delivered to the midbody during cytokinesis, establishing an apical

membrane at the interface of the first two daughter cells (Schluter et al., 2009). Proper

abscission and midbody positioning is required, in addition to proper spindle orientation,

for MDCK lumen formation (Lujan et al., 2016; Reinsch and Karsenti, 1994). Polarized

trafficking during cytokinesis has been shown to promote lumen formation in other

systems as well. Abscission is also delayed in acentrosomal blastomeres of the mouse

embryo to generate a MTOC that directs delivery of apical membrane markers to the

plasma membrane (Zenker et al., 2017). The midbody has also been shown to define

the site of polarization for dendrite extension in neurons (Pollarolo et al., 2011) and is

required for a polarizing cue in the C. elegans embryo necessary for the establishment

of dorsoventral axis formation (Singh and Pohl, 2014; Waddle et al., 1994). In addition,

the midbody can play a role in cilium formation (Bernabe-Rubio et al., 2016). Further

effort is required to understand how cytokinesis and the midbody regulates pattern

formation in tissues.

In order to further investigate patterns of cytokinesis during development, we examined

the invariant *C. elegans* lineage. We find that cytokinesis follows a lineage specific

pattern and that furrow symmetry and midbody inheritance is highly reproducible.

During morphogenesis, we observe striking midbody migration events in the developing

digestive and sensory tissues in *C. elegans*, likely before abscission. Interestingly, AIR-

2 migrates with midbodies and remains at several apical surfaces after internalization of

different ring components. Coordinated movements of midbodies and differential fates of midbody components are novel behaviors during cytokinesis and are programmed at specific divisions in the embryo. Additionally, inactivation of temperature sensitive midbody proteins disrupt proper formation of several tissues, indicating an important role for specialized cytokinesis during morphogenesis.

Results

Cytokinesis in the first two mitotic divisions

In order to systematically examine cytokinesis during the stereotypical divisions of the C. elegans embryo, we observed different components that allow us to visualize the central spindle and cytokinetic furrow among other mitotic structures. We also chose markers that localize to the flank and ring sub-structures of the midbody (Green et al., 2012). To observe the midbody flank region, we imaged the Aurora B kinase AIR-2, microtubules and the membrane trafficking regulator RAB-11 (Fig. 2.1 B-F, Q-U, Fig.2.3 D-E and Movie S11). Endogenous AIR-2 can also be observed on the central spindle and midbody as expected (Fig. A5 A-E). We also imaged midbody ring markers including the non-muscle myosin NMY-2, and the centralspindlin component ZEN-4 (Fig. 2.1 G-P and Movie S11). While the first mitotic furrow shows some variable asymmetry as previously demonstrated (Maddox et al., 2007), the midbody forms in a relatively central position between daughter cells (Fig. 2.1 B-C, G-H and L-M). AIR-2::GFP and tubulin show the expected pattern of localization on the central spindle throughout furrowing (Fig. 2.1 B-C, Fig. 2.3 D-E and Movie S11). We confirm previous
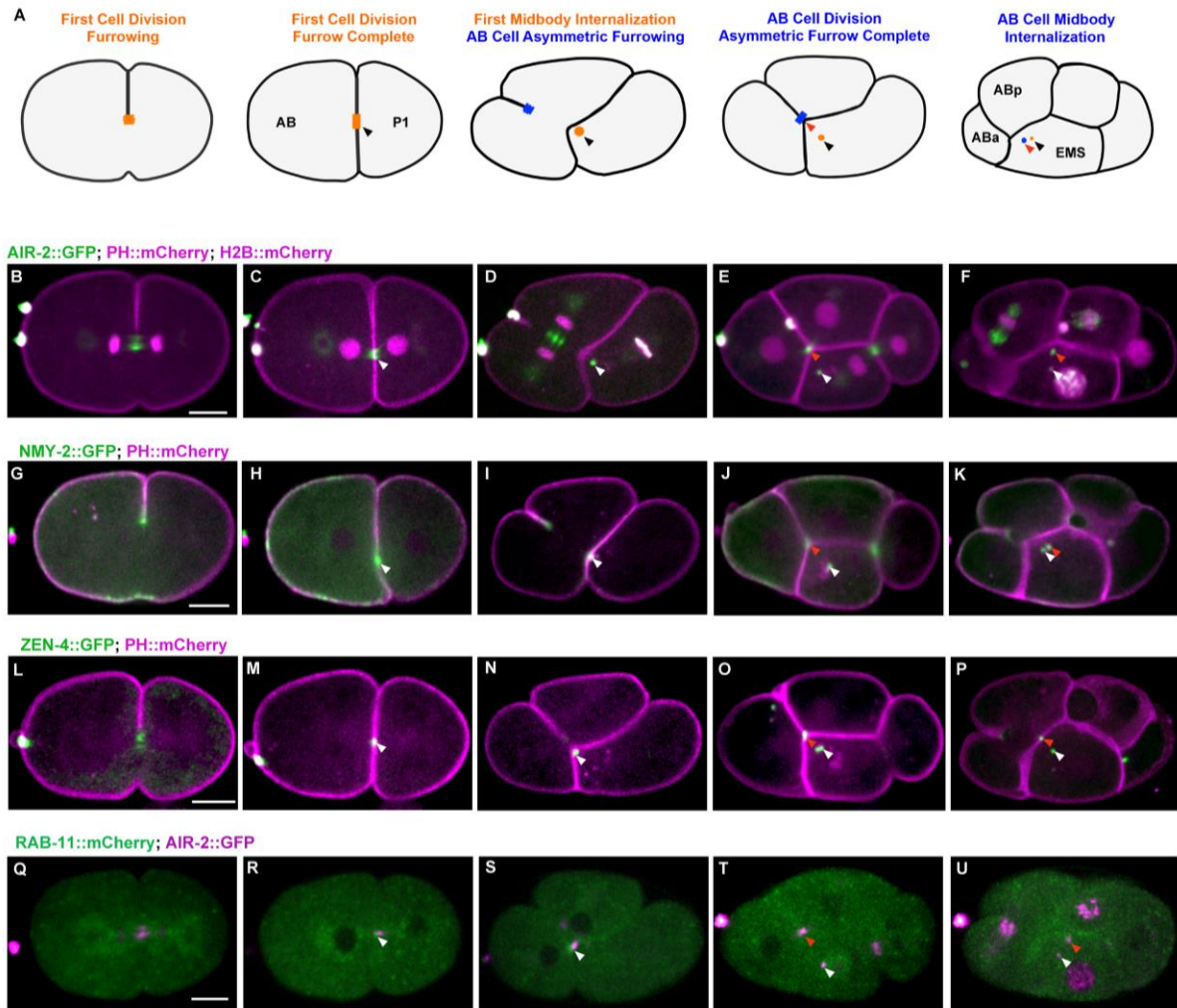
Figure 2. 1 Cytokinesis in the first two mitotic divisions.

(A) Illustration of the cytokinesis in the first two mitotic divisions and the behavior of midbody during the division. Cytokinesis in the one cell embryo labeled with (B-C) AIR-2::GFP (green) and PH::mCherry (magenta), H2B::mCherry (magenta). Aurora B shows the expected pattern on the central spindle during anaphase and furrowing, and remains on the midbody (white arrow head) until it is internalized by AB daughter cell during the second cell division (D). The furrow is highly asymmetric and initiates from the outside of the embryo and finishes in contact with EMS (D-E). The second midbody (red arrowhead) forms in a highly asymmetric position adjacent to EMS (E), and EMS engulfs the midbody instead of either of the AB daughter cells (F). Midbody ring markers NMY-2::GFP (green) myosin (G-K), ZEN-4::GFP (green) centralspindlin (L-P), membrane trafficking marker RAB-11 (green) small GTPase (Q-U) and PH::mCherry (magenta) as well as AIR-2::GFP (magenta in Q-U) all remain on the midbody until it is internalized into EMS like AIR-2. Scare Bar, 10 μm.

63

observations that the midbody from the first mitotic division is always inherited by the P1

daughter cell (Fig. 2.1 A) (Bembenek et al., 2013; Singh and Pohl, 2014). The midbody

microtubule signal diminishes 450s after furrowing onset, which is a general indicator of

abscission timing (Fig. 2.3 E, L) (Green et al., 2013; Konig et al., 2017). AIR-2 is lost

from the flank over time but can be observed on the midbody remnant even after it is

internalized into P1 (Fig. 2.1 D-E and Movie S11). Additionally, each of the ring

components behave similarly to AIR-2, as expected (Fig. 2.1 I-J and N-O). Therefore,

AIR-2 and other ring components remain colocalized on the midbody throughout the

final stages of cytokinesis and are reproducibly inherited by the P1 daughter cell,

consistent with previous results (Bembenek et al., 2013; Ou et al., 2014; Singh and

Pohl, 2014).

During the second round of division, we observed substantial changes in the pattern of

cytokinesis, beginning with furrow symmetry. During the AB daughter cell division, the

furrow ingresses from only the outer surface until it reaches the opposite plasma

membrane in contact with EMS. We calculated a symmetry parameter using the ratio of

furrow ingression distance from each side of the furrow at completion (Maddox et al.,

2007). On average, the furrow symmetry parameter is 1.7 in the first division, while the

AB furrow is 21.6 and the P1 furrow is 16.1, indicating a highly asymmetric furrow in the

second division (Fig. 2.3 A-C). The central spindle is swept from the middle of the AB

cell into contact with EMS during furrow ingression (Fig. 2.1 E, Movie S11). AIR-2

localizes to the central spindle, then the midbody flank and remains associated with the

midbody remnant after it is engulfed (Fig. 2.1 D-E, S-T and Movie S11). NMY-2 and

ZEN-4 also follow the expected pattern during cytokinesis and appear on the midbody that forms in contact with EMS (Fig. 2.1 I-J, N-O and Movie S11). Interestingly, the midbody from the AB cell division is invariably engulfed by EMS instead of either of the AB daughter cells (Fig. 2.1 F, K, P, U and Movie S11). The pattern of cytokinesis in the P1 daughter cell does not show any substantial change from the first division and the midbody is always inherited by EMS. Microtubules in the midbody flank disappear 480s after furrowing in both AB and P1 cell divisions, indicative of relatively fast abscission (Fig. 2.3 F-G and L). Therefore, a consistent pattern of cytokinesis is observed during the first two divisions, involving reproducible furrow ingression symmetry and midbody inheritance. Multiple mechanisms operating during cytokinesis must be properly regulated in order to achieve this highly reproducible pattern. While this analysis may reveal interesting information about the regulation of cytokinesis during the entire lineage, we focused next on novel cytokinesis patterns in three tissues during morphogenesis.

Cytokinesis in the intestine epithelia

During morphogenesis, cells undergo terminal divisions and start to form tissues by polarizing and changing shape. The intestine is a well-studied epithelial tube derived from the E blastomere that undergoes five well defined divisions (Leung et al., 1999). Around 280 minutes after the first cleavage the E8 to E16 division occurs, after which cells undergo epithelial polarization and subsequently organize into a tube (Leung et al., 1999). Our observations demonstrate that these cells are performing the final stages of

Figure 2. 2 Cytokinesis in the intestine epithelia

(A) Illustration of the cytokinesis in the intestinal E8-E16 mitotic divisions and the fate of midbody post mitotic division. Cytokinesis at the E8-E16 division. (B-D) Aurora B AIR-2::GFP (green) migrates with midbodies (labelled as 1-8) to midline and persists well after polarization is complete (rectangle box). (E) Kymograph of the single E8 cell division showing the midbody formation and migration to apical midline (time in minute: second indicated on left bottom). The E8 cell labeled with AIR-2::GFP (green) and PH::mCherry (magenta). Time in minutes indicated below. (F-H) NMY-2 (green) centralspindlin is midbody ring component that move to the midline but do not persist like AIR-2 (rectangle box). (I) Kymograph showing the single midbody migrating to midline. (J-K) High temporal resolution (10 seconds time interval) imaging of individual intestine cell indicated that midbody formed in the center of the cell, AIR-2::GFP (J) flank marker change the shape and migrate to midline of the apical and persist, as well as the ZEN-4 (K) rapid internalization to cytosol (time in minute: second indicated on right top). (L) Quantification of midline duration of different midbody components. (M-N) Illustration and Quantification of midbody flank length during different cell divisions. Scare Bar, 10 µm. Error bars indicated standard deviation of the mean.
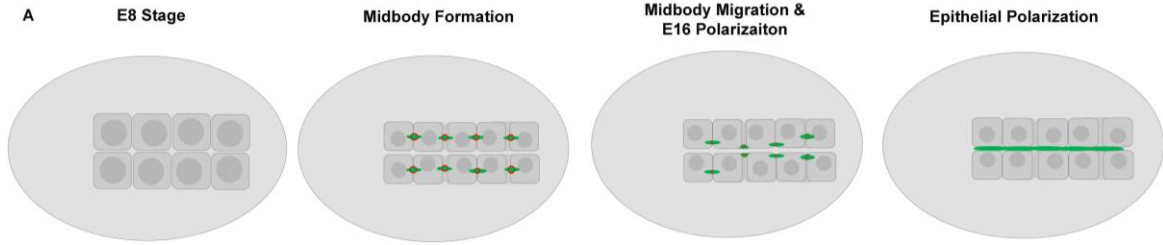
A E8 Stage | Midbody Formation | Midbody Migration & E16 Polarizaiton | Epithelial Polarization

AIR-2::GFP; H2B::mCherry; PH::mCherry

B 00:00

C 12:00

D 54:00

E

Time (Minutes) 0   10   20   28

NMY-2::GFP; TBB-1::mCherry

F 00:00

G 30:00

H 63:00

I

Time (Minutes) 0   10   20   28

J AIR-2::GFP; H2B::mCherry; PH::mCherry

00:00   10:00   15:40

K ZEN-4::GFP; PH::mCherry

00:00   33:40   47:30

L Midline Perdurance (Seconds)

ZEN-4   NMY-2   AIR-2

M Cell Length

Midbody Flank Length

$$\frac{\text{Cell Length}}{\text{Midbody Flank Length}} = \text{Midbody Flank Parameter}$$

N Midbody Flank Length Parameter

First Cell Division   Second Cell Division   Intestinal Cell Division

67
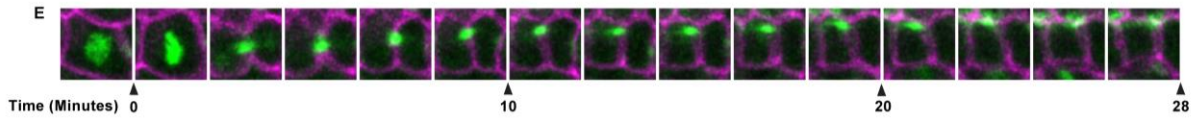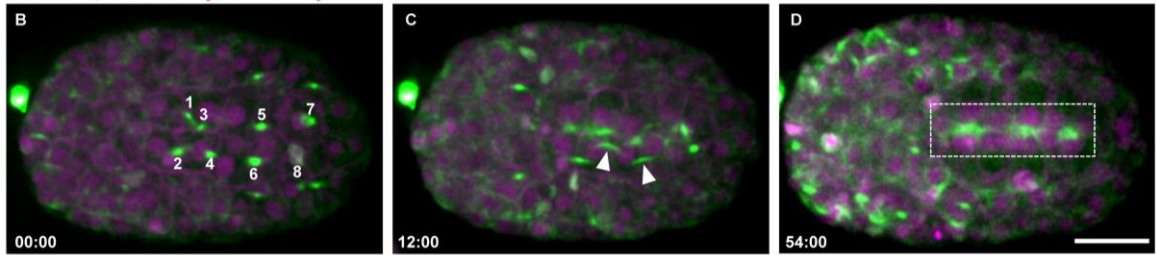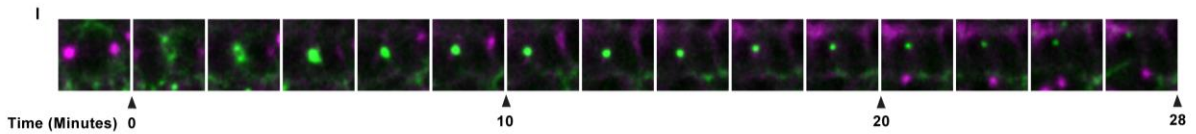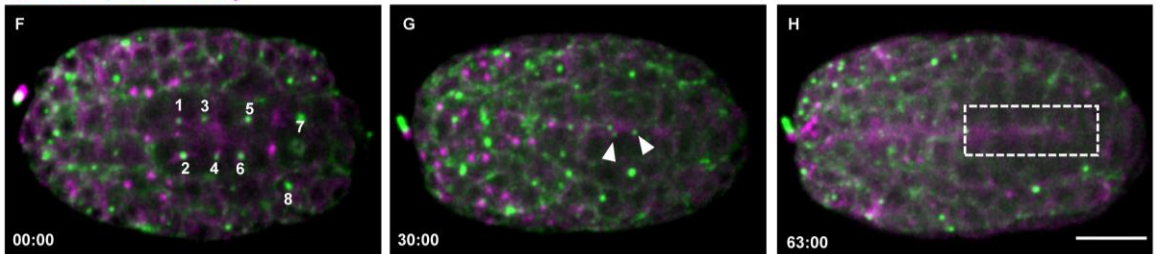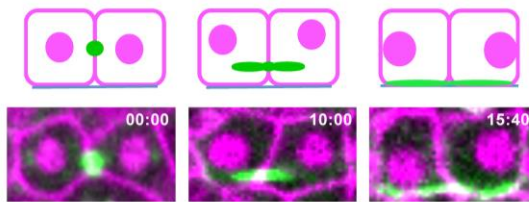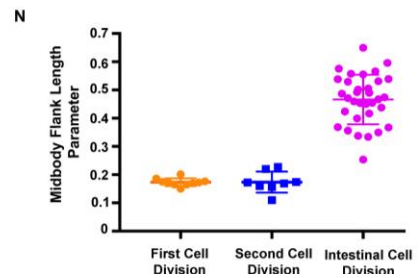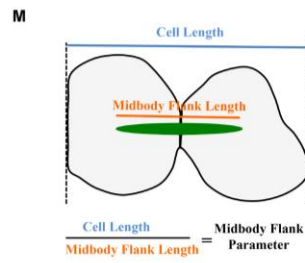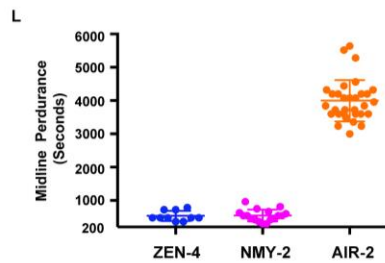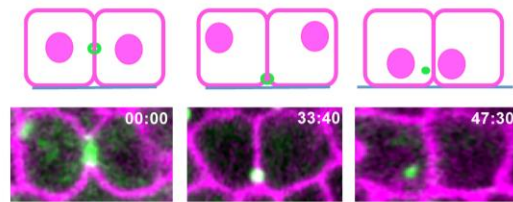
cytokinesis as they undergo polarization, which has not been previously reported (Fig. 2.2 A). Interestingly, the E8 cells undergo relatively symmetrical furrowing that produces a centrally placed midbody (Fig. 2.2, Fig. A 6 and Movie S12-13) with a 1.0 symmetry parameter (Fig 2.3 B, C). Therefore, unlike the AB division during the second mitosis, these cells have symmetrical furrowing.

Strikingly, in the central gut cells (Ealp, Earp, Epla and Epra), we observe that the centrally located midbody from both left and right daughter cell pairs migrate across the width of the cell after furrowing has completed to the apical midline of the gut tissue, which completes in about 30 minutes after furrow ingression (Fig. 2.2 C, E, G, I, J, K, Fig. A6 B, D and Movie S12-13). The ring markers ZEN-4 and NMY-2 are quickly internalized (553±140 seconds and 545±179 seconds, respectively) after the midbody reaches the apical midline (Fig. 2.2 L and Movie S12-13). The flank maker AIR-2::GFP appears on the central spindle, remains on the midbody flank region and migrates on the flank of the midbody to the intestinal apical midline similar to the midbody ring components. Interestingly, AIR-2 and tubulin localize to an elongated midbody flank region through the entire migration process (Fig. 2.3 I, K-L). The ratio of the length of this midbody flank relative to the cell is 0.47 (average 4.6 μm / 9.8 μm) in the intestinal cell division, which is more than twice that of the early two cell divisions 0.17 (average 9.3 μm / 53.4 μm) in P0 and 0.17 (average 7.7 μm/ 44.3 μm) in AB) (Fig. 2.2 M-N). Given that the flank region disappears after abscission has occurred in the one cell embryo, the persistence of an extended flank region observed with AIR-2 and tubulin in the gut cells suggests that the midbody migration event may occur prior to abscission.

Figure 2. 3 Variations of Cytokinesis during Different Mitotic Divisions

(A-C) Quantification of furrow symmetry during first two cell divisions and intestinal cell division. The asymmetry parameter was measured as illustrated in 2-D images (A-B). (C) Quantification of furrow asymmetry parameter during different cell division. (D-L) tubulin dissembling in different mitotic divisions. (D) Tubulin TBB-1::mCherry (magenta) and AIR-2::GFP (green) show the localization on the central spindle during anaphase and furrowing in first cell division. (E) Kymograph showed the tubulin dissembling during cytokinesis in the first mitotic division. Time in seconds indicated below. (F) Tubulin TBB-1::mCherry (green) show the localization on the central spindle near the EMS cell cortex during highly asymmetric furrowing. (G) Kymograph showed the tubulin dissembling during cytokinesis in the AB cell division (insert is TBB-1::mCherry only). Time in seconds indicated below. (H-J) Tubulin TBB-1::mCherry (magenta) and AIR-2::GFP (GFP) localize to an extended flank region around the midbody through the entire intestinal midbody migration process (arrowhead). (J) Tubulin and AIR-2 persist at the intestine midline after the E16 polarization (rectangle box). (G) Kymograph showed the tubulin dissembling during E8 cell Epra cell division and midbody migration to midline. The arrowhead indicated the extended flank region of tubulin. Time in seconds indicated below. (L) Quantification of tubulin dissemble time during different cell divisions. Scale Bar, 10 μm. Error bars indicated standard deviation of the mean.

A First Cell Division / Second Cell Division

Long / Short = Asymmetry Parameter

B Intestinal Cell Division

Long / Short = Asymmetry Parameter

C Furrow Asymmetry Parameter

First Cell Division / Second Cell Division / Intestinal Cell Division

D AIR-2::GFP; TBB-1::mCherry

E MERGE / AIR-2 / TBB-1

Furrow Initiation   90   180   270   360   Tubulin Diminished

Time (Seconds Post Furrwo Initiation)

F AIR-2::GFP; TBB-1::mCherry

G MERGE

Furrow Initiation   120   240   360   Tubulin Diminished

Time (Seconds Post Furrwo Initiation)

H I J AIR-2::GFP; TBB-1::mCherry

00:00   12:00   58:00

K TBB-1

Furrow Initiation   180   360   540   720   1080

Time (Seconds Post Furrwo Initiation)

L Tubulin Disassble Time (Seconds)

First Cell Division / Second Cell Division / Intestinal Cell Division

70

In contrast to the midbody ring components, AIR-2 persists at the midline well after the time that ring components are internalized and polarization is complete (Fig. 2.2 D, E, L and Movie S12-13) colocalizing with the apical polarity marker PAR-6 (Fig A6 E-G). Endogenous AIR-2 can also be observed at the apical midline as expected (Fig. A5 F-H). High temporal resolution confocal imaging and lattice light sheet imaging of individual midbodies confirm the elongated AIR-2::GFP flank localization and persistence at the apical midline as well as the rapid internalization of ZEN-4::GFP after the migration event (Fig. 2.2 J-K and Movie S13-14). Therefore, E8 cells undergo an additional step during cytokinesis consisting of a midbody migration event instead of having an asymmetrical furrow lead to the formation of an apically localized midbody as observed in the AB cell division. In addition, different midbody components have different fates after this migration event, with ring markers being internalized while AIR-2 remains at the apical surface.

In other lumen forming systems, such as MDCK cells, RAB-11 vesicle trafficking during cytokinesis transports apical membrane components to the midbody to establish the apical membrane (Schluter et al., 2009). In *C. elegans*, RAB-11 endosomes control trafficking at the apical surface of the intestine throughout the life of the animal (Sato et al., 2014). We imaged RAB-11 during the E8-E16 division to examine when apical localization occurs. Interestingly, RAB-11::mCherry colocalizes with AIR-2::GFP once the midbody is formed, and migrates to the apical surface with the midbody (Fig. A6 H-J). RAB-11::mCherry is also localized at spindle poles, as in other mitotic cells (Albertson et al., 2005), which also migrate to the apical surface (Feldman and Priess,

2012). Similar to AIR-2, RAB-11 remains localized to the apical surface and appears to remain at this position throughout the life of the animal (Fig. A6 J). These observations indicate that the apical localization of RAB-11 is established during cytokinesis in the E8-E16 division and is delivered at least in part by both the midbody and centrosome. Therefore, cytokinesis is programmed to occur in specialized way during the E8-E16 division, which may contribute to intestinal epithelial polarization.

Interestingly, the anterior and posterior pair of E16 cells (Ealaa, Earaa, Eplpp and Eprpp) undergo one last division to achieve the E20 intestine stage. In the four central E8 cells that do not divide again, the midbody migrates to the midline at E8-E16 as described above. However, the midbodies from the other four E8 cells (Eala, Eara, Eplp and Eprp), which undergo another division, did not migrate all the way to the midline and the AIR-2 signal disappeared quickly during E16 polarization (image not shown). Interestingly, during the terminal E16-E20 division, the midbodies of Ealaa, Earaa, Eplpp and Eprpp undergo the apical migration after symmetrical furrowing (Fig. A6 K-M and Movie S15). Further, the midbody ring components are quickly internalized while AIR-2 and RAB-11 remain at the apical surface during the E16-E20 divisions. Therefore, the midbody migration event in the intestine does not happen only during the polarization event that occurs during E8-E16, suggesting that it is specifically programmed to occur during the terminal divisions. It is interesting to note that post-embryonic divisions in the intestinal cells occur without completion of cytokinesis leading to the formation of polyploid cells in the adult animal (Hedgecock and White,

1985). Therefore, cytokinesis in the intestinal lineage undergoes distinct regulatory phases at different stages of development.

Cytokinesis in the pharynx

Unlike the intestine, which originates from a single blastomere that undergoes a very well defined series of divisions, the pharynx has a more complicated structure, containing more than 80 pharyngeal precursor cells (PPCs) that arise from both AB and MS founder cells (Sulston et al., 1983). The PPCs organize into a double plate structure prior to the final division which occurs at around 310-325 minutes after the first cleavage and then polarize, undergo apical constriction to become wedge shaped cells that form a lumen by 355 minutes (Rasmussen et al., 2013; Rasmussen et al., 2012). To obtain optimal images of this large complex structure, we filmed at least a 15-micron Z-depth section of the embryo from both dorsal and ventral aspects with confocal microscopy (Movie S 16-17). We also filmed the whole embryos with lattice light sheet microscopy, which provides higher spatial resolution during the pharyngeal cell division (Movie S18). Similar to our observations in the intestine, PPCs are in the final stages of cell division as they polarize, which has not been previously described. PPCs undergo a symmetric furrowing event that yields a centrally placed midbody (Fig. 2.4 A-C, F, G-H, K, L-M, P and Movie S16-17). Also similar to the intestine, PPC midbodies migrate from their central position between daughter cells to the apical midline of the forming pharyngeal bulb (Fig. 2.4 D, F, I, K, N, P and Movie S16-17). In PPC terminal divisions, AIR-2::GFP appears as a midbody flank structure that migrates to the apical midline and persists at the apical surface after cyst formation (Fig. 2.4 D, E and Movie S16-17). AIR-2 partially

73

Figure 2. 4 Cytokinesis in the pharynx

(A) Illustration of the cytokinesis in the pharyngeal mitotic divisions and the fate of midbody post mitotic division. (B-E) Cytokinesis in the pharynx. View of the AIR-2::GFP (green) in early and late stages of pharynx development (nuclei in magenta) from both ventral and dorsal views. AIR-2::GFP (D-E) flank marker change the shape and migrate to midline of the apical and persist. Time in minutes indicated below. (F) Kymograph showing the single midbody migrating to midline. (G-J) ZEN-4 (green) centralspindlin and (L-O) NMY-2 (green) myosin are both midbody ring components that move to the midline. ZEN-4 does not persist at the apical midline like AIR-2, NMY-2 persists at the pharyngeal midline as AIR-2. (K, P) Kymograph showing the midbody ring markers ZEN-4::GFP and NMY-2::GFP remain on the single midbody and migrate to pharyngeal midline. Time in minutes: seconds indicated right bottom. Scale Bar, 10 µm.

A

Pharyngeal Cell Division   Midbody Formation and Migration   Pharyngeal Polarization

B AIR-2::GFP; H2B::mCherry; Ventral View   Dorsal View after E16 Polarization

00:00   03:00   15:00

F

Time (Minutes)   0   10   20   30

G ZEN-4::GFP; TBB-1::mCherry; Ventral View   Dorsal View after E16 Polarization

00:00   03:00   27:00

K

Time (Minutes)   0   10   20   30

L NMY-2::GFP; TBB-1::mCherry; Ventrall View   Dorsal View after E16 Polarization

00:00   03:00   21:00

P

Time (Minutes)   0   10   20   30

co-localized with the apical polarity marker, PAR-6, after polarization (Fig. A7 G-I). We confirmed this localization with staining and show that endogenous AIR-2 can be observed on the apical surface of the pharynx (Fig. A5 I-K). ZEN-4::GFP appears on midbodies, migrates to the apical surface and is rapidly degraded, similar to the intestinal divisions (Fig. 2.4 J and Movie S16-17). Interestingly, NMY-2::GFP also labels the midbodies and moves to the apical surface, but persists at the apical surface during apical constriction (Fig. 2.4 O, P and Movie S16-17) (Rasmussen et al., 2012). Similar to AIR-2, RAB-11 and tubulin accumulate and remain localized to the apical surface after polarization (Fig. A7 A-F). Cytokinesis in the gut and pharynx show similar patterns where midbodies migrate to the apical midline and specific midbody components, especially AIR-2, remain localized at the cortex even after the midbody ring is removed. Therefore, cytokinesis may play an important function during epithelial morphogenesis of the digestive tract in *C. elegans*.

Midbody components label dendrites of sensilla neurons

The *C. elegans* amphid sensilla is a sensory organ that contains 12 neurons with dendrites that extend processes through the cuticle and two sheath cells. During morphogenesis, amphid neurons bundle together, anchor at the tip of the animal and migrate back to extend dendrites (Heiman and Shaham, 2009). From the lineage of the 12 sensilla neurons, there are 10 precursor cell divisions that occur between 280 and 400 minutes after the first cleavage (Fig. 2.5 A). These terminal divisions including two daughter cell pairs (ADF/AWB and ASG/AWA) and several where one daughter differentiates into a sensilla neuron while the other daugher undergoes apoptosis (ADL,

76

Figure 2. 5 Midbody components label dendrites of sensilla neurons

(A) Timeline of the cellular events during sensilla precursor cell division. (B) Illustration of cytokinesis in the sensilla mitotic divisions and the fate of midbody post mitotic division. (C-E) Cytokinesis in the sensilla. Multiple midbodies (arrowheads) forming in the anterior lateral region of the embryo flowed by migration of the midbodies into a cluster at the lateral sides of the embryos. Later AIR-2::GFP (green) persists in the clusters. (F-H) Midbody ring marker ZEN-4::GFP (green) appears near the forming sensilla cluster, but rapidly internalized into cytosol and degraded. (G) NMY-2::GFP (green) and (G) PAR-6::GFP (green) localized to the cluster and persist at the tip of the dendrites (arrowheads). (I-K) After midbodies cluster, a focus of AIR-2::GFP extend anteriorly until sensilla dendrite extension anchors at the tip of the animal. AIR-2::GFP localized to the tip (red arrowheads) of the dendritic extension and labels a substantial portion of the dendrite. Insert is anterior view of sensilla neuron (K). Time in minutes: seconds indicated left bottom. Scale Bar, 10 μm.

A Sensilla Development at 20 °C

First Cytokinesis 8E-16E — End of Last Cytokinesis 8E-16E — Cytokinesis of Sensilla Precursor Cells — Completion of Midbody Migration to Sensilla Foci — Extension of Sensilla Dendrite to Posterior Tip of Animal

Midbody Migration to Midline — Midbody Migration to Midline — AIR-2::GFP Persistence at Midline

230   262   280   310   340   420

B

Sensilla Cell Division   Midbody Formation and Migration   Sensilla Cell Cluster

AIR-2::GFP; H2B::mCherry;
C Midbody Formation   **D** Midbody Migration   **E** Midbody Clusting

00:00   06:00   46:30

F ZEN-4::GFP; TBB-1::mCherry   **G** NMY-2::GFP; TBB-1::mCherry   **H** AIR-2::GFP; PAR-6::mCherry

I AIR-2::GFP; Clustering   **J** Dendrite Extension Initiation   **K** Dendrite Extension

00:00   28:30   55:30

78

ASE, ASK, ASI), or differentiates into another neuron (AWC, ASH, AFD, ASJ). Our

observations show that these cells undergo a unique form of cytokinesis just before they

undergo dendrite morphogenesis (Fig. 2.5 B). These cells undergo a symmetrical

furrowing event before midbodies form centrally between the daughter cells (Fig. 2.5 C

and Movie S19-20). A group of at least 6 daughter cell pairs divide initially forming

multiple midbodies as observed with both confocal and lattice light sheet imaging (Fig.

2.5 D and Movie S19-20). Interestingly, these midbodies migrate into a cluster at the

extreme lateral sides of the embryo within 20 minutes. The midbodies migrate an

average 3.4 microns to reach the cluster over a 60-minute time window after the

appearance of the first midbody. After the initial clustering event, at least 4 more

midbodies form and migrate to join the cluster (data not shown). Interestingly, AIR-

2::GFP, RAB-11 and tubulin persist in these clusters (Fig. 2.5 E, Fig. A8 A-F and Movie

S19-20), while ZEN-4::GFP rapidly disappears after midbody clustering (Fig. 2.5 F and

Movie S19-20). Endogenous AIR-2 can be observed in these lateral clusters (Fig. A5 L-

N). We observe PAR-6 at the tip of the sensilla cluster colocalized with AIR-2, indicating

that it is the apical surface of these cells (Fig. 2.5 H, Fig. A8 J-L). In contrast to ZEN-

4::GFP, NMY-2::GFP migrates with the midbody to the cluster and persists at the very

tip of the dendrites (Fig. 2.5 G and Movie S19-20). To our knowledge, this is the first

detailed examination of the division and initial steps of organization of these neuronal

cell precursors.

After formation of the cluster, we observe this apical region extend anteriorly until the

amphid bundle anchors at the tip of the animal. AIR-2 remains localized along a

substantial length of the dendritic extension, as does tubulin (Fig. 2.5 I-K, Fig. A8 G-I and Movie S21). Around 80 minutes after sensilla precursor cell division, most of the neuronal sensory neurons have formed and AIR-2::GFP can be clearly observed along the length of the dendrites. As the amphid dendrites extend, other foci of AIR-2 form within the anterior region of the embryo and migrate toward the tip until six sensilla appear at the anterior tip (Fig. 2.5 K inset, and Movie S21). Although the individual cell divisions cannot be easily discerned in this crowded anterior region, these data suggest that a number of sensilla in the tip of the animal form through a similar process. These results demonstrate that directly after cytokinesis a midbody migration event brings several midbody components to the apical tip of the amphid dendrites, which remain localized there as dendrite extension occurs. Therefore, the midbody migrates from its original position at the end of furrowing to the position of the apical surface in several developing tissues during morphogenesis. Interestingly, AIR-2 remains localized at the apical surface of these tissues well after cytokinesis has occurred. The neuronal cell polarization has been suggested to share mechanisms of epithelial morphogenesis (McLachlan and Heiman, 2013), suggesting that these modified cytokinesis events may play a role in cells that undergo epithelial polarization.

Tissue Morphogenesis is Disrupted in Cytokinesis Mutants

Given the pattern of cytokinesis during morphogenesis and the localization of AIR-2::GFP to apical structures, we tested whether inactivation of AIR-2 in temperature sensitive mutant *air-2 (or207 ts)* embryos later in development would have an effect on epithelial morphogenesis. Although *air-2 (or207 ts)* mutants fail cytokinesis within
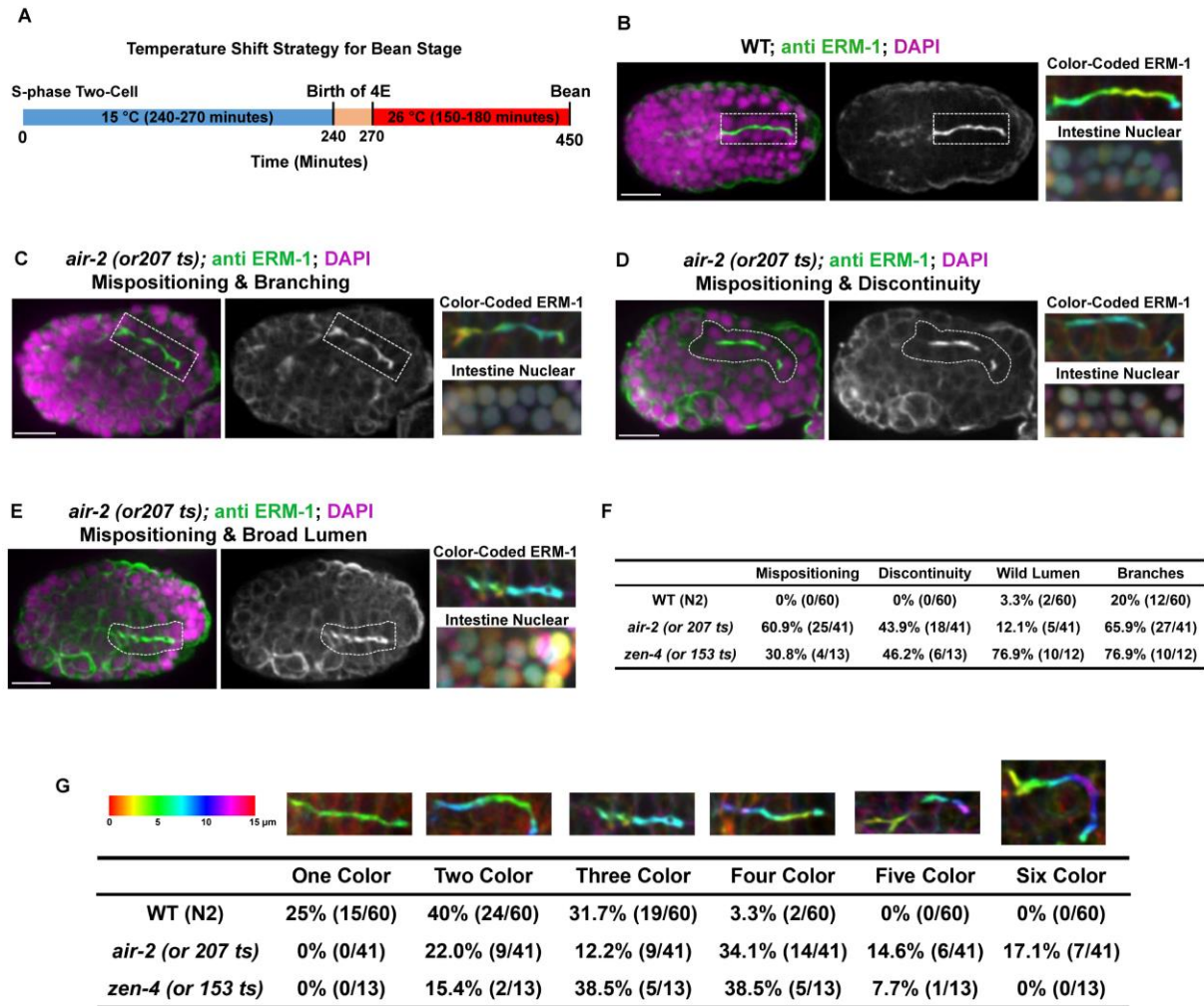
Figure 2. 6 Cytokinesis mutants have disrupted intestinal morphogenesis

Temperature sensitive mutant *air-2 (or207 ts)* and *zen-4 (or153 ts)* had severe morphogenetic defects during intestinal development. (A) Illustration of the temperature shift strategy of the ts mutants. (B) The immunostaining of apical marker ERM-1 showed that in wild type embryos, ERM-1 (middle) enriched at the apical cell cortex of the hypodermis and at the midline intestinal primordium (dotted rectangle). Images of the color-coding depth of intestinal ERM-1 and nuclei show the detailed z-depth distribution of intestine primordium. (C-E) there were various defects in intestinal tubulogenesis in *air-2 (or207 ts)* embryos, including mispositioning (C-E), branches (C), discontinuous lumen (D) and broad lumen (E). (F) Quantification of air-2 (or 207 ts) and *zen-4 (or 153 ts)* embryos with morphogenesis defects. (G) Summary of the color-coding depth of intestinal ERM-1 shows wider z-depth distribution of ERM-1 in cytokinesis ts mutants than wildtype.

minutes after shifting to non-permissive temperature in one cell embryos (Severson et al., 2000), we did not observe significant cytokinesis failures in later development unless embryos were shifted for several hours. Therefore, we shifted *air-2 (or207 ts)* embryos around the E4 stage for 2.5-3 hours when they reach the bean stage (Fig. 2.6 A) and examined the apical Ezrin-Radixin-Moesin homologue (ERM-1) by staining (van Furden et al., 2004). In wild-type and *air-2(or207 ts)* embryos, ERM-1 was localized to apical surfaces of the intestine and pharynx (Fig. 2.6 B, Fig. A9 A, C). However, the intestine often had an abnormal position within the embryo, with broadened ERM-1 staining, and apical surfaces that were branched or discontinuous in *air-2 (or207 ts)* embryos (Fig. 2.6 C-F, Fig. A9 B-C). Irregular localization of ERM-1 was also observed in comma stage *air-2 (or207 ts)* embryos, which were shifted for 4.5-5 hours (Fig. A9 B-C). The localization of other apical markers, such as PAR-3, DLG-1, IFB-2, were similarly disrupted (Fig. A9 D-I, DLG-1 and IFB-2 data not shown).

To investigate whether other cytokinesis regulators also regulate later epithelial morphogenesis, we inactivated midbody ring marker MKLP-1/ZEN-4, in temperature sensitive mutants later in different tissue development to observe any effects on morphogenesis. The *zen-4 (or153 ts)* embryos were shifted around the E4 stages for 2.5-3 hours until they reached the bean stage. Cytokinesis failure was more penetrant in *zen-4 (or153 ts)* embryos shifted to nonpermissive temperature at around 300 cell-stage of development during the E8-E16 divisions (Fig. A9 J-K). ERM-1 staining showed that intestinal and pharyngeal tubulogenesis in *zen-4 (or153 ts)* embryos was disrupted at restrictive temperature (Fig. 2.6 F, G and Fig. A9 J-L). These observations suggested

that the cytokinesis may play an important function to ensure proper epithelial morphogenesis of the digestive tract in *C. elegans*.

Additionally, we also detected whether the remodeling of microtubule (MT) cytoskeleton occurs normally in temperature sensitive mutants. The *air-2 (or207 ts)* embryos with expressing Tubulin::GFP were shifted around E4 stages until they reached the bean stage. High-laser-intensity images show the irregular tubulin distribution at the apical surface of intestine and pharynx tissues (Fig. A10 A-H). Previous studies identified that Aurora B kinase phosphorylates microtubule-depolymerizing enzyme KLP-7 to regulate MT growth (Han et al., 2015). Therefore, we decided to observe whether tubulin dynamics in *air-2 (or207 ts)* embryos was disrupted. Interestingly, we saw a localization of tubulin to an extended flank region around the midbody through the entire migration process and tubulin persists at apical surface after E16 polarization (Fig. A10 I-L). However, the tubulin localization on flank region disappeared in *air-2 (or 207 ts)* embryo (Fig. A10 M-N), but still accumulated at apical surface (Fig. A10 O-P). This suggests that AIR-2 may phosphorylate a putative substrate to stabilize the microtubule-dependent midbody or central spindle structures during midbody movement to apical surface.

We also investigated whether the developing sensory neurons formed normally in temperature sensitive mutants. *C. elegans* amphid neurons can take up lipophilic dyes such as DiI when they form properly and generate cilia that are exposed to the environment (Hedgecock and White, 1985; Perkins et al., 1986). We maintained

embryos at the permissive temperature (15 °C) and shifted them to non-permissive temperature at different embryo stages until they hatched and stained L1 larvae with DiI. This allowed us to rigorously test the role of AIR-2 in viability later in development as well as examine its role in sensilla development. As expected, 100% of wildtype embryos hatch under these conditions. In contrast, *air-2 (or207 ts)* embryos have only 39.7% (27/68) hatching even when left at 15 °C, indicating that this mutant is sick even at permissive temperature. Shifting *air-2 (or207 ts)* embryos to non-permissive temperature around the E4 stage causes significantly more lethality (10-20% hatching), consistent with the penetrant cytokinesis failures and gut morphogenesis defects we observed (Fig. 2.6 and Fig. A10). Interestingly, we observe significantly higher lethality over basal rate at permissive temperature when we shift embryos up to the comma or later stages. The lethality in *air-2 (or207 ts)* embryos decreases to the same level as observed when kept at 15 °C when we shift at comma or later stage, consistent with an essential role of AIR-2 during the last cell divisions in the embryonic lineage. These data suggest that AIR-2 function is required, even after the time window when most embryonic cell divisions have completed and support an important post mitotic function during late development. For comparison, we examined *zen-4 (or153 ts)* mutants, which have much more severe and penetrant cytokinesis defects later during morphogenesis as compared with *air-2 (or207 ts)*. In contrast to AIR-2 disruption we see almost 100% hatch rate of shifted embryos. Additionally, much less percentages of hatched *zen-4 (or153 ts)* animals, which were shifted at comma or later stage, display the defects of neuronal DiI staining (Fig. 2.7 A) and other tissue morphogenesis (Data not shown).

Genotype/ (Stage before Shifting)	No DiI Signal	Weak DiI Signal	Shape & Position Defect	Diffused DiI Staining	Hatch Rate
WT (N2) / (E8-E16)	0% (0/29)	0% (0/29)	0% (0/29)	0% (0/29)	100% (45/45)
WT (N2) / (Comma-1.5 Fold)	0% (0/21)	0% (0/21)	0% (0/21)	0% (0/21)	100% (36/36)
air-2 (or 207 ts) / (15 °C)	3.7% (1/27)	0% (0/27)	0% (0/27)	0% (0/27)	39.7% (27/68)
air-2 (or 207 ts) / (E4-E8)	20% (4/20)	15% (3/20)	35% (7/20)	0% (0/20)	20.6% (22/107)
air-2 (or 207 ts) / (E8-E16)	19.7% (13/66)	4.5% (3/66)	31.8% (21/66)	1.5% (1/66)	15.1% (89/588)
air-2 (or 207 ts) / (Polarized E16)	8.3% (1/12)	41.7% (5/12)	8.3% (1/12)	0% (0/12)	8.2% (14/170)
air-2 (or 207 ts) / (Comma-1.5 Fold)	0% (0/65)	3.1% (2/65)	18.5% (12/65)	21.5% (14/65)	63.1% (82/130)
zen-4 (or 153 ts) / (15 °C)	0% (0/18)	0% (0/18)	0% (0/18)	0% (0/18)	100% (28/28)
zen-4 (or 153 ts) / (Polarized E16)	30% (3/10)	0% (0/10)	0% (0/10)	0% (0/10)	NA
zen-4 (or 153 ts) / (Comma-1.5 Fold)	0% (0/32)	0% (0/32)	6.3% (2/32)	25% (8/32)	97.4% (37/38)
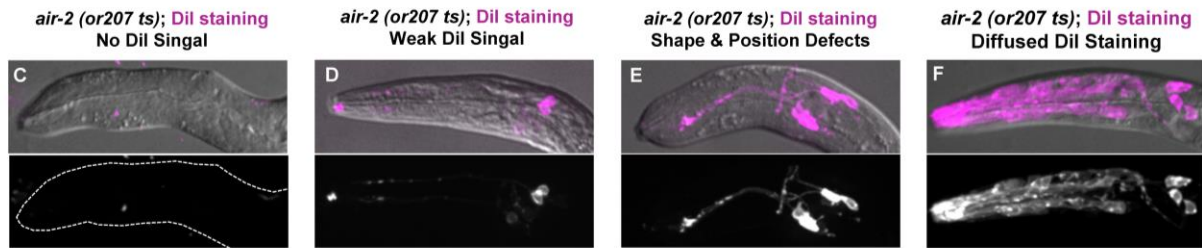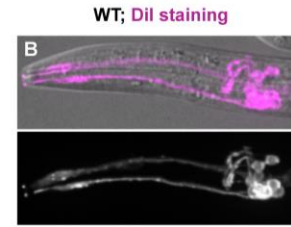
Figure 2. 7 Cytokinesis mutants have disrupted sensilla neuron morphogenesis

(A-E) The DiI dye process allowed visualizing neurite processes in live animals. (A) Quantification of DiI staining showed that around 40-60% of *air-2 (or207 ts)* and 20-30% of *zen-4 (or153 ts)* hatched larva had DiI staining defects at different temperature shift conditions. For wildtype, amphid neuron cell bodies, amphid dendrites, and phasmid neurons were clearly visualized by DiI staining (B). (C-F) *air-2 (or207 ts)* larvae displayed variety of neurite defects, including No-DiI signal (C), Weak signal (D), Shape and positioning defects (E) and Diffused staining (F).

This suggests that AIR-2 may perform other important roles for morphogenesis in addition to cytokinesis. In addition to observing hatching rates, we used DiI staining to observe sensilla morphology. In wildtype, amphid neuron cell bodies, amphid dendrites, and phasmid neurons were clearly labeled by DiI and appeared normal as expected (Fig. 2.7 A, F). In *air-2 (or207 ts)* mutant embryos, we observed numerous defects in the subset of surviving embryos that did not fail to hatch and became L1 larvae. Animals with no observed DiI staining were more common under longer inactivating conditions and were not observed if animals were shifted after dendrite morphogenesis at the comma and two-fold stage (Fig. 2.7 A), indicating that AIR-2 function is required during the specialized cytokinesis events described above. Importantly, shifting the AIR-2 mutant around the comma stage after the cytokinesis events are completed still caused significant defects in neuron shape, positioning and DiI staining intensity (Fig. 2.7 A). These data strongly indicate a post mitotic function for AIR-2 in dendrite morphogenesis well after the completion of cytokinesis. In contrast, *zen-4 (or153 ts)* ZEN-4 does not show the same defects when shifted after cytokinesis has completed, consistent with the observation that AIR-2 localization persists well after cytokinesis in the dendrite whereas ZEN-4 is internalized and degraded quickly after cytokinesis and cluster formation. Therefore, proper execution of cytokinesis and AIR-2 function especially are required late in embryo development for proper morphogenesis of the apical lumen of the gut and pharynx and proper formation of the sensilla neurons.

Figure 2. 8 Multiple microtubule-based organelles contribute to morphogenesis

(A-C) *spd-1 (oj5ts)* alters AIR-2::GFP dynamics. Shifting spd-1ts to non-permissive temperature did not prevent AIR-2::GFP localization to metaphase plate (A, arrowhead), but prevents AIR-2::GFP localization to the midbody (B). AIR-2::GFP localizes to the spindle poles after *spd-1 (oj5ts)* shifted to the restrictive temperature (B, arrowheads). AIR-2::GFP still accumulates at the intestinal apical midline (C, arrowhead). (D-F) Centrosome marker γ-tubulin::GFP (green) and α-tubulin::mCherry (magenta) colocalized at intestinal primordium (rectangle). (G-I) γ-tubulin::GFP (white arrowheads) and AIR-2::GFP (red arrowheads) migrate to apical midline simultaneously and persist at the tip of sensilla dendrite (I). (J) Quantification of AIR-2::GFP signal at intestinal apical midline after E16 polarization in both wildtype and *spd-1 (oj5 ts)* embryos. Time in minutes: seconds indicated left bottom. Scale Bar, 10 µm.

AIR-2::GFP; *spd-1 (oj5 ts)*

γ-Tublin::GFP; AIR-2::GFP

α-TUBULIN::mCherry; γ-TUBULIN::GFP; H2B::GFP

γ-TUBULIN::GFP; H2B::GFP

α-TUBULIN::mCherry
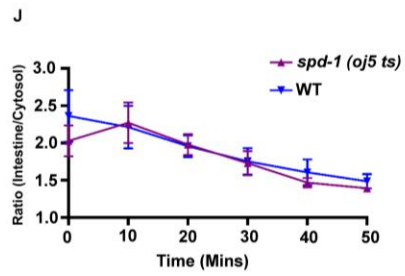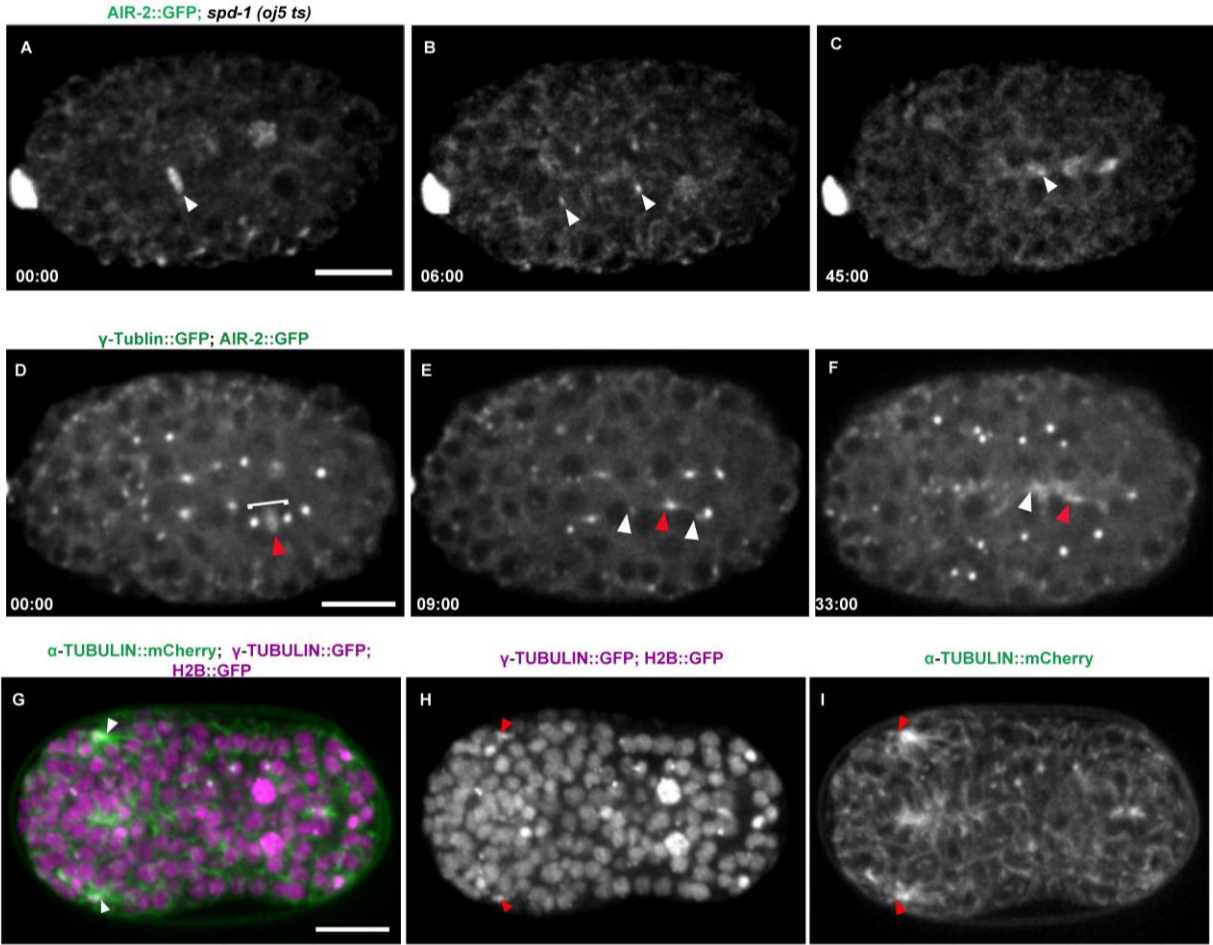
Multiple microtubule-based organelles contribute to morphogenesis

Next, we asked whether the functions of midbody proteins in morphogenesis are affected by midbody formation during late terminal cell division. In our study, we have shown a stereotypical migration of midbodies during tissue formation. Our observations also identified the localization of AIR-2::GFP at the flank central spindle region and midbody during its migration. Intriguingly, AIR-2::GFP persists prominently at the apical surfaces of different tissues post division. To further investigate the functions of midbody and its migration during tissue morphogenesis, we decided to inactivate the microtubule binding and bundling protein SPD-1, which is the orthologue of PRC1 in *C. elegans*. Interestingly, disruption of SPD-1 in *C. elegans* does not invariably prevent cytokinesis in the first cell division and intestinal cell divisions, but perturbed the microtubule bundling and disorganized central spindles in these cells. To inactivate SPD-1 during intestinal division, *spd-1 (oj5ts)* embryos were shifted at E4 stage to E8 prophase for live imaging (Fig. A11 A). As expected, the inhibition of SPD-1 during intestinal cell divisions prevent the recruitment of AIR-2::GFP to the midbody (Fig. 2.8 A-B). Interestingly, AIR-2::GFP expressed in *spd-1 (oj5 ts)* mutants shifted to the restrictive temperature localizes primarily to the spindle poles instead of the midbody (Fig. 2.8 B). However, AIR-2::GFP still accumulates at the midline of intestinal primordium after moving there with the poles (Fig. 2.8 C). Quantification of AIR-2::GFP signals in the intestinal primordium midline shows that there is no significant reduction of AIR-2::GFP signal strength and duration in *spd-1 (oj5ts)* mutant compared with wildtype (Fig. 2.8 J).

Previous studies showed a novel patterns of midbody-centrosome collaboration pattern to regulate ciliogenesis in MDCK cells (Bernabe-Rubio et al., 2016). Additionally, various midbody proteins can also be found in centrosomes, which reach the apical base of the cilium (Fabbro et al., 2005; Ott, 2016; Smith et al., 2011). In *C. elegans*, the apical surface ultimately becomes elaborated with microvilli supported by PCM material donated by the centrosome during intestinal development, while the centrioles are discarded (Feldman and Priess, 2012; Yang and Feldman, 2015). Therefore, we propose a possible mechanism behind the re-location of AIR-2::GFP to spindle pole and their subsequent migration to the apical surface. We hypothesize that microtubule-based organelles, like the midbody and centrosome, may collaborate each other to deliver identical signaling materials to initiate architectural arragement of apical surfaces. To delineate the relationship between these two organelles during intestinal development, we imaged embryos expressing both centrosome marker γ-tubulin::GFP and midbody marker AIR-2::GFP during the E8-E16 division. Interestingly, the data shows that centrosome and midbody migrate to apical midline simultaneously, and both γ-tubulin::GFP and AIR-2::GFP persist prominently at intestinal apical surface (Fig. A11 B-D). Interestingly, the same migration pattern has also been observed in sensilla and pharynx tissues (data not shown), γ-tubulin::GFP persists at the tip of sensilla dendrites and pharyngeal apical surface (Fig. 2.8 G-I, Fig. A11 E-G). Our observations suggest that the centrosome might be a complementary machinery to direct the critical midbody passenger molecules, such as Aurora B kinase, to apical surface when spindle microtubules bundling was disrupted. Delineating the precise relationship between these two organelles and deciphering the regulatory process that leads to proper

cellular organizations underlying proper morphogenesis will be a major focus of future studies.

Discussion

Our results have revealed surprisingly complex and reproducible patterns of cytokinesis during the invariant embryonic divisions in *C. elegans*. The entire invariant lineage has been known for several decades and our results suggest that cytokinesis also follows a specific pattern during the lineage. We observe reproducible alterations to furrow symmetry, central spindle length, abscission timing, midbody movement and inheritance. The traditional view of the embryo lineage is that cells are born and subsequently undergo changes that produce the differentiated organization within a tissue. However, our data demonstrate that cells in multiple tissues are completing cytokinesis, and are thus in "C phase," which has significant implications for understanding their behavior and regulation. Given that the entire cell is reconfigured during mitosis and cytokinesis is the transition period back into the interphase state, this is an ideal time window to reorganize cellular architecture.

We observe consistent changes to the symmetry of furrow ingression where the first mitosis is relatively symmetric and the second mitosis is highly asymmetric. Previously, the furrow asymmetry in the first division was shown to be a consequence of asymmetric accumulation of contractile ring components during ingression (Maddox et al., 2007). The adhesion between cells may also reinforce this asymmetry to drive the highly asymmetric furrow observed in the second round of divisions (Padmanabhan and

Zaidel-Bar, 2017). Whether due to cell intrinsic or extrinsic factors, the asymmetric

furrows have previously been postulated to drive efficient furrowing or help maintain

proper cell-cell contacts during cytokinesis (Maddox et al., 2007; Morais-de-Sa and

Sunkel, 2013). Our data suggest another hypothesis: the asymmetric furrow may be

required for the AB midbody to be engulfed by EMS instead of either daughter cell.

Given that the midbody has been proposed to deliver signals to cells that inherit it, it is

worth noting that the MS cell collects up to four midbodies over time (Singh and Pohl,

2014). Unexpectedly, we see relatively symmetric furrowing in several tissues later in

morphogenesis. This is striking because an asymmetric furrow would be sufficient to

position the midbody at the nascent apical surface. Given that the polarization

mechanisms are not completely understood, for example the extracellular matrix

component laminin is required in the pharynx but not the intestine (Rasmussen et al.,

2012), the symmetrical furrow followed by midbody migration may be important for

defining the apical surface. Perhaps there is no good reference for such asymmetric

furrowing prior to epithelial polarization that would allow cells in different locations to

position the midbody through an asymmetric furrow mechanism. We hypothesize that

lumen formation in the gut and pharynx is analogous to that described in MDCK cells

with the formation of a midbody-derived apical-membrane initiation site with the addition

of midbody migration for correct positioning of this domain (Li et al., 2014).

The coordinated, directed movement of the midbody we observe in several tissues

represents a new phenomenon during cytokinesis. Our data also suggest that

abscission has not taken place before the midbody migrates. This would mean that the

two daughter cells polarize while connected at the midbody, which might facilitate their positioning. These data are somewhat different than what is observed in already polarized epithelia where the furrow constricts from the basal to the apical surface to position the midbody. It is tempting to consider that performing cytokinesis in this particular fashion has an important function in the polarization process. Since these cells are undergoing a mesenchymal to epithelial transition, it is interesting to consider whether cytokinesis may have some general function in executing this process. Previously, midbodies have been shown to reposition after forming under normal or mutant conditions (Bernabe-Rubio et al., 2016; Herszterg et al., 2013; Morais-de-Sa and Sunkel, 2013; Singh and Pohl, 2014), but this phenomenon is only appreciated in isolated cases and poorly understood. It will be important to investigate how the midbody moves to the apical surface after furrowing is completed. The entire cortex is controlled by several actin cytoskeletal regulators in order to perform cytokinesis (Jordan and Canman, 2012), perhaps this is also employed to control the movement of the midbody.

In the tissues we investigated, the cells are undergoing their terminal cell division before morphogenesis, although some cells like those in the gut undergo post-embryonic divisions. These cells are also undergoing epithelial polarization and a mesenchymal to epithelial transition. After midbody movement, RAB-11, AIR-2 and possibly other molecules are recruited to the apical surface. Certainly these different tissues have unique gene expression programs, part of which might involve proteins delivered to the midbody and the apical surface. Interestingly, a transmembrane protein that binds to an

93

extracellular partner is expressed in the tip of the dendrites in amphid sensilla, which is required to maintain dendrite attachment at the tip of the embryo (Heiman and Shaham, 2009). It is unknown how this protein localizes to the tip of the dendrite, one speculative possibility is that it could be delivered through cytokinesis-directed membrane trafficking. A stem cell marker protein is released in extracellular membrane particles by neuroepithelial cells from the cilium and midbody, showing a similarity between these two organelles (Dubreuil et al., 2007). Interestingly, the worm releases exosomes from the sensory cilia later in life for communication between animals (Wang et al., 2014a). Perhaps the initial secretory apparatus built during cytokinesis to promote cell division is recruited to the apical surface of these neurons to recruit machinery involved in exosome release. Further investigation is required to define the molecular contributions provided by the midbody to the apical surface of these tissues.

Once the midbody moves to the apical surface, we observe that different components of the midbody have different fates. Typically, once the midbody is abscised from the cell, it is thought that most midbody proteins are discarded with the remnant. Strikingly, we observe Aurora B kinase remains at the apical surface well after other midbody components like ZEN-4 are removed. The limit of the resolution of light microscopy does not allow us to characterize in detail how this occurs. The most likely model is that the midbody is cut from the plasma membrane and flanking proteins like Aurora B, RAB-11 and microtubules are left behind. Among the many mitotic functions of Aurora B, it is a critical regulator of the timing of abscission (Mathieu et al., 2013; Steigemann et al., 2009). Based on our observations of microtubules at the central spindle and

94

midbody, abscission may occur after the midbody migration event, which might require

Aurora B activity. Interestingly, inhibition of Aurora B kinase in mouse embryos caused

the loss of midbody derived interphase bridges and a reduction of RAB-11 and cell

adhesion molecules delivered to apical membranes (Zenker et al., 2017). Aurora B also

regulates a number of cytoskeletal regulators during cytokinesis that control cell shape

(Ferreira et al., 2013; Floyd et al., 2013; Goto et al., 2003; Kettenbach et al., 2011), and

it will be interesting to determine whether any are involved with the events we observed.

It is striking that in the intestine, the central spindle elongates dramatically as the

midbody migrates. Along these lines, altered expression of the central spindle protein

PRC-1 (the homologue of SPD-1) contributes to variant midzone microtubule density in

different tissues in the *Xenopus* embryo, which correlates with changes to furrow

ingression and midbody behavior (Kieserman et al., 2008). While we observe the

centralspindlin component, ZEN-4, becoming internalized and degraded in the three

tissues, it was previously implicated in morphogenesis of the epidermis and pharynx

(Hardin et al., 2008; Portereiko et al., 2004; Von Stetina et al., 2017). It remains to be

determined whether this role is related to the dynamics of cytokinesis, or a cytokinesis

independent function of ZEN-4 as previously suggested. Therefore, further study will be

required to understand the role of the central spindle components in the formation of the

apical surface.

In the sensilla, the centriole moves to tip of the dendrite to template the cilia that form

sensory endings of these neurons (Dammermann et al., 2009; Nechipurenko et al.,

2017; Perkins et al., 1986). Interestingly, multiple central spindle proteins localize to the

95

base of cilia in Xenopus epithelial cells and are required for cilia morphology after the divisions are completed in *C. elegans* (Kieserman et al., 2008; Smith et al., 2011). In the apical membrane of the gut, gamma tubulin and other pericentriolar material is delivered from the centrosome, while the centrioles are discarded. The gut apical membrane ultimately becomes elaborated with microvilli (Feldman and Priess, 2012; Leung et al., 1999). We also observed gamma tubulin at the apical surface of the pharynx and sensilla dendrites. Therefore, different material provided by the midbody and centrosome may contribute to the final architecture of the apical surface. Delineating the precise relationship between these two organelles and deciphering the regulatory process that leads to proper cellular organizations underlying proper morphogenesis will be a major focus of future studies.

Materials and Methods

C. elegans Strains

C. elegans strains were maintained with standard protocols. Integrated *C. elegans* strains expressing midbody components proteins driven by *pie-1* promoter are listed in Table 1. All temperature sensitive mutants were obtained from the Caenorhabditis Genetics Center.

Embryo Preparation and Imaging

For live imaging, young gravid hermaphrodites were dissected in M9 buffer containing polystyrene microspheres and sealed between two coverslips with vaseline (Pohl and Bao, 2010). Live cell imaging was performed on a spinning disk confocal system that

uses a Nikon Eclipse inverted microscope with a 60 X 1.40NA objective, a CSU-22 spinning disc system and a Photometrics EM-CCD camera from Visitech International. Images were acquired by Metamorph (Molecular Devices) and analyzed by ImageJ/FIJI Bio-Formats plugins (National Institutes of Health) (Linkert et al., 2010; Schindelin et al., 2012). Whole embryo live imaging was performed on a lattice light sheet microscope created by Dr. Eric Betzig's lab and Dr. Bi-Chang Chen's lab (Chen et al., 2014).

Immunostaining and DiI Staining Assay

Freeze-crack methanol protocol was used in the study and the staining procedure is adapted from previous studies (Gonczy et al., 1999; Leung et al., 1999). 15-20 gravid worms were dissected in 15 μl M9 on a subbed slide which were covered by 3% gelatin subbing solution. Place an 18 mm^2 coverslip onto the drop and wick away the excess fluid with 3 MM Whatman paper. Freeze the slide on the metal block in -80 °C freezer for 5 minutes. Flick off the coverslip with a razor blade and plunge the slide into -20 °C methanol for 15 minutes or more. Rehydrate the slide in 1xPBS for 5 minutes. Incubate the slide with 50-100 μl of primary antibody in PBS for 45 minutes at room temperature or 4 °C overnight in a wet chamber. Wash slides for 5 minutes in PBT (PBS-0.05% Tween 20), 5 minutes in PBS. Incubate the slide with 50-100 μl of secondary antibody in PBS for 45 minutes at room temperature or 4 °C overnight in a wet chamber. 1:200-400 dilutions of Alexa 588 and 468 secondary antibodies were used in the study. Wash slide 2-3 times in PBS for 5 minutes, and mount the slides in 7-10 μl mounting buffer. Immunostaining to AIR-2 was performed as described (Schumacher et al., 1998). Primary antibodies and (dilutions) used were anti-ERM-1 (1:150-200); P4A1/PAR-3

(1:200); DLG-1 (1:200); MH33 (1:150); AIR-2 (1:50). Immunostaining to the temperature sensitive mutants, two-cell stage embryos were dissected from gravid worms, mounted in 10 μl of M9 buffer. All the processes were operated on the ice-bucket. The two-cell stage embryos incubated at 15 °C for 4~7 hours till specific stages, then the embryos were shifted to restrictive temperature (25 °C) for 2-4 hours and followed the freeze-crack staining protocol described above.

DiI staining in *C. elegans*

DiI staining to the wildtype N2 and temperature sensitive mutants is adapted from the previous study (Tong and Burglin, 2010). The two-cell stage embryos incubated at 15 °C for different time periods, then the embryos were shifted to restrictive temperature (25 °C) with 1:200 dilution of stock DiI dye solution containing 2 mg/ml DiI in dimethyl formamide for 18-24 hours. Transfer the hatched larvae to M9 and wash twice before transferring them onto agar pads with levamisole to visualize by confocal microscope.

Temperature-Shift Experiments

Temperature sensitive mutants were maintained at 15 °C. To perform terminal cell divisions temperature shifts on staged embryos, gravid adults were transferred to a dissection chamber (< 4 °C), which was precooled in ice bucket, with 20 μl of ice-cold M9 Buffer. Two-Cell stage embryos were quickly transferred via mouth pipette (Aspirator tube assemblies, Sigma) to hanging drop slides (Fisher) on ice. The slide was placed into a humidified chamber after collecting 20-30 two-cell embryos (process takes

5-10 minutes) at 15 °C. Embryos were incubated at 15 °C until the appropriate stages were reached and then shifted to 26 °C to inactivate cytokinesis regulator proteins. Incubation times were determined based on C. elegans embryonic lineage timing and adjusted according to our DAPI staining assay (data not shown), which define the stage of embryonic development based on the number of nuclei number and positioning of nuclei in embryos. The specific programs for each shift were listed below: E4-E8 shift: 4.5 hours at 15 °C, 3 hours at 26 °C to reach the bean stage; 5 hours at 26 °C to reach the comma stage. E8-E16 shift: 6 hours at 15 °C, 2 hours at 26 °C to reach the bean stage; 4 hours at 26 °C to reach the comma stage. Comma/1.5 Fold shift: 10-11 hours at 15 °C, 18 hours at 26 °C to L1 larvae.

Statistics

Quantification of AIR-2::GFP at the intestinal apical surface was performed in Image J by measuring the fluorescent intensity in frames with the brightest signal after E16 cells polarized. To decrease the phototoxicity, embryos were imaged when E8 cells Eplp and Eprp start dividing. To account for variation in imaging and z-depth, we calculated the ratio of the intensity at the apical surface relative to intestinal cytoplasm.

CHAPTER 3

Mounting *Caenorhabditis elegans* Embryos for Live Imaging during

Early Embryonic Divisions and Morphogenesis

This chapter contains one publication.

Bai X., Joshua N. Bembenek 2017. Orchestrating Early Embryonic Division (Bai and Bembenek, 2017a)

This chapter will be submitted for publications

Bai X., ….. 2018. The programmed Variations of Cytokinesis Contribute to Morphogenesis in the *C. elegans* Embryo.

Bai X., ….2018. Mounting *Caenorhabditis elegans* embryos for live imaging during meiotic division. Methods paper.

Bai X. will be considered the first author in all three publications. My contribution included: (1) designing experiments, (2) performing experiments, (3) collecting data and data analysis, (4) creating figures and writing the manuscript. Dr. Joshua N. Bembenek assisted with (1), (4). Dr. Bi-Chang Chen and Po-Yi Lee assisted with (1), (2), (3) and (4). Only small revisions to the original figures have been made for the purposes of this dissertation.

Abstract

Transparency of *C. elegans* embryos provides many benefits for imaging with light microscopy. To study the role of essential cell cycle regulators in early cell division and later developmental events, we have developed several methods for imaging *C. elegans* embryos using both high-resolution confocal microscopy and next-generation

lattice light sheet microscopy. In Chapter III, we described these live-cell imaging approaches to study cellular functions of the master regulators during sequential cell cycle events, including cortical granule exocytosis, meiotic division, and mitotic division in both one-cell stage embryo and multicellular tissues. Firstly, in order to image cortical granule exocytosis which occurs during anaphase I, we generated a mechanical and osmotic stress-free mounting method to avoid any external stress during filming the embryos without matured eggshell and permeable barrier. Additionally, we carefully characterized the spatiotemporal window of embryonic morphogenesis, which provides detailed timing windows to image the tissue-specific cell divisions from invariant lineage. Finally, this chapter also provides a brief process of analyzing the image data which were generated by lattice light microscope using Amira 3D software.

Introduction

Caenorhabditis elegans is a powerful model system for addressing fundamental cell cycle events. The observation of cellular processes within living cells (including oogenesis, fertilization, meiotic and mitotic cell division, and embryogenesis) can be performed with relative ease. *C. elegans* hermaphroditic adults contain a U-shaped gonad where the oocytes are produced in both proximal gonad arms (McCarter et al., 1999). Interestingly, the hermaphrodite animals contain a spermatheca to produce sperm cells. When the oocytes mature, they move through the spermatheca to become fertilized (McCarter et al., 1999). Once sperm enters the oocyte, fertilization triggers anaphase onset during egg activation. Egg activation encompasses a large number of events including cortical granule exocytosis and progression through the cell cycle that

102

transforms the highly differentiated oocyte into a totipotent egg (Bembenek et al., 2007). Therefore, studying cortical granule exocytosis is an ideal way to learn more about how cells regulate secretion during anaphase.

Cortical granule exocytosis (CGE) helps to rebuild the embryo's extracellular environment and forms an impermeable layer responsible for blocking polyspermy (Wessel et al., 2001). The ovulated embryos are lack of matured eggshell and the impermeable barrier, which could cause mechanical and osmotic stress during imaging with a regular agarose pad. To avoid this limitation of imaging, we created several imaging methods to diminish external stress in filming the embryos without an impermeable barrier, such as dissection-hanging drop and immobilization methods. The dissection method involves mobilizing adult worms in a liquid medium. Dissection of animals is performed under a dissection microscope and requires experienced hand-eye coordination to isolate the fertilized embryos before anaphase I (Bembenek et al., 2007). However, only healthy fertilized embryos were collected by the dissection method. Therefore, an alternative immobilization method is used for observing oocytes to embryo transition in uterus. Anesthetic agents, such as levamisole, and agarose-polystyrene nanoparticles, achieve immobilization. In this chapter, we evaluate the methods of hanging drop dissection and polystyrene beads to observe the dynamics of cell cycle regulators during sequential cell cycle events from oocyte maturation until later morphogenesis. Our techniques are relatively simple and avoid exposure of the worm to toxic substances, helping us understand the molecular mechanisms of egg activation during development.

C. elegans has unique advantages that make it well-suited for studying single cell division in multicellular tissues and observing the phenotype during later morphogenesis. Simplified anatomic structures, transparency of embryos, and essentially invariant development allowed the determination of the invariant embryonic cell lineage (Sulston et al., 1983). Such invariant embryonic lineage allows the characterization of cell cycle regulators at the level of single cells in different tissues. In this chapter, we also attempted to obtain the optimal images of several large complex structures, including developing intestine, neuronal sensilla, and pharynx. The usage of immunostaining and DAPI staining assays allowed us to streamline the determination of stages of developing embryos compared with the usage of Nomarski (DIC) microscopy only. We describe the preparation of agar mounts and other approaches for immobilizing embryos. We also carefully titrated the temperature shifting conditions to incubate staged embryos of various temperature sensitive mutants prior to performing standard 3D or 4D imaging. Lastly, Dr. Bi-Chang Chen and Po-Yi Lee helped us optimizing and analyzing the images captured by light sheet microscope with striking engineering software Amira 3D. This imaging analysis enables us to show the impressive details of cell division and midbody migration patterns in several complex tissues.

Methods and Protocols

1) Hanging Drop Dissection and Mounting Method

1.1) Worm culture for live cell imaging. Maintain *C. elegans* strains expressing the fluorescent proteins on OP50 plates at 20 °C with standard protocols. Some care must be taken to ensure that the worms are not starved for food. For imaging, select the healthy gravid worms from OP50 plates. Note: worm plates should not be overcrowded or contaminated. For live fluorescence imaging, worms are cultured at warmer temperatures (~ 25 °C) often have brighter fluorescence expression than worms cultured at lower temperatures (16-20 °C). The timing of meiotic cell cycle events can vary significantly with slight changes in maintaining temperature. We utilize both of 20 °C and 25 °C as culture and live imaging temperatures.

1.2) Prepare Blastomere Culture Medium (BCM). Dilute Inulin to 5 mg/ml in embryonic transfer water. Dilute PVP to 50 mg/ml in Schneider's medium. Mix 8 ml Schneider's medium, 1 ml 5 mg/ml Inulin, 1ml 50 mg/ml PVP, 100 μl BME vitamins, 100 μl Penicillin-Streptomycin, 100 μl Lipid Concentration for 10 ml blastomere culture medium (BCM). Sterilize the BCM by syringe filter, and add 35 % heat-inactivated FBS to BCM before using.

1.3) Prepare hanging drop slide. Melt the Vaseline with heat block; suck in 5 ml liquid Vaseline in 10 ml syringe. Leave the syringe with Vaseline at room temperature until Vaseline is completely solidified. Attach 23 G x 3/4" needle to the syringe tightly. Gently squeeze the Vaseline from syringe along the slide's surface to create a circular chamber with a cut for releasing the osmotic and mechanical pressure.

1.4) Before the worms are cut open, we need to pick worms from OP50 plates and transfer them to clean NGM plates for removing the bacteria. Simultaneously, load 15 μl of BCM on the cover glasses. Gently pick one or two clean worms to the BCM, and dissect the worms under the dissection microscope. Suck the mother worm carcass to avoid a toxicity effect.

1.5) Very gently attach the hanging drop slide on the cover glasses and gently tap the cover glasses by syringe.

2) Immobilization of Worms Using Anesthetic Agents

2.1) Maintain worms as described previously in 1.1).

2.2) Prepare a 2% agarose solution in a microcentrifuge tube by dissolving 0.02g of agarose in 1mL M9. Maintain solution on a heat block to ensure the solution remains molten.

2.3) Prepare molten Vaseline by thawing an aliquot of it a falcon tube inserted into a heat block. Prepare thawed levamisole aliquot by thawing tubes on ice.

2.4) Preparing the agarose pad. Apply approximately 150μL of molten agarose to the slide situated between two slides wrapped in tape. Apply an additional slide over the molten agarose to form the agarose pad. Allow the agarose pad to cool and solidify. After the agarose pad has solidified, remove the top slide and prepare the pad for worm mounting.

2.5) Mounting worms. Apply 5µL M9 buffer with levamisole on the coverslip, transfer the gravid worms to buffer and wait for 1-2 minutes till worm immobilized. Gently placing over the agarose pad over coverslip will help immobilize the worms. Seal the edges of the coverslip with molten Vaseline.

3) Immobilization of Embryos via Polystyrene Beads

3.1) Maintain worms as described previously in method (1).

3.2) Embryos were dissected from gravid hermaphrodites, mounted in 2.5 µl of an M9 buffer suspension containing 20 or 25 µm polystyrene microspheres and sealed between coverslips with molten vaseline.

4) Embryo Freeze-Cracking Method

4.1) Dissect the gravid worms in the M9 buffer, transfer them to humid chamber till embryos reach specific stage.

4.2) Freeze the metal block at -80 °C at least 30 minutes.

4.3) Transfer the embryos with mouth pipette to a slide, and gently place over a coverslip on the slide. Transfer the slide to frozen metal block surface for 5-10 minutes, and flick off coverslip with a razor, and plunge the slide into -20 °C methanol for 15 minutes.

4.4) Rehydrate the slide with 1xPBS buffer for 5-10 minutes.

4.5) Incubate the slide with antibody buffer or mount the slide with mounting buffer with DAPI for further assessments.

4.6) Seal slides with nail polish before imaging.

5) Microscopy and Image acquisition

5.1) Warm up the confocal microscope system. Before mounting embryos for imaging, everything should be ready to go, including warming up the imaging system, opening the imaging software, adjusting the imaging temperature, and the microscope pre-focus test. From the time the worm is dissected, there are only approximately three to five minutes until imaging needs to begin.

5.2) Place a drop of oil on the 60x objective; place the hanging drop slide on an inverted microscope.

5.3) Focus on the plane of the embryos with chromosomes and ensure that the embryos will not float in the BCM buffer. Make sure to start image acquisition of the embryos before anaphase I or other required stages.

5.4) Program the image acquisition software to take GFP, RFP, DAPI, and DIC (optional) images of the embryos. For this experiment, we used MetaMorph to capture the images with 300 ms (conditional) exposure time for both GFP and RFP filter. To capture the single cortical granule during anaphase I, we used the single z-plane to track the cortical granule exocytosis process around the central focus point of the chromosome.

5.5) Images were taken every 3 seconds for anaphase I imaging. The exposure time can be adjusted according to the protein of interest and transgene expression in different strains. Note: the overexposure condition will be phototoxic to embryos. Therefore, the image conditions need to be optimized to allow the embryos develop properly.

5.6) Acquire images till the embryos complete the cortical granule exocytosis and chromosome segregation as observed by the fluorescent signals labeled with marker proteins. The whole imaging process only takes 2 minutes or other time till acquired cellular events complete.

5.7.1) Analyze the images using Fiji Image J software. Open the image series for any one of the wavelengths in Image J.

5.7.2) Click on Image>Transform>Rotate the embryos to lateral view.

5.7.3) Click on the ImageJ toolbar> Image> Adjust the brightness and contrast.

6) Materials

6.1) NGM media (2% agar, 3g/L NaCl, 2.5g/L peptone, 5 mg/ml cholesterol, I M KH_2PO4, 1 M $CaCl_2$, 1 M $MgSO_4$, 2 mg/ml uracil).

6.2) M9 liquid media (5g/L NaCl, 3 g/L KH_2PO_4, 6 g/L Na_2HPO_4).

6.3) LB liquid media (10g/L tryptone, 5 g/L yeast extract, 10 g/L NaCl).

6.4) Blastomere Culture medium (Schneider's medium (Gibco, 21720024), Inulin (Sigma-Aldrich I2255), Polyvinyl Pyrrolidone (Sigma-Aldrich, PVP40), BME vitamins

(Sigma-Aldrich B6891), Penicillin-Streptomycin (Gibco 15140-148), Lipid concentration (Gibco, 11905-031), Embryo transfer water (Sigma-Aldrich W1503), Heat Inactivated FBS (Gibco, 10082-147), Vaseline (Fisher Scientific, 18-999-1820).

6.5) Spinning disk confocal system (Nikon Eclipse inverted microscope with a 60 X 1.40NA objective, CSU-22 spinning disc system, Photometrics EM-CCD camera (Visitech International, UK). Images were acquired by Metamorph (Molecular Devices).

6.6) ImageJ/FIJI Bio-Formats plugins (National Institutes of Health) (Schindelin et al., 2012, Linkert et al., 2010).

6.7) Microscope slides (Fisher Scientific 12-550-15), cover glasses squares (Fisher Scientific 12-540C).

6.8) Polystyrene Beads, 2% volume, 0.1μm (Fisher Scientific, NC9081186).

6.9) Fisherbrand Razor Blades (12-640), Vaseline (Fisher Scientific, 18-999-1820).

6.10) Spinning disk confocal system (Nikon Eclipse inverted microscope with a 60 X 1.40NA objective, CSU-22 spinning disc system, Photometrics EM-CCD camera (Visitech International, UK). Images were acquired by Metamorph (Molecular Devices).

6.11) ImageJ/FIJI Bio-Formats plugins (National Institutes of Health) (Schindelin et al., 2012, Linkert et al., 2010).

6.12) Microscope slides (Fisher Scientific 12-550-15), cover glasses squares (Fisher Scientific 12-540C).

6.13) Aspirator tube assemblies for calibrated microcapillary pipettes (Sigma A5177).

Representative Results

Figure 3. 1 Making a standard hanging-drop and agar mount.

(A-B) Aspirator tube assemblies, worm pick, and Vaseline syringes were used to dissect and collect embryos. (C) Use the Vaseline-filled syringe to make a circular chamber with a cut in the center of the coverslip for releasing osmotic and mechanical pressure. Dissect the worms under the dissection microscope. (D) Remove the mother worm carcass to avoid the toxicity effect. Very gently attach the hanging drop slide on the cover glasses and gently tap the cover glasses by syringe. (E-G) Representative images illustrating cortical granule exocytosis (green, arrowheads) and chromosome segregation (red, bracket) during anaphase I in SEP-1^{PD}::GFP embryo. Data were collected with 60X lens and every 3 seconds. Images were rotated such that the posterior side is to the left. (H-K) Representative images of first mitotic division from metaphase (H-I) to cytokinesis (J-K) in the embryo expressing SEP-1^{PD}::GFP. Hanging drop mounting will release mechanical and osmotic stress when imaging the embryos with RNAi treatment to eliminate the expression of core exocytosis machinery genes, which may cause permeable barrier defects, such as *syx-4* RNAi. (H-I) Processes to make a standard agar mount for immobilizing worms using anesthetic agents, such as levamisole. Place three slides on the bench, with the outer two slides taped down to the bench. Drop molten agar on the center slide. Place the fourth slide onto the three original slides to compress over the agar. (J) Representative image of the syncytial germ line which generating oocytes that undergo ovulation into the spermatheca. Separase (green) localizes on cortical granules and chromosome (magenta) during anaphase I embryo (right).
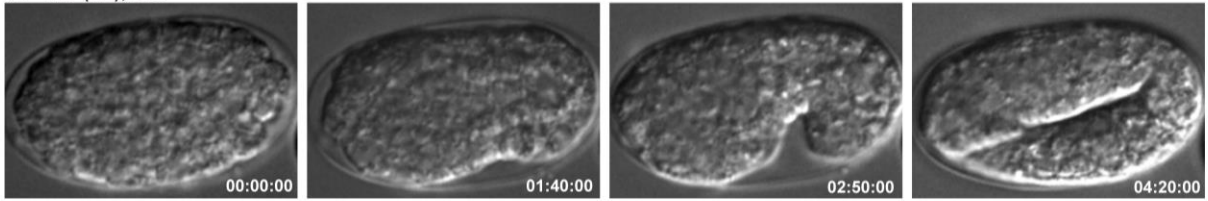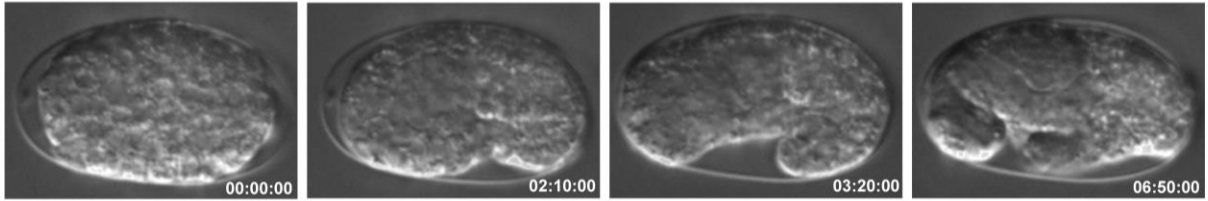
SEP-1^PD^::GFP; H2B::mCherry

DIC; Metaphase   SEP-1^PD^::GFP   DIC; Furrowing   SEP-1^PD^::GFP
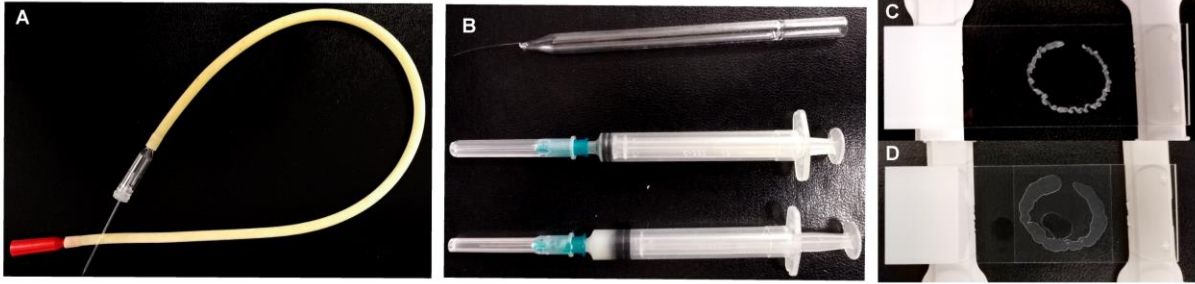
SEP-1::GFP; H2B::mCherry
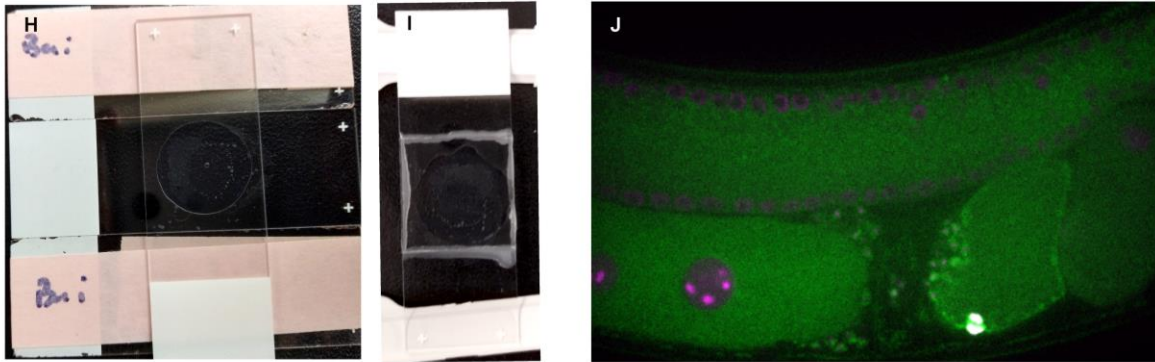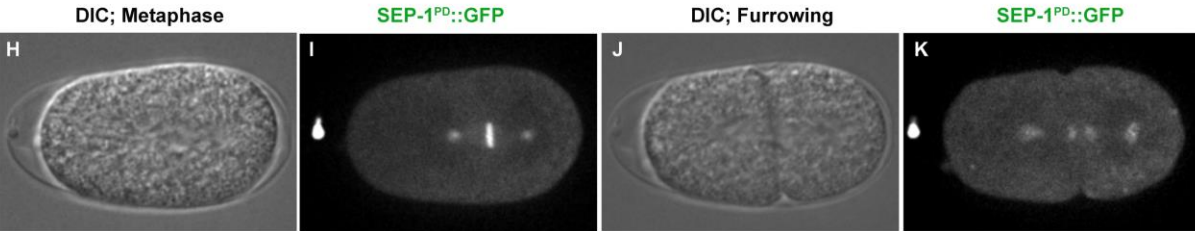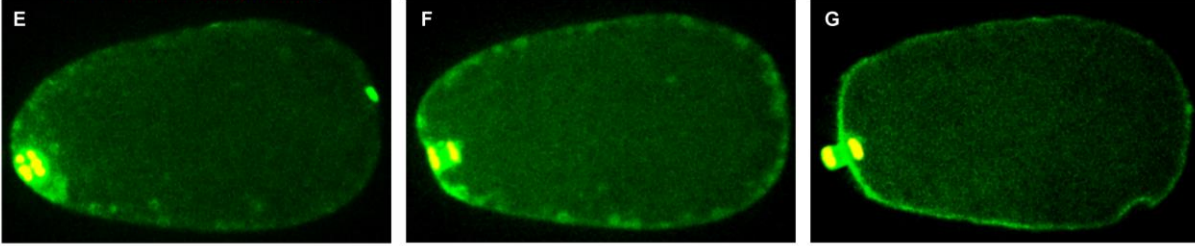
Figure 3. 2 Timing the stage of embryonic development.

Embryos were dissected from gravid hermaphrodites, mounted in 2.5 µl of an M9 buffer suspension containing 20 or 25 µm polystyrene microspheres and sealed between coverslips with molten vaseline. (A-C) Both *air-2 (or207 ts)* and *zen-4 (or153 ts)* mutants had severe morphogenetic defects. (A-C) *air-2 (or207 ts)* and *zen-4 (or153 ts)* embryos elongated much slower than wild-type embryos and arrested before reaching two-fold elongation. Time in an hour: minute: second indicated on right bottom. (D-L) To carefully characterize the loss function of midbody proteins during morphogenesis, we designed temperature-shift strategy using DAPI staining assay to define the stage of embryonic development. The two-cell stage of embryos were maintained at 15 °C until specific stages, such as E2 metaphase, E2 anaphase, E4 S-phase, E4 prophase, E4 metaphase, E8 S phase, E16, and E16 ventral enclosure which were listed as (D-L). Then, embryos were shifted to 25/26 °C to disrupt the functions of midbody proteins or cytokinetic proteins, which caused a variety of morphogenesis defects (data were shown in Chapter 2). The detailed timing for specific stages for wild-type (N2) and other temperature sensitive mutants are listed in Figure A12.
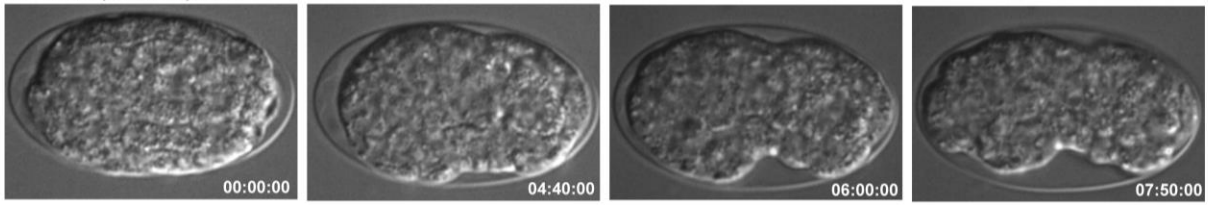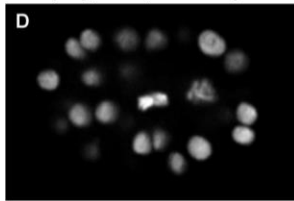
A   WT (N2); DIC

00:00:00   01:40:00   02:50:00   04:20:00

B   *air-2 (or207 ts)*; DIC

00:00:00   02:10:00   03:20:00   06:50:00

C   *zen-4 (or 153 ts)*, DIC

00:00:00   04:40:00   06:00:00   07:50:00

WT (N2); DAPI; E2 Metaphase   E2 Anaphase   E4 S-Phase   E4 Prophase

D   E   F   G
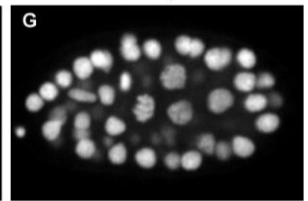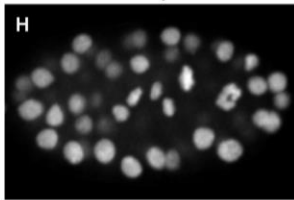
E4 Metaphase   E8 S-Phase   E16   E16 Ventral Enclosure

H   I   J   L
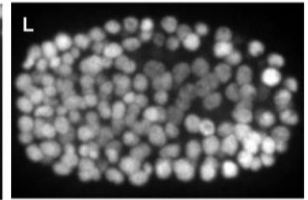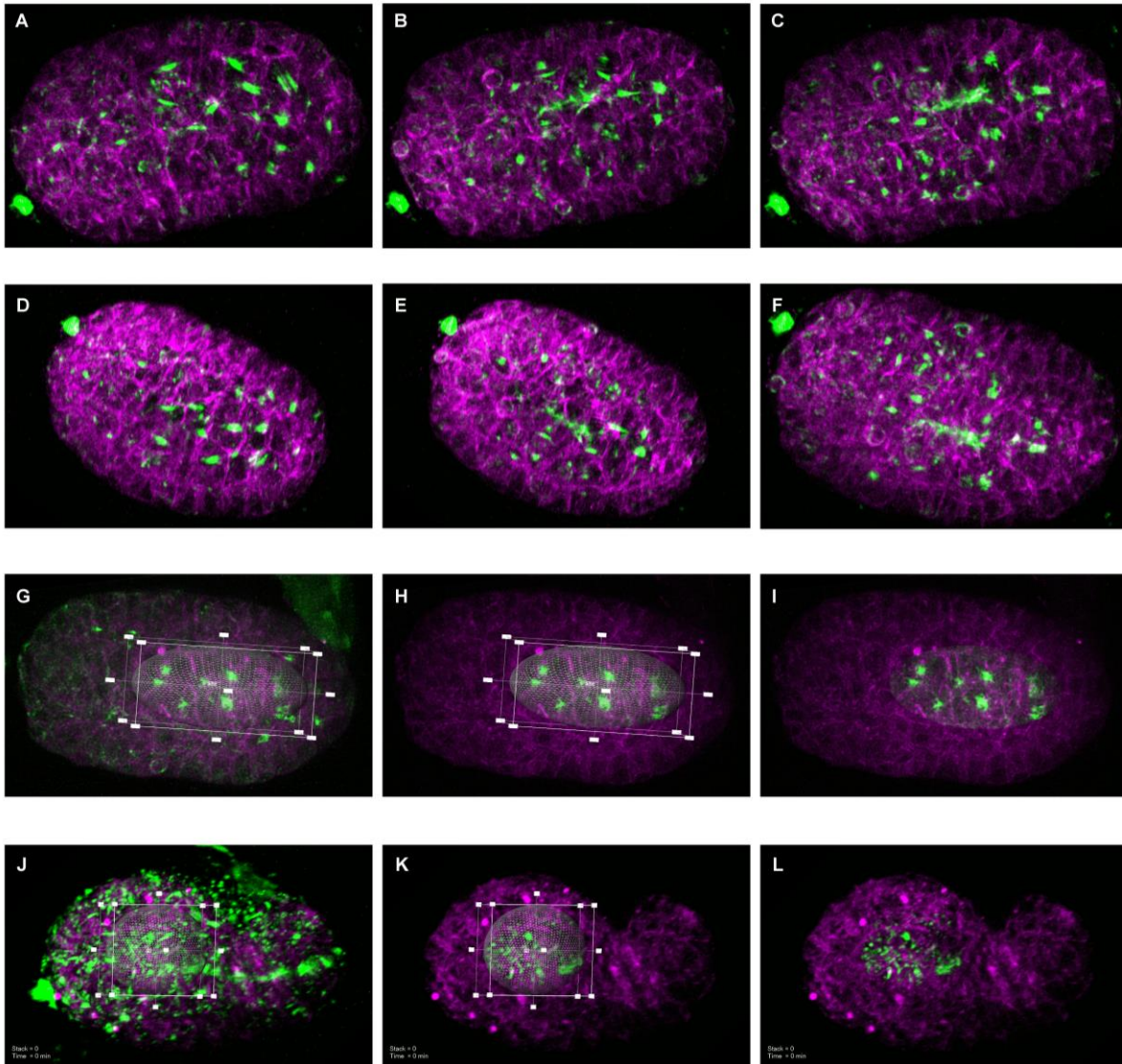
Figure 3. 3 Example of cytokinesis in intestinal cell divisions with lattice light sheet microscopy.

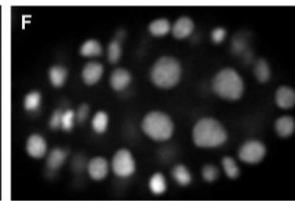The embryos expressing midbody flank marker AIR-2::GFP (green) with PH::mCherry (magenta). Images were captured by lattice light sheet microscopy every 90 seconds with 61 *z*-planes. (A-C) Intestinal midbody migration from division positions to the intestinal apical surface, and AIR-2::GFP (green) persists at the apical midline. (D-F) Mirror-symmetric images of (A-C) after rotating the images 180 ° along *x*-axis using Amira 3-D software. (G-L) To emphasize the tissue-specific cell divisions (intestine G-I; pharynx J-L), Volume Edit tool was used to select the intestine (G-H) and pharynx regions (J-K) from whole embryos to emphasize the intestinal (I) and pharyngeal cell divisions (L).

Discussion

A primary challenge for live imaging is to preserve the integrity and viability of embryos. In this chapter, we created some approaches to diminish external stress during filming embryos, including hanging drop and polystyrene beads mounting. We also utilized DIC microscopy for imaging the long-term morphogenesis process to avoid the excessive heating and phototoxicity from the laser source to embryos. Additionally, the transparency of *C. elegans* embryos benefits from the use of DIC microscopy to detect changes in cell shape, including cytokinesis. DIC also enables us to observe other cellular structures, such as the mitotic spindle, nuclear eyes, developing apical lumen and epidermal structures. Mounting *C. elegans* embryos on an agar pad provide a stable, long-term environment for DIC microscopic analysis of tissue morphogenesis. The utilization of specific proteins tagged with a fluorescent reporter complements DIC microscopy to visualize the cellular localization of these proteins and study the role of these proteins in cell division. To compromise the quality of imaging and phototoxicity of embryos during fluorescence imaging, we usually increase the CCD camera digital gain and lower the fluorescent intensity and duration of exposure. Our collaborator Dr. Bi-Chang Chen provided deconvolution algorithms to reassign out-of-focus light, which reduced background and improved the quality of the captured images with lattice sheet microscopy. In the future, other extensions live imaging, such as live cell super-resolution imaging microscopy, will be applied in our lab to study membrane trafficking, midbody migration and morphogenesis in *C. elegans*.

CONCLUSION

The collection of work outlined here attempts to address some important questions regarding the functions of cell cycle regulators during cytokinesis and later developmental events. The first question of this work is whether the proteolytic activity of separase is involved in its membrane trafficking roles. Additionally, we tried to decipher how cytokinesis and other aspects of cell division control developmental events in several tissues. Lastly, this work suggests possible post-mitotic roles for the subcellular structure midbody/midbody remnant in *C. elegans*. Collectively, these studies provide insight into how the separase and other master cell cycle regulators control cytokinesis, cell division, and later developmental events to maintain invariant embryogenesis in *C. elegans*.

Our lab and other colleagues found novel roles for separase in membrane trafficking and exocytosis during cortical granule exocytosis and cytokinesis in *C. elegans* (Bembenek et al., 2007; Bembenek et al., 2010; Richie et al., 2011). In this study, we aimed to investigate whether an unknown substrate of separase is involved in regulating exocytosis and how the proteolytic activity of separase controls exocytosis. To address these questions, we utilized several separase mutants and microscopy techniques to explore the cellular functions of separase in exocytosis and membrane trafficking. Intriguingly, our previous studies show that protease-dead separase (SEP-1[PD]::GFP), which contains a point mutation at the catalytic active site, is dominant negative and interferes with endogenous separase function during chromosome segregation and cytokinesis (Bai and Bembenek, 2017b; Bembenek et al., 2010; Mitchell et al., 2014). In

this study, we also observed that depletion of the cohesin subunit SCC-1 significantly

rescues mitotic chromosome segregation defects and embryonic lethality in the

embryos expressing protease-dead separase. Depletion of cohesin does not alleviate

the cytokinesis defects caused by disrupting separase function. All of these

observations suggest that separase has another substrate besides cohesin, the

cleavage of which promotes exocytosis during anaphase. Chromosome segregation

and cytokinesis are spatiotemporally related cell cycle events. In several systems,

chromosome segregation defects (such as chromatin bridges) induce a delay in the

physical abscission of daughter cells and cause failure of cytokinesis (Bembenek et al.,

2013; Hauf et al., 2001; Norden et al., 2006). Our data suggested that SEP-1[PD]::GFP

blocked cleavage of an unknown substrate to interfere the exocytosis of RAB-11

vesicles in anaphase rather than other chromosome bridging conditions.

The protease activity of separase is to hydrolyze substrates, of which there are several

in *C. elegans,* yeast, and mammalian cells (Lee and Rhee, 2012; Matsuo et al., 2012;

Sullivan et al., 2004; Sullivan et al., 2001; Zou et al., 2002). Further studies are needed

to identify the substrates of separase, which may be involved in the regulation of

exocytosis during anaphase. Additionally, investigation of how the proteolytic activity of

separase mediates exocytosis is also required for fully understanding of the molecular

mechanisms of cell division.

RAB-11 performs multiple roles during the oocyte-to-embryo transition. The localization of RAB-11 moves through recycling endosome, cortical granules, and Golgi membranes after fertilization (Sato et al., 2008). After vesicles are delivered to plasma membrane, RABs recruit a number of effectors to promote vesicle tethering to promote the SNARE-mediated fusion and later exocytosis (Wickner and Schekman, 2008). Our study showed that both SEP-1^{WT}::GFP and SEP-1^{PD}::GFP colocalize with RAB-11::mCherry in the cleavage furrow and cortical granules, implying that these two proteins may interact either directly or indirectly. We found that RAB-11 did not remain associated with the plasma membrane in SEP-1^{PD}::GFP embryo after exocytosis, suggesting that RAB-11 may not be the substrate of separase during exocytosis (Bai and Bembenek, 2017b). However, it is still possible that RAB-11 related proteins may interact with separase and be one of separase's direct substrates. Further investigations with genetic interaction, biochemical, and super-resolution imaging assays are required to investigate the interaction between separase and RAB-11 or RAB-11 effectors, such as the newly found RAB-11 GEF protein REI-1 (Sakaguchi et al., 2015). Studying the molecular mechanism of the interaction between separase and other vesicle regulators, including RABs would help to determine whether separase affects a different step in exocytosis than the membrane docking or tethering functions. It would also provide insights into temporal regulation of separase during exocytosis, for example, separase may cleave an inhibitor of exocytosis at early steps. Therefore, identifying a putative vesicle target that separase cleaves to promote exocytosis is a critical step for future investigation.

Previous studies using genetic screens identified several separase mutations, which localize outside the protease domain. Despite the fact that none of these mutation sites are localized inside the protease domain, these amino acid substitution mutants cause defects in chromosome segregation, cortical granule exocytosis, and cytokinesis (Richie et al., 2011). These observations beg the question of whether the non-proteolytic domains coordinate with the proteolytic activity to regulate exocytosis? Genetic suppressors provide a powerful tool for exploring gene expression and interaction by mutagenizing a second mutations in the mutant under study. Our recent study to identify the suppressor of the separase non-proteolytic mutant (*e2406*) provided some ideas that the phosphatase 5 (PPH-5) and Heat Shock Protein-90 (HSP-90) might represent a signaling pathway that controls exocytosis (Melesse et al., 2018). This study may help to address another hypothesis that non-proteolytic functions of separase may also impact exocytosis through regulating the CDK or other signaling pathways. Additionally, the newly reported crystal structures of separase in *C. elegans* and other systems add strong structural information for studying the regulation between protease domains and other motifs in separase (Boland et al., 2017; Luo and Tong, 2017). Collectively, the study presented here provides novel insights into the molecular mechanism of how separase promotes exocytosis. Identification of a putative vesicle substrate that separase cleaves to promote exocytosis will be important goals of future investigation.

Perhaps of all the work presented here, the most interesting findings are derived from the study of cytokinesis patterns during the invariant embryonic divisions in *C. elegans.* In Chapter 2, we carefully characterized several surprising phenomena during cell

division, which provide a novel case of cytokinesis in a multicellular context and open a new link between cell division and later development. The use of next-generation lattice light sheet microscopy enabled us to obtain the incredible details of cytokinesis during invariant embryonic divisions and showed a few novel lineage-specific cytokinesis patterns.

Cytokinesis is one of the most dynamic cellular processes with dramatic changes in cell shape and reorganization of the cytoskeleton (D'Avino et al., 2015). Successful execution of cytokinesis requires multiple key mechanisms, factors, and signals to precisely control various cytokinetic events including positioning of the cleavage site, symmetry of ingression furrow, nascent membrane synthesis, midbody formation, and final abscission (D'Avino et al., 2015; Green et al., 2012; Pollard, 2017). Our study attempted to characterize lineage-specific cytokinesis patterns in *C. elegans*. First, we observed variations in furrow symmetry during the first two cell divisions. Symmetric furrow ingression has been observed during the first cell division, however we saw a significant change during AB cell division (during the second round of cell division). The cleavage furrow ingressed in an asymmetric fashion from one side of AB cell towards the EMS cell, and the midbody formed near the cortex of EMS cell. Remarkably, we observed symmetric furrows during cytokinesis in intestine, pharynx, and sensilla precursor cells, which is different from the highly asymmetric furrowing during AB cell division and cell divisions in other polarized multicellular tissues, such as various epithelial and vertebrate neuroepithelium (Das et al., 2003; Kosodo et al., 2004; Kosodo et al., 2008). In epithelial tissues, including the *Drosophila* embryonic ectoderm and

follicular epithelium, asymmetric furrowing is driven by the close attachment of contractile ring with apical junctions at the apical side (Guillot and Lecuit, 2013; Morais-de-Sa and Sunkel, 2013). In *C. elegans*, polarized distribution of the scaffold proteins Anillin and Septin, as well as the cytoskeleton motor protein Myosin II at an asymmetrical contractile ring, produce the cortical tension to control asymmetric furrowing (Maddox et al., 2007; Singh and Pohl, 2014). Despite the fact that asymmetric furrowing was considered a general property of dividing epithelial cells, symmetric furrow ingression did exist in some epithelial tissues, such as the *Drosophila* pupal wing (Herszterg et al., 2013). Perhaps, there is no good reference for symmetric furrowing prior to epithelial polarization that would position midbody to asymmetric apical surface, which is observed in our case.

Another interesting feature of cytokinesis in epithelial tissues is that asymmetric furrowing results in midbody formation and positioning at the apical domain (Herszterg et al., 2013; Herszterg et al., 2014; Morais-de-Sa and Sunkel, 2013). Recent studies have characterized asymmetric furrow ingression during AB cell division in *C. elegans* (Singh and Pohl, 2014). Our data suggested that asymmetric furrowing is required for inheritance of the AB midbody by the EMS cell instead of either AB daughter cell. Strikingly, apical positioning of the midbody also occurs in epithelial tissues with symmetric furrow ingression, such as the *Drosophila* pupal wing (Herszterg et al., 2013). The dividing pupal wing cells are extruded to reposition their geometrical center and help the midbody relocate at the apical domain. Probably the most interesting observation is that the midbody crosses the cell and to reach an apical position in

several tissues. Detailed analysis of abscission indicated that disassembly of the microtubule scaffold occurs prior to abscission in the early *C. elegans* embryo (Green et al., 2013; Konig et al., 2017). Additionally, the longer persistence of spindle microtubules suggests that abscission in these cells has not taken place until the completion of midbody migration and polarization of daughter cells to the apical domain. Collectively, further studies are needed to delineate how the midbody moves to apical surface after furrowing is completed but before abscission occurs.

Notably, we observed coordinated and orientated midbody migration events to the apical position in three tissues. Although some midbody migration patterns have been shown in different cell models, the migration patterns are only appreciated in specific cellular cortexes and the molecular mechanisms are poorly understood (Bernabe-Rubio et al., 2016; Herszterg et al., 2013; Morais-de-Sa and Sunkel, 2013; Singh and Pohl, 2014). In our study, the novel patterns of midbody migration and positioning are somewhat different from what has been observed in polarized epithelia with asymmetric and symmetric furrowing. Therefore, there may be other mechanisms and factors to regulate midbody migration in *C. elegans*. Recent studies in *Drosophila* identified that cadherin-catenin complex mediated recruitment of midbody to the apical side (Morais-de-Sa and Sunkel, 2013). It is tempting to consider that apical junction (AJ) components may be delivered to the midbody region, where they coordinate with enriched F-actin around the midbody to drive midbody migration. Meanwhile, it is plausible to speculate that membrane trafficking machinery, such as RAB-11 positive vesicle trafficking, helps to deliver AJ components to the midbody region as previously reported in MDCK system

123

(Schluter et al., 2009). It is possible that cytokinetic regulators may also control midbdoy movement after symmetric furrowing is completed. Potential candidates in this regulation are tubulin, actin and a set of other cytoskeletal regulators, such as Rac- and Arp2/3- dependent regulators. Another surprising observation is that the midbody flank marker AIR-2::GFP consistently persisted at the extended central spindle region during the migration process; it is possible that Aurora B kinase may phosphorylate some putative targets at the central spindle to regulate movement of the midbody. Intriguingly, we observed that the central spindle protein ZEN-4::GFP was internalized to the cytosol after midbody movement. Other central spindle proteins, such as PRC-1 contribute to midzone microtubule density in *Xenopus* and are required for cilia morphogenesis in the worm (Kieserman et al., 2008; Smith et al., 2011). Additional evidence is recommended to define the role of different spindle regulators in midbody migration and their regulation of tissue morphogenesis. Lastly, much less is known about the functions of the midbody migration process. Perhaps the midbody movement may contribute to epithelial polarization or a mesenchymal-to-epithelial transition and initiating the nascent apical surfaces. Further studies could address these questions by damaging the midbody structure or blocking midbody migration. If our hypothesis is correct, then epithelial morphogenesis after either of these manipulations would be disrupted. Additionally, further work should target putative regulators, which are involved in the movement of the midbody, and their regulation in coordinating the formation of the contractile ring, symmetric furrowing, midbody migration, and midbody positioning during the mesenchymal-epithelial transition.

Although the mechanisms of midbody movement remain largely unknown, it is apparent that the midbody is delivered and positioned to apical surfaces in various epithelial tissues. The midbody has been long thought to be useless cellular junk, which was discarded and degraded by the cell after cytokinesis, hence the word remnant (Crowell et al., 2014; Schink and Stenmark, 2011). However, besides its canonical role in regulating abscission, a number of other surprising non-cytokinetic functions that come from recent midbody literature, such as the midbody helping to deliver the apical marker to the lumen sites in MDCK cells (Schluter et al., 2009). Physical removal of the midbody from the periphery of MDCK cells disrupted ciliogenesis (Bernabe-Rubio et al., 2016). Additionally, extensive studies indicated that apical positioning of the midbody after cell division contributes to the epithelial architecture. Disruption of apical localization of the midbody under different mutant conditions would result in ectopic lumen formation, disturbing the overall epithelial architecture (Bryant et al., 2010; Jaffe et al., 2008; Li et al., 2014; Overeem et al., 2015; Schluter et al., 2009). The apical membrane initiation site (AMIS) is also guided by the midbody, which allows RAB-11 endosomes to deliver cargo during lumenogenesis (Li et al., 2014). Another interesting study showed that the delivery of exogenous and ectopic midbodies to an apical structure induces a shift in localization of apical markers (Lujan et al., 2017). Collectively, all of these studies suggest that midbody might act as an active signal unit to regulate apical polarity and formation of apical surface.

Numerous recent studies have recognized the potential roles of midbody post-abscission. However, midbody fate post-abscission and the explicit function of the midbody or the midbody remnant during lumenogenesis remained unexplored. In our

125

study, we realized that the midbody flank structure persists for a long time at the apical surface instead of being degraded. Interestingly, after midbody movement, we observed RAB-11 and AIR-2 are recruited to apical surface, suggesting a role of the midbody or midbody remnant after cell division in polarity maintenance or regulating the apical surface through generating apical membrane.

Other questions that must be answered so that we fully understand the function of the midbody are: 1) what regions of the midbody execute delivery of membrane components to target position and 2) which midbody proteins are involved in transportation? In our study, we observed that midbody ring markers, such as central spindle regulators MKLP-1/ZEN-4, were internalized into the cytosol and degraded quickly after cytokinesis. However, we were unable to delineate the details of how the midbody ring was severed and internalized due to the resolution limit of light microscopy. One hypothesis is that the midbody ring structure may be cut from the plasma membrane by the assistance of ESCRT proteins. However, the flanking proteins, such as Aurora B kinase and microtubules, somehow persist at apical surface after midbody movement. Structured illumination microscopy (SIM), and electron microscopy will be used to define the ultrastructural details of this process.

Based on previous ultrastructural analysis of the midbody, we know that the midbody is a plastic proteinaceous scaffold. To date, about three hundred midbody proteins, including a large number of kinases and phosphatases, have been identified by mass spectrometry, immunostaining, and other biochemical assays (Chen et al., 2009; Huang

et al., 2015; Skop et al., 2004). If the midbody plays key signaling roles in maintaining

epithelial polarity or initiating the architecture of apical surface, it would be of great

interest to identify midbody-dependent signaling pathways post-mitosis. In our study, we

observed an interesting pattern of Aurora B kinase during midbody migration and

location on apical structure. Aurora B regulates a number of cytoskeletal regulators

during cytokinesis that control cell shape (Ferreira et al., 2013; Floyd et al., 2013; Goto

et al., 2003; Kettenbach et al., 2011), and it will be interesting to determine whether any

are involved with the events we observed. Additionally, Aurora B specifically

phosphorylates intermediate filaments at the cleavage furrow (Izawa and Inagaki, 2006;

Kawajiri et al., 2003). Therefore, Aurora B kinase may rely on its phosphorylation to

putative substrates to regulate cytoskeleton components during tissue morphogenesis.

Given that the major components of a few signaling pathways have been identified in

the midbody, it is likely that these pathways play some roles in post-mitotic midbody

activity. For example, several key components of the Wnt signaling pathway, including

catenin and Frizzled, localize and persist at the midbody (Fumoto et al., 2012; Kaplan et

al., 2004). The Wnt signaling pathway is extensively studied for cell migration and stem

cell fate specification through the asymmetric distribution of signaling components to

activate downstream signaling (Clevers et al., 2014). Therefore, it is plausible to

speculate that the midbody may recruit lipid-modified Wnt proteins to activate

downstream signaling once the midbody reaches the apical surface to regulate apical

membrane fusion or degradation of the midbody. Another interesting finding is that

several receptors of stem-cell mesenchymal-related Chemokin signaling pathway have

been found in the midbody (Andreas et al., 2014; Cho and Kehrl, 2007; Dionne et al., 2015; Naito et al., 2006). Chemokin signaling should be considered as a candidate pathway for the midbody to regulate the mesenchymal-to-epithelial transition in the intestinal or pharyngeal tissues that we observed. Lastly, a set of MAP kinases is associated with the midbody; however, the function and regulation of MAP kinase activity in midbody fate are not well understood (Kasahara et al., 2007; Willard and Crouch, 2001). Collectively, the post mitotic midbody may regulate fundamental biological events via many signaling components. However, the multiple functions of these signaling components in other cellular events become an arduous limit to specifically understand midbody-related signaling. For example, Aurora B kinase performs critical roles in chromosome segregation, cytokinesis, and other cellular events in the early embryo. Therefore, deciphering their midbody-specific roles requires an innovative and lineage-specific protein degradation system, which is suitable to inactivate midbody proteins such as Aurora B kinase during a specific cell division.

We observed novel midbody migration events during neuronal precursor cell divisions. Not only would this add further support for the idea that our midbody migration pattern occurs during the terminal cell division in invariant lineage, but this would also highlight the possibility that midbody may deliver identical signaling components in different tissues. During epithelial and neuronal morphogenesis, the midbody plays an identical role to maintain tissue polarity(Li et al., 2014; Pollarolo et al., 2011; Singh and Pohl, 2014), however neuronal sensilla have unique gene expression program compared with digestive tract tissues. For example, the extracellular matrix proteins, DEX-1 and DYF-7

are expressed at the tip of amphid dendritic tips to anchor the neuronal cells at the tip of the embryo (Heiman and Shaham, 2009). Interestingly, midbody formed in neuroepithelial cells release the stem cell marker Prominin in neural tube fluid, which potentially influences cell proliferation and differentiation (Dubreuil et al., 2007). Therefore, further study is required to define the molecular contributions provided by the midbody as well as midbody-dependent signaling pathways to different epithelial and neuronal-epithelial structures.

In our study, we have shown a stereotypical migration pattern of the midbody and centrosome in different tissues and that centrosome marker gamma tubulin persists at the apical surface of the intestine, pharynx and sensilla dendrites. Therefore, multiple microtubule-based organelles may contribute to the final architecture of the apical surface. The centrosome and the midbody may work as supplementary machinery during ciliogenesis and establishing the architecture of apical surfaces. However, the interaction and precise coordination mechanisms between midbody and centrosome/centriole to control cellular organization and tissue morphogenesis remain to be elucidated. In stem cells, midbody inheritance depends on mother centriole inheritance (Kuo et al., 2011). RAB-11/FIP3 endosomes may play a critical role in the midbody-centrosome collaboration since RAB-11 positive vesicles accumulate around the centriole at metaphase, and translocate to the cleavage furrow during cytokinesis (Schiel et al., 2011; Schiel et al., 2012). This translocation may determine midbody fate during abscission. Inhibition of RAB-11 translocation may provide feedback signals to the centrioles or centrosome to activate these complementary roles in tissue

development. Therefore, additional studies, including comparative proteomic and transcriptomic analysis of the midbody and the centrosome in different tissues and cell types will be required to fully understand the roles of these organelles during development.

Ultimately, we observed that AIR-2 localizes to the tip of the dendritic extension and labels a substantial portion of the dendrite post mitosis. Inactivation of Aurora B kinase post-mitosis disrupts tissue morphogenesis. Recent studies showed that inhibition of Aurora B kinase in mouse embryos caused the loss of midbody derived interphase bridges and significant reduction of RAB-11 and cell adhesion molecules during apical membrane formation. Additionally, loss of Aurora B kinase causes aberrant neuronal axon morphology, and overexpression of Aurora B causes extended axonal outgrowth in Zebrafish (Gwee et al., 2018). Therefore, these results implied that Aurora B kinase may regulate neuronal and epithelial development after abscission. As a component of the chromosomal passenger complex, Aurora B kinase requires other components, such as BIR-1 (Survivin), for its localization at cytoskeletal structures and chromosome in *C. elegans* (Adams et al., 2001). It is well studied that Aurora B specifically phosphorylates intermediate filament at the cleavage furrow (Izawa and Inagaki, 2006; Kawajiri et al., 2003). We also observed that inactivation of Aurora B kinase disrupts tubulin localization at the central spindle region during midbody movement. Therefore, Aurora B kinase may rely on its phosphorylation to putative substrates to regulate cytoskeleton components during tissue morphogenesis instead of CPC complex-

dependent regulation. Identification of the phosphorylation substrates of Aurora B

kinase at the apical surface after abscission will be a major focus of future studies.

In conclusion, our study casts light on the protease activity of separase during

exocytosis, suggesting that an unknown substrate might be involved in separase

regulation of exocytosis and cytokinesis. Our observations of variations in cytokinesis in

the *C. elegans* invariant lineage highlight the complexity of proper execution of

cytokinesis and determination of cell fate. Additionally, the novel midbody inheritance

patterns in different tissues scratches the surface of the post-mitotic function of the

midbody and led us to postulate that the midbody can function as a transportation tool

for the delivery of signaling molecules or proteins to nascent apical positions. More

studies in this newly emerging field are needed to better understand the role of the

midbody during development and the link between cell division and morphogenesis.

LIST OF REFERENCE

Adams, R.R., Carmena, M., and Earnshaw, W.C. (2001). Chromosomal passengers and the (aurora) ABCs of mitosis. Trends Cell Biol *11*, 49-54.

Agromayor, M., and Martin-Serrano, J. (2013). Knowing when to but and run: mechanisms that control cytokinetic abscission. Trends Cell Biol *23*, 433-441.

Albertson, D.G., and Thomson, J.N. (1982). The Kinetochores of Caenorhabditis-Elegans. Chromosoma *86*, 409-428.

Albertson, R., Riggs, B., and Sullivan, W. (2005). Membrane traffic: a driving force in cytokinesis. Trends Cell Biol *15*, 92-101.

Andreas, K., Sittinger, M., and Ringe, J. (2014). Toward in situ tissue engineering: chemokine-guided stem cell recruitment. Trends Biotechnol *32*, 483-492.

Archambault, V., and Carmena, M. (2012). Polo-like kinase-activating kinases. Cell Cycle *11*, 1490-1495.

Bacac, M., Fusco, C., Planche, A., Santodomingo, J., Demaurex, N., Leemann-Zakaryan, R., Provero, P., and Stamenkovic, I. (2011). Securin and Separase Modulate Membrane Traffic by Affecting Endosomal Acidification. Traffic *12*, 615-626.

Bai, X., and Bembenek, J.N. (2017a). Orchestrating early embryonic divisions. Mol Reprod Dev.

Bai, X.F., and Bembenek, J.N. (2017b). Protease dead separase inhibits chromosome segregation and RAB-11 vesicle trafficking. Cell Cycle *16*, 1902-1917.

Ban, R., Irino, Y., Fukami, K., and Tanaka, H. (2004). Human mitotic spindle-associated protein PRC1 inhibits MgcRacGAP activity toward Cdc42 during the metaphase. J Biol Chem *279*, 16394-16402.

Bembenek, J.N., Richie, C.T., Squirrell, J.M., Campbell, J.M., Eliceiri, K.W., Poteryaev, D., Spang, A., Golden, A., and White, J.G. (2007). Cortical granule exocytosis in C-elegans is regulated by cell cycle components including separase. Development *134*, 3837-3848.

Bembenek, J.N., Verbrugghe, K.J.C., Khanikar, J., Csankovszki, G., and Chan, R.C. (2013). Condensin and the Spindle Midzone Prevent Cytokinesis Failure Induced by Chromatin Bridges in C. elegans Embryos. Curr Biol *23*, 937-946.

Bembenek, J.N., White, J.G., and Zheng, Y.X. (2010). A Role for Separase in the Regulation of RAB-11-Positive Vesicles at the Cleavage Furrow and Midbody. Curr Biol *20*, 259-264.

Bernabe-Rubio, M., Andres, G., Casares-Arias, J., Fernandez-Barrera, J., Rangel, L., Reglero-Real, N., Gershlick, D.C., Fernandez, J.J., Millan, J., Correas, I.*, et al.* (2016). Novel role for the midbody in primary ciliogenesis by polarized epithelial cells. J Cell Biol *214*, 259-273.

Boland, A., Martin, T.G., Zhang, Z.G., Yang, J., Bai, X.C., Chang, L.F., Scheres, S.H.W., and Barford, D. (2017). Cryo-EM structure of a metazoan separase-securin complex at near-atomic resolution. Nat Struct Mol Biol *24*, 414-+.

Boucrot, E., and Kirchhausen, T. (2007). Endosomal recycling controls plasma membrane area during mitosis. P Natl Acad Sci USA *104*, 7939-7944.

Bringmann, H., and Hyman, A.A. (2005). A cytokinesis furrow is positioned by two consecutive signals. Nature *436*, 731-734.

Bryant, D.M., Datta, A., Rodriguez-Fraticelli, A.E., Peranen, J., Martin-Belmonte, F., and Mostov, K.E. (2010). A molecular network for de novo generation of the apical surface and lumen. Nat Cell Biol *12*, 1035-U1024.

Cabral, G., Sans, S.S., Cowan, C.R., and Dammermann, A. (2013). Multiple Mechanisms Contribute to Centriole Separation in C. elegans. Curr Biol *23*, 1380-1387.

Campa, C.C., and Hirsch, E. (2017). Rab11 and phosphoinositides: A synergy of signal transducers in the control of vesicular trafficking. Adv Biol Regul *63*, 132-139.

Carlton, J.G., Caballe, A., Agromayor, M., Kloc, M., and Martin-Serrano, J. (2012). ESCRT-III Governs the Aurora B-Mediated Abscission Checkpoint Through CHMP4C. Science *336*, 220-225.

Carmena, M., Earnshaw, W.C., and Glover, D.M. (2015). The Dawn of Aurora Kinase Research: From Fly Genetics to the Clinic. Front Cell Dev Biol *3*, 73.

Carmena, M., Wheelock, M., Funabiki, H., and Earnshaw, W.C. (2012). The chromosomal passenger complex (CPC): from easy rider to the godfather of mitosis. Nat Rev Mol Cell Bio *13*, 789-803.

Chen, B.C., Legant, W.R., Wang, K., Shao, L., Milkie, D.E., Davidson, M.W., Janetopoulos, C., Wu, X.F.S., Hammer, J.A., Liu, Z.*, et al.* (2014). Lattice light-sheet microscopy: Imaging molecules to embryos at high spatiotemporal resolution. Science *346*, 439-+.

Chen, C.T., Ettinger, A.W., Huttner, W.B., and Doxsey, S.J. (2013). Resurrecting remnants: the lives of post-mitotic midbodies. Trends Cell Biol *23*, 118-128.

Chen, T.C., Lee, S.A., Hong, T.M., Shih, J.Y., Lai, J.M., Chiou, H.Y., Yang, S.C., Chan, C.H., Kao, C.Y., Yang, P.C.*, et al.* (2009). From midbody protein-protein interaction network construction to novel regulators in cytokinesis. J Proteome Res *8*, 4943-4953.

Chin, C.F., Bennett, A.M., Ma, W.K., Hall, M.C., and Yeong, F.M. (2012). Dependence of Chs2 ER export on dephosphorylation by cytoplasmic Cdc14 ensures that septum formation follows mitosis. Mol Biol Cell *23*, 45-58.

Cho, H., and Kehrl, J.H. (2007). Localization of Gi alpha proteins in the centrosomes and at the midbody: implication for their role in cell division. J Cell Biol *178*, 245-255.

Clevers, H., Loh, K.M., and Nusse, R. (2014). An integral program for tissue renewal and regeneration: Wnt signaling and stem cell control. Science *346*, 54-+.

Crowell, E.F., Gaffuri, A.L., Gayraud-Morel, B., Tajbakhsh, S., and Echard, A. (2014). Engulfment of the midbody remnant after cytokinesis in mammalian cells. J Cell Sci *127*, 3840-3851.

D'Avino, P.P., and Capalbo, L. (2016). Regulation of midbody formation and function by mitotic kinases. Semin Cell Dev Biol *53*, 57-63.

D'Avino, P.P., Giansanti, M.G., and Petronczki, M. (2015). Cytokinesis in Animal Cells. Csh Perspect Biol *7*.

Dammermann, A., Pemble, H., Mitchell, B.J., McLeod, I., Yates, J.R., Kintner, C., Desai, A.B., and Oegema, K. (2009). The hydrolethalus syndrome protein HYLS-1 links core centriole structure to cilia formation. Gene Dev *23*, 2046-2059.

Das, T., Payer, B., Cayouette, M., and Harris, W.A. (2003). In vivo time-lapse imaging of cell divisions during neurogenesis in the developing zebrafish retina. Neuron *37*, 597-609.

Dionne, L.K., Wang, X.J., and Prekeris, R. (2015). Midbody: from cellular junk to regulator of cell polarity and cell fate. Curr Opin Cell Biol *35*, 51-58.

Dubreuil, V., Marzesco, A.M., Corbeil, D., Huttner, W.B., and Wilsch-Brauninger, M. (2007). Midbody and primary cilium of neural progenitors release extracellular membrane particles enriched in the stem cell marker prominin-1. J Cell Biol *176*, 483-495.

El Amine, N., Kechad, A., Jananji, S., and Hickson, G.R. (2013). Opposing actions of septins and Sticky on Anillin promote the transition from contractile to midbody ring. J Cell Biol *203*, 487-504.

Ettinger, A.W., Wilsch-Brauninger, M., Marzesco, A.M., Bickle, M., Lohmann, A., Maliga, Z., Karbanova, J., Corbeil, D., Hyman, A.A., and Huttner, W.B. (2011). Proliferating versus differentiating stem and cancer cells exhibit distinct midbody-release behaviour. Nat Commun *2*, 503.

Fabbro, M., Zhou, B.B., Takahashi, M., Sarcevic, B., Lal, P., Graham, M.E., Gabrielli, B.G., Robinson, P.J., Nigg, E.A., Ono, Y.*, et al.* (2005). Cdk1/Erk2- and Plk1-dependent phosphorylation of a centrosome protein, Cep55, is required for its recruitment to midbody and cytokinesis. Dev Cell *9*, 477-488.

Feldman, J.L., and Priess, J.R. (2012). A role for the centrosome and PAR-3 in the hand-off of MTOC function during epithelial polarization. Curr Biol *22*, 575-582.

Ferreira, J.G., Pereira, A.J., Akhmanova, A., and Maiato, H. (2013). Aurora B spatially regulates EB3 phosphorylation to coordinate daughter cell adhesion with cytokinesis. J Cell Biol *201*, 709-724.

Fletcher, A.I., Shuang, R.Q., Giovannucci, D.R., Zhang, L., Bittner, M.A., and Stuenkel, E.L. (1999). Regulation of exocytosis by cyclin-dependent kinase 5 via phosphorylation of Munc18. Journal of Biological Chemistry *274*, 4027-4035.

Floyd, S., Whiffin, N., Gavilan, M.P., Kutscheidt, S., De Luca, M., Marcozzi, C., Min, M., Watkins, J., Chung, K., Fackler, O.T.*, et al.* (2013). Spatiotemporal organization of Aurora-B by APC/CCdh1 after mitosis coordinates cell spreading through FHOD1. J Cell Sci *126*, 2845-2856.

Fox, D.T., and Duronio, R.J. (2013). Endoreplication and polyploidy: insights into development and disease. Development *140*, 3-12.

Fumoto, K., Kikuchi, K., Gon, H., and Kikuchi, A. (2012). Wnt5a signaling controls cytokinesis by correctly positioning ESCRT-III at the midbody. J Cell Sci *125*, 4822-4832.

Glotzer, M. (2009). The 3Ms of central spindle assembly: microtubules, motors and MAPs. Nat Rev Mol Cell Biol *10*, 9-20.

Gonczy, P., Schnabel, H., Kaletta, T., Amores, A.D., Hyman, T., and Schnabel, R. (1999). Dissection of cell division processes in the one cell stage Caenorhabditis elegans embryo by mutational analysis. J Cell Biol *144*, 927-946.

Gorr, I.H., Boos, D., and Stemmann, O. (2005). Mutual inhibition of separase and Cdk1 by two-step complex formation. Mol Cell *19*, 135-141.

Gorr, I.H., Reis, A., Boos, D., Wuhr, M., Madgwick, S., Jones, K.T., and Stemmann, O. (2006). Essential CDK1-inhibitory role for separase during meiosis I in vertebrate oocytes. Nat Cell Biol *8*, 1035-U1120.

Goto, H., Yasui, Y., Kawajiri, A., Nigg, E.A., Terada, Y., Tatsuka, M., Nagata, K., and Inagaki, M. (2003). Aurora-B regulates the cleavage furrow-specific vimentin phosphorylation in the cytokinetic process. J Biol Chem *278*, 8526-8530.

Green, R.A., Mayers, J.R., Wang, S., Lewellyn, L., Desai, A., Audhya, A., and Oegema, K. (2013). The midbody ring scaffolds the abscission machinery in the absence of midbody microtubules. J Cell Biol *203*, 505-520.

Green, R.A., Paluch, E., and Oegema, K. (2012). Cytokinesis in Animal Cells. Annu Rev Cell Dev Bi *28*, 29-+.

Greenbaum, M.P., Ma, L., and Matzuk, M.M. (2007). Conversion of midbodies into germ cell intercellular bridges. Developmental Biology *305*, 389-396.

Gruneberg, U., Neef, R., Honda, R., Nigg, E.A., and Barr, F.A. (2004). Relocation of Aurora B from centromeres to the central spindle at the metaphase to anaphase transition requires MKlp2. J Cell Biol *166*, 167-172.

Guillot, C., and Lecuit, T. (2013). Adhesion Disengagement Uncouples Intrinsic and Extrinsic Forces to Drive Cytokinesis in Epithelial Tissues. Dev Cell *24*, 227-241.

Guizetti, J., Schermelleh, L., Mantler, J., Maar, S., Poser, I., Leonhardt, H., Muller-Reichert, T., and Gerlich, D.W. (2011). Cortical constriction during abscission involves helices of ESCRT-III-dependent filaments. Science *331*, 1616-1620.

Gwee, S.S.L., Radford, R.A.W., Chow, S., Syal, M.D., Morsch, M., Formella, I., Lee, A., Don, E.K., Badrock, A.P., Cole, N.J.*, et al.* (2018). Aurora kinase B regulates axonal outgrowth and regeneration in the spinal motor neurons of developing zebrafish. Cell Mol Life Sci.

Haglund, K., Nezis, I.P., and Stenmark, H. (2011). Structure and functions of stable intercellular bridges formed by incomplete cytokinesis during development. Commun Integr Biol *4*, 1-9.

Hardin, J., King, R., Thomas-Virnig, C., and Raich, W.B. (2008). Zygotic loss of ZEN-4/MKLP1 results in disruption of epidermal morphogenesis in the C. elegans embryo. Dev Dyn *237*, 830-836.

Hauf, S., Waizenegger, I.C., and Peters, J.M. (2001). Cohesin cleavage by separase required for anaphase and cytokinesis in human cells. Science *293*, 1320-1323.

Hedgecock, E.M., and White, J.G. (1985). Polyploid Tissues in the Nematode Caenorhabditis-Elegans. Developmental Biology *107*, 128-133.

Hehnly, H., Chen, C.T., Powers, C.M., Liu, H.L., and Doxsey, S. (2012). The Centrosome Regulates the Rab11-Dependent Recycling Endosome Pathway at Appendages of the Mother Centriole. Curr Biol *22*, 1944-1950.

Heiman, M.G., and Shaham, S. (2009). DEX-1 and DYF-7 establish sensory dendrite length by anchoring dendritic tips during cell migration. Cell *137*, 344-355.

Hellmuth, S., Pohlmann, C., Brown, A., Bottger, F., Sprinzl, M., and Stemmann, O. (2015). Positive and Negative Regulation of Vertebrate Separase by Cdk1-Cyclin B1 May Explain Why Securin Is Dispensable. Journal of Biological Chemistry *290*, 8002-8010.

Herszterg, S., Leibfried, A., Bosveld, F., Martin, C., and Bellaiche, Y. (2013). Interplay between the Dividing Cell and Its Neighbors Regulates Adherens Junction Formation during Cytokinesis in Epithelial Tissue. Dev Cell *24*, 256-270.

Herszterg, S., Pinheiro, D., and Bellaiche, Y. (2014). A multicellular view of cytokinesis in epithelial tissue. Trends Cell Biol *24*, 285-293.

Herzog, F., Primorac, I., Dube, P., Lenart, P., Sander, B., Mechtler, K., Stark, H., and Peters, J.M. (2009). Structure of the Anaphase-Promoting Complex/Cyclosome Interacting with a Mitotic Checkpoint Complex. Science *323*, 1477-1481.

Hime, G.R., Brill, J.A., and Fuller, M.T. (1996). Assembly of ring canals in the male germ line from structural components of the contractile ring. Journal of Cell Science *109*, 2779-2788.

Holland, A.J., Bottger, F., Stemmann, O., and Taylor, S.S. (2007). Protein phosphatase 2A and separase form a complex regulated by separase autocleavage. Journal of Biological Chemistry *282*, 24623-24632.

Hu, C.K., Coughlin, M., and Mitchison, T.J. (2012). Midbody assembly and its regulation during cytokinesis. Mol Biol Cell *23*, 1024-1034.

Huang, Z.N., Ma, L.L., Wang, Y.B., Pan, Z.C., Ren, J., Liu, Z.X., and Xue, Y. (2015). MiCroKiTS 4.0: a database of midbody, centrosome, kinetochore, telomere and spindle. Nucleic Acids Res *43*, D328-D334.

Izawa, I., and Inagaki, M. (2006). Regulatory mechanisms and functions of intermediate filaments: A study using site- and phosphorylation state-specific antibodies. Cancer Sci *97*, 167-174.

Jaffe, A.B., Kaji, N., Durgan, J., and Hall, A. (2008). Cdc42 controls spindle orientation to position the apical surface during epithelial morphogenesis. J Cell Biol *183*, 625-633.

Jakobsen, M.K., Cheng, Z.L., Lam, S.K., Roth-Johnson, E., Barfield, R.M., and Schekman, R. (2013). Phosphorylation of Chs2p regulates interaction with COPII. J Cell Sci *126*, 2151-2156.

Jantsch-Plunger, V., and Glotzer, M. (1999). Depletion of syntaxins in the early Caenorhabditis elegans embryo reveals a role for membrane fusion events in cytokinesis. Curr Biol *9*, 738-745.

Jordan, S.N., and Canman, J.C. (2012). Rho GTPases in Animal Cell Cytokinesis: An Occupation by the One Percent. Cytoskeleton *69*, 919-930.

Kachur, T.M., Audhya, A., and Pilgrim, D.B. (2008). UNC-45 is required for NMY-2 contractile function in early embryonic polarity establishment and germline cellularization in C-elegans. Dev Biol *314*, 287-299.

Kaplan, D.D., Meigs, T.E., Kelly, P., and Casey, P.J. (2004). Identification of a role for beta-catenin in the establishment of a bipolar mitotic spindle. J Biol Chem *279*, 10829-10832.

Kasahara, K., Nakayama, Y., Nakazato, Y., Ikeda, K., Kuga, T., and Yamaguchi, N. (2007). Src signaling regulates completion of abscission in cytokinesis through ERK/MAPK activation at the midbody. J Biol Chem *282*, 5327-5339.

Kawajiri, A., Yasui, Y., Goto, H., Tatsuka, M., Takahashi, M., Nagata, K., and Inagaki, M. (2003). Functional significance of the specific sites phosphorylated in desmin at cleavage

furrow: Aurora-B may phosphorylate and regulate type III intermediate filaments during cytokinesis coordinatedly with Rho-kinase. Mol Biol Cell *14*, 1489-1500.

Kettenbach, A.N., Schweppe, D.K., Faherty, B.K., Pechenick, D., Pletnev, A.A., and Gerber, S.A. (2011). Quantitative Phosphoproteomics Identifies Substrates and Functional Modules of Aurora and Polo-Like Kinase Activities in Mitotic Cells. Sci Signal *4*.

Kieserman, E.K., Glotzer, M., and Wallingford, J.B. (2008). Developmental regulation of central spindle assembly and cytokinesis during vertebrate embryogenesis. Curr Biol *18*, 116-123.

Kimura, K., and Kimura, A. (2012). Rab6 is required for the exocytosis of cortical granules and the recruitment of separase to the granules during the oocyte-to-embryo transition in Caenorhabditis elegans. J Cell Sci *125*, 5897-5905.

Konig, J., Frankel, E.B., Audhya, A., and Muller-Reichert, T. (2017). Membrane remodeling during embryonic abscission in Caenorhabditis elegans. J Cell Biol.

Kosodo, Y., Roper, K., Haubensak, W., Marzesco, A.M., Corbeil, D., and Huttner, W.B. (2004). Asymmetric distribution of the apical plasma membrane during neurogenic divisions of mammalian neuroepithelial cells. Embo J *23*, 2314-2324.

Kosodo, Y., Toida, K., Dubreuil, V., Alexandre, P., Schenk, J., Kiyokage, E., Attardo, A., Mora-Bermudez, F., Arii, T., Clarke, J.D.W.*, et al.* (2008). Cytokinesis of neuroepithelial cells can divide their basal process before anaphase. Embo J *27*, 3151-3163.

Krenn, V., and Musacchio, A. (2015). The Aurora B kinase in chromosome bi-orientation and spindle checkpoint signaling. Front Oncol *5*.

Kudo, N.R., Wassmann, K., Anger, M., Schuh, M., Wirth, K.G., Xu, H.L., Helmhart, W., Kudo, H., Mckay, M., Maro, B.*, et al.* (2006). Resolution of chiasmata in oocytes requires separase-mediated proteolysis. Cell *126*, 135-146.

Kuilman, T., Maiolica, A., Godfrey, M., Scheidel, N., Aebersold, R., and Uhlmann, F. (2015). Identification of Cdk targets that control cytokinesis. Embo J *34*, 81-96.

Kuo, T.C., Chen, C.T., Baron, D., Onder, T.T., Loewer, S., Almeida, S., Weismann, C.M., Xu, P., Houghton, J.M., Gao, F.B.*, et al.* (2011). Midbody accumulation through evasion of autophagy contributes to cellular reprogramming and tumorigenicity (vol 13, pg 1214, 2011). Nat Cell Biol *13*, 1467-1467.

Lacroix, B., and Maddox, A.S. (2012). Cytokinesis, ploidy and aneuploidy. J Pathol *226*, 338-351.

Lampson, M.A., and Cheeseman, I.M. (2011). Sensing centromere tension: Aurora B and the regulation of kinetochore function. Trends Cell Biol *21*, 133-140.

Lara-Gonzalez, P., Westhorpe, F.G., and Taylor, S.S. (2012). The spindle assembly checkpoint. Curr Biol *22*, R966-980.

Lee, K., and Rhee, K. (2012). Separase-dependent cleavage of pericentrin B is necessary and sufficient for centriole disengagement during mitosis. Cell Cycle *11*, 2476-2485.

Leung, B., Hermann, G.J., and Priess, J.R. (1999). Organogenesis of the Caenorhabditis elegans intestine. Dev Biol *216*, 114-134.

Li, D.Y., Mangan, A., Cicchini, L., Margolis, B., and Prekeris, R. (2014). FIP5 phosphorylation during mitosis regulates apical trafficking and lumenogenesis. Embo Rep *15*, 428-437.

Li, R. (2007). Cytokinesis in development and disease: variations on a common theme. Cell Mol Life Sci *64*, 3044-3058.

Lin, Z., Luo, X., and Yu, H. (2016). Structural basis of cohesin cleavage by separase. Nature *532*, 131-134.

Linkert, M., Rueden, C.T., Allan, C., Burel, J.M., Moore, W., Patterson, A., Loranger, B., Moore, J., Neves, C., MacDonald, D*., et al.* (2010). Metadata matters: access to image data in the real world. J Cell Biol *189*, 777-782.

Lu, Y., and Cross, F. (2009). Mitotic Exit in the Absence of Separase Activity. Mol Biol Cell *20*, 1576-1591.

Lujan, P., Rubio, T., Varsano, G., and Kohn, M. (2017). Keep it on the edge: The post-mitotic midbody as a polarity signal unit. Commun Integr Biol *10*, e1338990.

Lujan, P., Varsano, G., Rubio, T., Hennrich, M.L., Sachsenheimer, T., Galvez-Santisteban, M., Martin-Belmonte, F., Gavin, A.C., Brugger, B., and Kohn, M. (2016). Phosphatase of regenerating liver (PRL)-3 disrupts epithelial architecture by altering the post-mitotic midbody position. J Cell Sci.

Luo, S., and Tong, L. (2017). Molecular mechanism for the regulation of yeast separase by securin. Nature *542*, 255-259.

Maddox, A.S., Habermann, B., Desai, A., and Oegema, K. (2005). Distinct roles for two C-elegans anillins in the gonad and early embryo. Development *132*, 2837-2848.

Maddox, A.S., Lewellyn, L., Desai, A., and Oegema, K. (2007). Anillin and the septins promote asymmetric ingression of the cytokinetic furrow. Dev Cell *12*, 827-835.

Malsam, J., Kreye, S., and Sollner, T.H. (2008). Membrane fusion: SNAREs and regulation. Cell Mol Life Sci *65*, 2814-2832.

Mathieu, J., Cauvin, C., Moch, C., Radford, S.J., Sampaio, P., Perdigoto, C.N., Schweisguth, F., Bardin, A.J., Sunkel, C.E., Mckim, K*., et al.* (2013). Aurora B and Cyclin B Have Opposite

Effects on the Timing of Cytokinesis Abscission in Drosophila Germ Cells and in Vertebrate Somatic Cells. Dev Cell *26*, 250-265.

Matsuo, K., Ohsumi, K., Iwabuchi, M., Kawamata, T., Ono, Y., and Takahashi, M. (2012). Kendrin Is a Novel Substrate for Separase Involved in the Licensing of Centriole Duplication. Curr Biol *22*, 915-921.

McCarter, J., Bartlett, B., Dang, T., and Schedl, T. (1999). On the control of oocyte meiotic maturation and ovulation in Caenorhabditis elegans. Dev Biol *205*, 111-128.

McLachlan, I.G., and Heiman, M.G. (2013). Shaping dendrites with machinery borrowed from epithelia. Curr Opin Neurobiol *23*, 1005-1010.

McLean, P.F., and Cooley, L. (2013). Protein Equilibration Through Somatic Ring Canals in Drosophila. Science *340*, 1445-1447.

Melesse, M., Sloan, D.E., Benthal, J.T., Caylor, Q., Gosine, K., Bai, X.F., and Bembenek, J.N. (2018). Genetic Identification of Separase Regulators in Caenorhabditis elegans. G3-Genes Genom Genet *8*, 695-705.

Mierzwa, B., and Gerlich, D.W. (2014). Cytokinetic Abscission: Molecular Mechanisms and Temporal Control. Dev Cell *31*, 525-538.

Miller, D.P., Hall, H., Chaparian, R., Mara, M., Mueller, A., Hall, M.C., and Shannon, K.B. (2015). Dephosphorylation of Iqg1 by Cdc14 regulates cytokinesis in budding yeast. Mol Biol Cell *26*, 2913-2926.

Mishima, M., Pavicic, V., Gruneberg, U., Nigg, E.A., and Glotzer, M. (2004). Cell cycle regulation of central spindle assembly. Nature *430*, 908-913.

Mitchell, D.M., Uehlein-Klebanow, L.R., and Bembenek, J.N. (2014). Protease-Dead Separase Is Dominant Negative in the C. elegans Embryo. Plos One *9*.

Mito, Y., Sugimoto, A., and Yamamoto, M. (2003). Distinct developmental function of two Caenorhabditis elegans homologs of the cohesin subunit Scc1/Rad21. Mol Biol Cell *14*, 2399-2409.

Monen, J., Hattersley, N., Muroyama, A., Stevens, D., Oegema, K., and Desai, A. (2015). Separase Cleaves the N-Tail of the CENP-A Related Protein CPAR-1 at the Meiosis I Metaphase-Anaphase Transition in C-elegans. Plos One *10*.

Morais-de-Sa, E., and Sunkel, C. (2013). Adherens junctions determine the apical position of the midbody during follicular epithelial cell division. Embo Rep *14*, 696-703.

Moschou, P.N., Smertenko, A.P., Minina, E.A., Fukada, K., Savenkov, E.I., Robert, S., Hussey, P.J., and Bozhkov, P.V. (2014). The caspase-related protease separase (extra spindle poles)

regulates cell polarity and cytokinesis in Arabidopsis (vol 25, pg 2171, 2013). Plant Cell *26*, 3823-3823.

Mullins, J.M., and Biesele, J.J. (1977). Terminal Phase of Cytokinesis in D-98s Cells. J Cell Biol *73*, 672-684.

Naito, Y., Okada, M., and Yagisawa, H. (2006). Phospholipase C isoforms are localized at the cleavage furrow during cytokinesis. J Biochem *140*, 785-791.

Nasmyth, K., and Haering, C.H. (2009). Cohesin: Its Roles and Mechanisms. Annu Rev Genet *43*, 525-558.

Nechipurenko, I.V., Berciu, C., Sengupta, P., and Nicastro, D. (2017). Centriolar remodeling underlies basal body maturation during ciliogenesis in Caenorhabditis elegans. Elife *6*.

Norden, C., Mendoza, M., Dobbelaere, J., Kotwaliwale, C.V., Biggins, S., and Barral, Y. (2006). The NoCut pathway links completion of cytokinesis to spindle midzone function to prevent chromosome breakage. Cell *125*, 85-98.

Oegema, K., and Hyman, A.A. (2006). Cell division. WormBook : the online review of C elegans biology, 1-40.

Onn, I., Heidinger-Pauli, J.M., Guacci, V., Unal, E., and Koshland, D.E. (2008). Sister Chromatid Cohesion: A Simple Concept with a Complex Reality. Annu Rev Cell Dev Bi *24*, 105-129.

Ott, C.M. (2016). Midbody remnant licenses primary cilia formation in epithelial cells. J Cell Biol *214*, 237-239.

Ou, G.S., Gentili, C., and Gonczy, P. (2014). Stereotyped distribution of midbody remnants in early C. elegans embryos requires cell death genes and is dispensable for development. Cell Res *24*, 251-253.

Ou, G.S., Stuurman, N., D'Ambrosio, M., and Vale, R.D. (2010). Polarized Myosin Produces Unequal-Size Daughters During Asymmetric Cell Division. Science *330*, 677-680.

Overeem, A.W., Bryant, D.M., and van, I.S.C. (2015). Mechanisms of apical-basal axis orientation and epithelial lumen positioning. Trends Cell Biol *25*, 476-485.

Padmanabhan, A., and Zaidel-Bar, R. (2017). Non-junctional E-Cadherin Clusters Regulate the Actomyosin Cortex in the C. elegans Zygote. Mech Develop *145*, S85-S85.

Palani, S., Meitinger, F., Boehm, M.E., Lehmann, W.D., and Pereira, G. (2012). Cdc14-dependent dephosphorylation of Inn1 contributes to Inn1-Cyk3 complex formation. J Cell Sci *125*, 3091-3096.

Paolini, A., Duchemin, A.L., Albadri, S., Patzel, E., Bornhorst, D., Avalos, P.G., Lemke, S., Machate, A., Brand, M., Sel, S.*, et al.* (2015). Asymmetric inheritance of the apical domain and

self-renewal of retinal ganglion cell progenitors depend on Anillin function. Development *142*, 832-839.

Papi, M., Berdougo, E., Randall, C.L., Ganguly, S., and Jallepalli, P.V. (2005). Multiple roles for separase auto-cleavage during the G2/M transition. Nat Cell Biol *7*, 1029-U1144.

Peel, N., Iyer, J., Naik, A., Dougherty, M.P., Decker, M., and O'Connell, K.F. (2017). Protein Phosphatase 1 Down Regulates ZYG-1 Levels to Limit Centriole Duplication. PLoS genetics *13*, e1006543.

Perkins, L.A., Hedgecock, E.M., Thomson, J.N., and Culotti, J.G. (1986). Mutant Sensory Cilia in the Nematode Caenorhabditis-Elegans. Developmental Biology *117*, 456-487.

Pohl, C., and Bao, Z. (2010). Chiral forces organize left-right patterning in C. elegans by uncoupling midline and anteroposterior axis. Dev Cell *19*, 402-412.

Pollard, T.D. (2017). Nine unanswered questions about cytokinesis. J Cell Biol *216*, 3007-3016.

Pollarolo, G., Schulz, J.G., Munck, S., and Dotti, C.G. (2011). Cytokinesis remnants define first neuronal asymmetry in vivo. Nat Neurosci *14*, 1525-1533.

Portereiko, M.F., Saam, J., and Mango, S.E. (2004). ZEN-4/MKLP1 is required to polarize the foregut epithelium. Curr Biol *14*, 932-941.

Rasmussen, J.P., Feldman, J.L., Reddy, S.S., and Priess, J.R. (2013). Cell Interactions and Patterned Intercalations Shape and Link Epithelial Tubes in C. elegans. Plos Genetics *9*.

Rasmussen, J.P., Reddy, S.S., and Priess, J.R. (2012). Laminin is required to orient epithelial polarity in the C. elegans pharynx. Development *139*, 2050-2060.

Reinsch, S., and Karsenti, E. (1994). Orientation of Spindle Axis and Distribution of Plasma-Membrane Proteins during Cell-Division in Polarized Mdckii Cells. J Cell Biol *126*, 1509-1526.

Richie, C.T., Bembenek, J.N., Chestnut, B., Furuta, T., Schumacher, J.M., Wallenfang, M., and Golden, A. (2011). Protein phosphatase 5 is a negative regulator of separase function during cortical granule exocytosis in C. elegans. J Cell Sci *124*, 2903-2913.

Sakaguchi, A., Sato, M., Sato, K., Gengyo-Ando, K., Yorimitsu, T., Nakai, J., Hara, T., Sato, K., and Sato, K. (2015). REI-1 Is a Guanine Nucleotide Exchange Factor Regulating RAB-11 Localization and Function in C. elegans Embryos. Dev Cell *35*, 211-221.

Salzmann, V., Chen, C., Chiang, C.Y., Tiyaboonchai, A., Mayer, M., and Yamashita, Y.M. (2014). Centrosome-dependent asymmetric inheritance of the midbody ring in Drosophila germline stem cell division. Mol Biol Cell *25*, 267-275.

Sato, K., Norris, A., Sato, M., and Grant, B.D. (2014). C. elegans as a model for membrane traffic. WormBook : the online review of C elegans biology, 1-47.

Sato, M., Grant, B.D., Harada, A., and Sato, K. (2008). Rab11 is required for synchronous secretion of chondroitin proteoglycans after fertilization in Caenorhabditis elegans. J Cell Sci *121*, 3177-3186.

Schiel, J.A., Childs, C., and Prekeris, R. (2013). Endocytic transport and cytokinesis: from regulation of the cytoskeleton to midbody inheritance. Trends Cell Biol *23*, 319-327.

Schiel, J.A., Park, K., Morphew, M.K., Reid, E., Hoenger, A., and Prekeris, R. (2011). Endocytic membrane fusion and buckling-induced microtubule severing mediate cell abscission. J Cell Sci *124*, 1411-1424.

Schiel, J.A., and Prekeris, R. (2013). Membrane dynamics during cytokinesis. Curr Opin Cell Biol *25*, 92-98.

Schiel, J.A., Simon, G.C., Zaharris, C., Weisz, J., Castle, D., Wu, C.C., and Prekeris, R. (2012). FIP3-endosome-dependent formation of the secondary ingression mediates ESCRT-III recruitment during cytokinesis. Nat Cell Biol *14*, 1068-+.

Schindelin, J., Arganda-Carreras, I., Frise, E., Kaynig, V., Longair, M., Pietzsch, T., Preibisch, S., Rueden, C., Saalfeld, S., Schmid, B.*, et al.* (2012). Fiji: an open-source platform for biological-image analysis. Nat Methods *9*, 676-682.

Schink, K.O., and Stenmark, H. (2011). Cell differentiation: midbody remnants - junk or fate factors? Curr Biol *21*, R958-960.

Schluter, M.A., Pfarr, C.S., Pieczynski, J., Whiteman, E.L., Hurd, T.W., Fan, S.L., Liu, C.J., and Margolis, B. (2009). Trafficking of Crumbs3 during Cytokinesis Is Crucial for Lumen Formation. Mol Biol Cell *20*, 4652-4663.

Schockel, L., Mockel, M., Mayer, B., Boos, D., and Stemmann, O. (2011). Cleavage of cohesin rings coordinates the separation of centrioles and chromatids. Nat Cell Biol *13*, 966-972.

Schumacher, J.M., Golden, A., and Donovan, P.J. (1998). AIR-2: An Aurora/Ipl1-related protein kinase associated with chromosomes and midbody microtubules is required for polar body extrusion and cytokinesis in Caenorhabditis elegans embryos. J Cell Biol *143*, 1635-1646.

Schvarzstein, M., Pattabiraman, D., Bembenek, J.N., and Villeneuve, A.M. (2013). Meiotic HORMA domain proteins prevent untimely centriole disengagement during Caenorhabditis elegans spermatocyte meiosis. P Natl Acad Sci USA *110*, E898-E907.

Severson, A.F., Hamill, D.R., Carter, J.C., Schumacher, J., and Bowerman, B. (2000). The Aurora-related kinase AIR-2 recruits ZEN-4/CeMKLP1 to the mitotic spindle at metaphase and is required for cytokinesis. Curr Biol *10*, 1162-1171.

Siller, K.H., and Doe, C.Q. (2009). Spindle orientation during asymmetric cell division. Nat Cell Biol *11*, 365-374.

Singh, D., and Pohl, C. (2014). Coupling of Rotational Cortical Flow, Asymmetric Midbody Positioning, and Spindle Rotation Mediates Dorsoventral Axis Formation in C. elegans. Dev Cell *28*, 253-267.

Siomos, M.F., Badrinath, A., Pasierbek, P., Livingstone, D., White, J., Glotzer, M., and Nasmyth, K. (2001). Separase is required for chromosome segregation during meiosis I in Caenorhabditis elegans. Curr Biol *11*, 1825-1835.

Skop, A.R., Bergmann, D., Mohler, W.A., and White, J.G. (2001). Completion of cytokinesis in C-elegans requires a brefeldin A-sensitive membrane accumulation at the cleavage furrow apex. Curr Biol *11*, 735-746.

Skop, A.R., Liu, H., Yates, J., 3rd, Meyer, B.J., and Heald, R. (2004). Dissection of the mammalian midbody proteome reveals conserved cytokinesis mechanisms. Science *305*, 61-66.

Smith, K.P., Kieserman, E.K., Wang, P.I., Basten, S.G., Giles, R.H., Marcotte, E.M., and Wallingford, J.B. (2011). A Role for Central Spindle Proteins in Cilia Structure and Function. Cytoskeleton *68*, 112-124.

Stegmeier, F., Visintin, R., and Amon, A. (2002). Separase, polo kinase, the kinetochore protein Slk19 and Spo12 function in a network that controls Cdc14 localization during early anaphase. Cell *108*, 207-220.

Steigemann, P., Wurzenberger, C., Schmitz, M.H.A., Held, M., Guizetti, J., Maar, S., and Gerlich, D.W. (2009). Aurora B-Mediated Abscission Checkpoint Protects against Tetraploidization. Cell *136*, 473-484.

Stemmann, O., Zou, H., Gerber, S.A., Gygi, S.P., and Kirschner, M.W. (2001). Dual inhibition of sister chromatid separation at metaphase. Cell *107*, 715-726.

Stenmark, H. (2009). Rab GTPases as coordinators of vesicle traffic. Nat Rev Mol Cell Bio *10*, 513-525.

Sullivan, M., Hornig, N.C., Porstmann, T., and Uhlmann, F. (2004). Studies on substrate recognition by the budding yeast separase. The Journal of biological chemistry *279*, 1191-1196.

Sullivan, M., Lehane, C., and Uhlmann, F. (2001). Orchestrating anaphase and mitotic exit: separase cleavage and localization of Slk19. Nat Cell Biol *3*, 771-777.

Sullivan, M., and Uhlmann, F. (2003). A non-proteolytic function of separase links the onset of anaphase to mitotic exit. Nat Cell Biol *5*, 249-254.

Sulston, J.E., Schierenberg, E., White, J.G., and Thomson, J.N. (1983). The embryonic cell lineage of the nematode Caenorhabditis elegans. Dev Biol *100*, 64-119.

Sun, Y.X., Kucej, M., Fan, H.Y., Yu, H., Sun, Q.Y., and Zou, H. (2009). Separase Is Recruited to Mitotic Chromosomes to Dissolve Sister Chromatid Cohesion in a DNA-Dependent Manner. Cell *137*, 123-132.

Tang, J., Maximov, A., Shin, O.H., Dai, H., Rizo, J., and Sudhof, T.C. (2006). A complexin/synaptotagmin 1 switch controls fast synaptic vesicle exocytosis. Cell *126*, 1175-1187.

Tong, Y.G., and Burglin, T.R. (2010). Conditions for dye-filling of sensory neurons in Caenorhabditis elegans. J Neurosci Meth *188*, 58-61.

Tsou, M.F., and Stearns, T. (2006). Mechanism limiting centrosome duplication to once per cell cycle. Nature *442*, 947-951.

Uehara, R., Tsukada, Y., Kamasaki, T., Poser, I., Yoda, K., Gerlich, D.W., and Goshima, G. (2013). Aurora B and Kif2A control microtubule length for assembly of a functional central spindle during anaphase. J Cell Biol *202*, 623-636.

Uhlmann, F., Wernic, D., Poupart, M.A., Koonin, E.V., and Nasmyth, K. (2000). Cleavage of cohesin by the CD clan protease separin triggers anaphase in yeast. Cell *103*, 375-386.

Viadiu, H., Stemmann, O., Kirschner, M.W., and Walz, T. (2005). Domain structure of separase and its binding to securin as determined by EM. Nat Struct Mol Biol *12*, 552-553.

Von Stetina, S.E., Liang, J., Marnellos, G., and Mango, S.E. (2017). Temporal regulation of epithelium formation mediated by FoxA, MKLP1, MgcRacGAP, and PAR-6. Mol Biol Cell *28*, 2042-2065.

Waddle, J.A., Cooper, J.A., and Waterston, R.H. (1994). Transient localized accumulation of actin in Caenorhabditis elegans blastomeres with oriented asymmetric divisions. Development *120*, 2317-2328.

Waizenegger, I.C., Gimenez-Abian, J.F., Wernic, D., and Peters, J.M. (2002). Regulation of human separase by securin binding and autocleavage. Curr Biol *12*, 1368-1378.

Welz, T., Wellbourne-Wood, J., and Kerkhoff, E. (2014). Orchestration of cell surface proteins by Rab11. Trends Cell Biol *24*, 407-415.

Wessel, G.M., Brooks, J.M., Green, E., Haley, S., Voronina, E., Wong, J., Zaydfudim, V., and Conner, S. (2001). The biology of cortical granules. Int Rev Cytol *209*, 117-206.

Wickner, W., and Schekman, R. (2008). Membrane fusion. Nat Struct Mol Biol *15*, 658-664.

Willard, F.S., and Crouch, M.F. (2001). MEK, ERK, and p90RSK are present on mitotic tubulin in Swiss 3T3 cells - A role for the MAP kinase pathway in regulating mitotic exit. Cell Signal *13*, 653-664.

Winter, A., Schmid, R., and Bayliss, R. (2015). Structural Insights into Separase Architecture and Substrate Recognition through Computational Modelling of Caspase-Like and Death Domains. Plos Comput Biol *11*.

Wong, J.L., Koppel, D.E., Cowan, A.E., and Wessel, G.M. (2007). Membrane hemifusion is a stable intermediate of exocytosis (vol 12, pg 653, 2007). Dev Cell *12*, 837-838.

Yang, R.Z., and Feldman, J.L. (2015). SPD-2/CEP192 and CDK Are Limiting for Microtubule-Organizing Center Function at the Centrosome. Curr Biol *25*, 1924-1931.

Zenker, J., White, M.D., Templin, R.M., Parton, R.G., Thorn-Seshold, O., Bissiere, S., and Plachta, N. (2017). A microtubule-organizing center directing intracellular transport in the early mouse embryo. Science *357*, 925-+.

Zheng, Z., Zhu, H.B., Wan, Q.W., Liu, J., Xiao, Z.N., Siderovski, D.P., and Du, Q.S. (2010). LGN regulates mitotic spindle orientation during epithelial morphogenesis. J Cell Biol *189*, 275-288.

Zou, H., Stemmann, O., Anderson, J.S., Mann, M., and Kirschner, M.W. (2002). Anaphase specific auto-cleavage of separase (vol 528, pg 246, 2002). Febs Lett *531*, 381-381.

APPENDIX
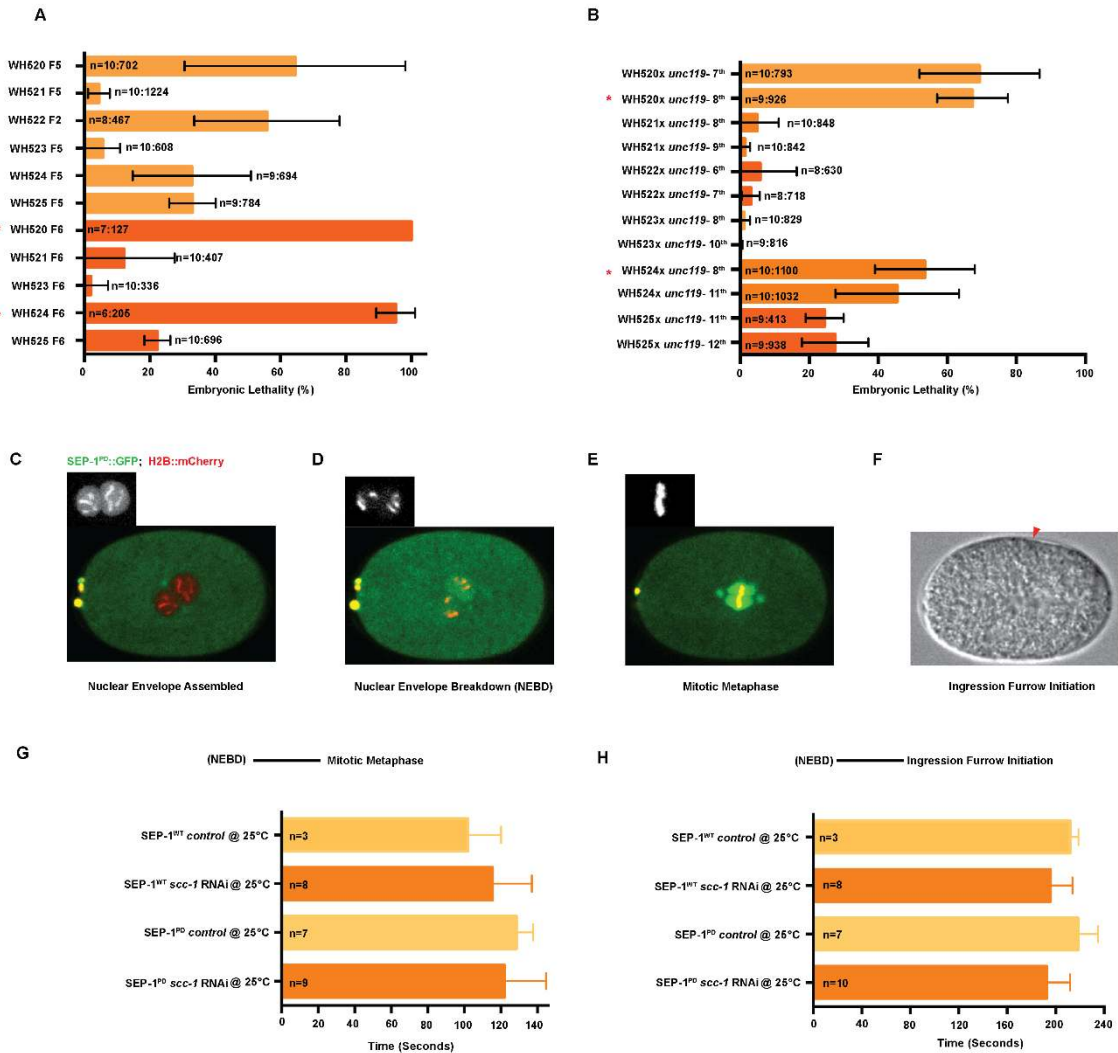
Figure A. 1 Testing different lines expressing SEP-1PD::GFP.

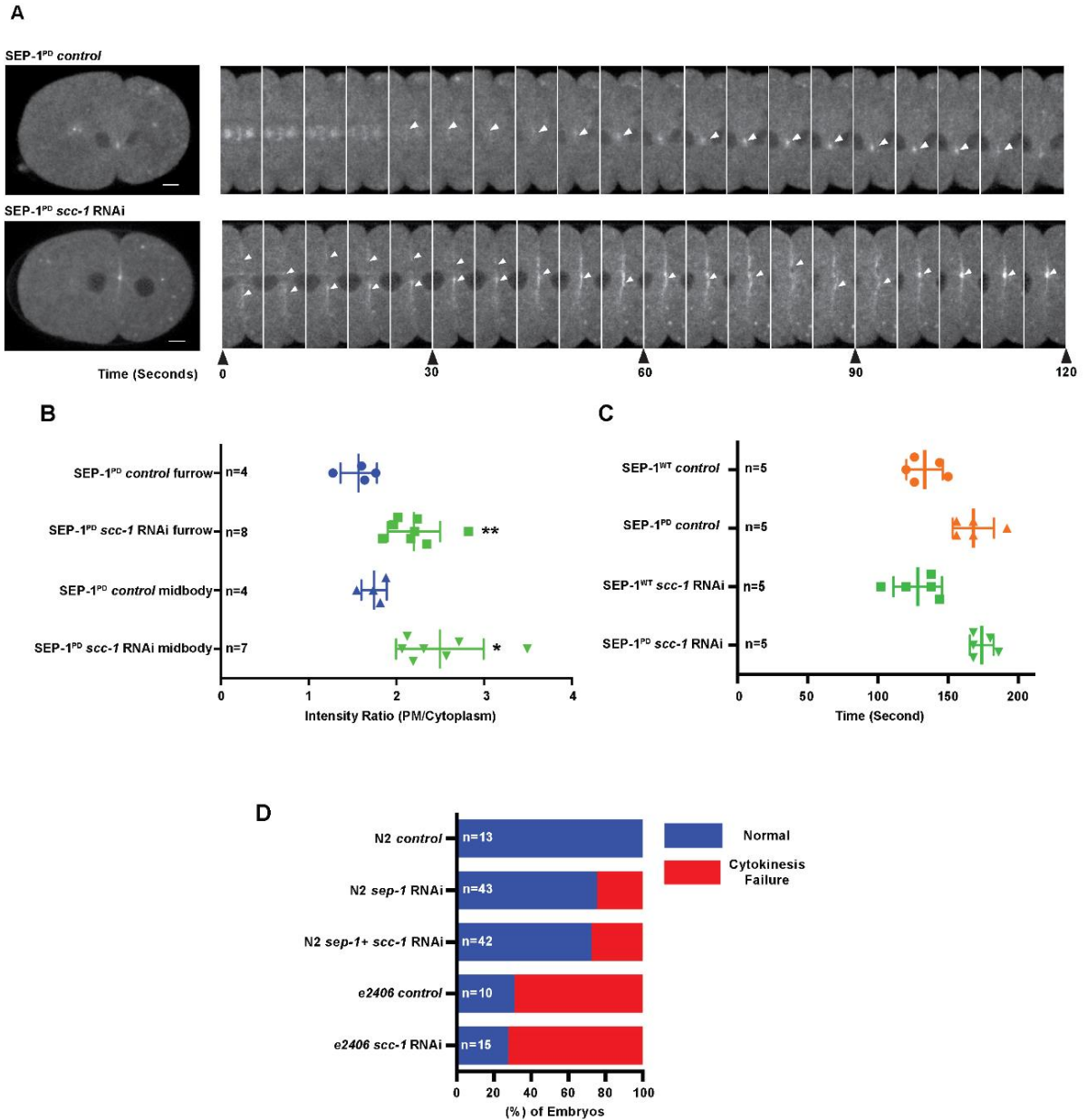(A) Embryonic lethality of homozygous SEP-1PD::GFP lines propagated off *gfp* (RNAi) for 5-6 generations. Each data with error bars represents the average of embryonic lethality from 6-10 singled worms (n=singled worm number: total embryo count). (B) Embryonic lethality in F2 broods from heterozygous SEP-1PD::GFP/+ transgenic hermaphrodites from backcrossing propagation strategy (see Materials and Methods). The number of generations the strain was backcrossed is also indicated. (C) Nuclear envelope intact in prophase, (D) Nuclear envelope breakdown (NEBD), indicated by separase in the nucleus and H2B::Cherry nucleoplasmic signal dispersing in prometaphase, (E) Chromosome alignment in metaphase and (F) Initiation of furrow ingression as observed by DIC acquired simultaneously with the fluorescent images. (G) Timing from NEBD to metaphase in SEP-1WT::GFP and SEP-1PD::GFP embryos with and without *scc-1* (RNAi) (n= number of embryos imaged). (H) Timing from NEBD to furrow ingression in SEP-1WT::GFP and homozygous SEP-1PD::GFP embryos with and without *scc-1* (RNAi) (n= number of embryos imaged). Error bars indicated the standard deviation of the mean. Red asterisks highlight the WH520 and WH524 which were used for analyzing the cellular phenotype.

149

**Figure A. 2 SEP-1^{PD}::GFP accumulated at centrosomes and centrioles, but does not inhibit disengagement in late anaphase.**

(A, B) Both SEP-1^{WT}::GFP (green) or SEP-1^{PD}::GFP (green) localize to centrioles (SPD-2::mCherry, red) during the first mitotic division. SEP-1^{PD}::GFP signal is more prominent and persistent at the centriole and centrosome, relative to SEP-1^{WT}::GFP embryos. Right insets show SPD-2::mCherry (red) and SEP-1::GFP (green) at centrioles. (C) Quantification of separase signals in the centrosome during centriole disengagement in the AB cell as indicated by the arrowhead (n= number of embryos imaged). (D) Kymograph of SPD-2::mCherry (red) during centriole disengagement in both SEP-1^{WT}::GFP and SEP-1^{PD}::GFP (green), showing no delay in SEP-1^{PD}::GFP expressing embryos (time in seconds indicated below). Each kymograph Image is 10 seconds apart. Scale Bars, 10 µm. P-values: ** =<0.01; ***=<0.001; **** =<0.0001 (*t*-test) (n= number of embryos imaged). Error bars indicated standard deviation of the mean.

A

SEP-1^WT::GFP | SPD-2::mCherry | SEP-1^WT::GFP; SPD-2::mCherry

SEP-1^WT
SPD-2
MERGE

B

SEP-1^PD::GFP | SPD-2::mCherry | SEP-1^PD::GFP; SPD-2::mCherry

SEP-1^PD
SPD-2
MERGE

C

AB Cell | P Cell

SEP-1^WT::GFP n=12
SEP-1^PD::GFP n=10

Ratio (Centriole/Cytoplasm)

Time (Seconds)

D

SEP-1^WT::GFP; SPD-2::mCherry; AB Cell Centrosome

SEP-1^WT::GFP
SPD-2::mCherry

Time (Seconds) 0   Centriole Disengagement   60   120   180

SEP-1^PD::GFP; SPD-2::mCherry; AB Cell Centrosome

SEP-1^PD::GFP
SPD-2::mCherry

Time (Seconds) 0   Centriole Disengagement   60   120   180

151

Figure A. 3 Depletion of cohesin enhances SEP-1^PD::GFP accumulation in the furrow.

(A) Kymograph of the furrow region shows SEP-1^PD::GFP accumulation in the furrow and midbody in control and *scc-1(RNAi)* embryos. The arrows show SEP-1^PD::GFP signal at the furrow and midbody. Each kymograph Image is 10 seconds apart. (B) Quantification of the SEP-1^PD::GFP signal indicates that cohesin depletion enhanced SEP-1^PD::GFP accumulation in the furrow (p=0.0038, *t*-test) and midbody (p=0.0182, *t*-test) compared with control SEP-1^PD::GFP embryos (n= number of embryos imaged). (C) Quantification of the furrow ingression time in different conditions as indicated (n= number of embryos imaged). (D) Percentage of embryos displaying normal cytokinesis (blue) or cytokinesis failure (red) in different conditions as indicated (n= number of embryos imaged). Scale Bars, 10 μm. P-values: * =<0.05; **=<0.01 (*t*-test). Error bars indicated standard deviation of the mean.

152
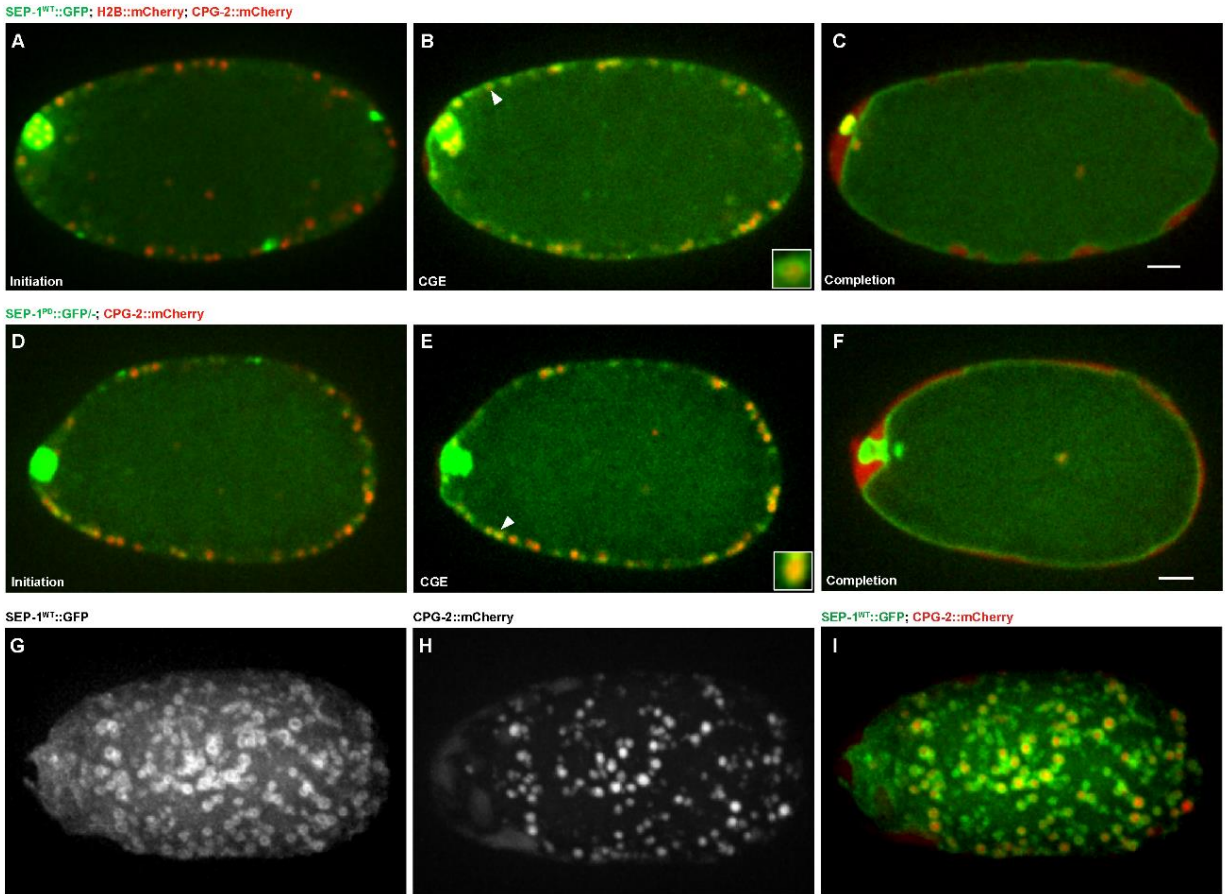
Figure A. 4 Both SEP-1^WT::GFP and SEP-1^PD::GFP/+ co-localized with cortical granule marker CPG-2::mCherry during cortical granule exocytosis.

Both SEP-1^WT::GFP (A-C, green) and SEP-1^PD::GFP/+ (D-F, green) colocalize with CPG-2::mCherry (red) at cortical granules. Cortical granules viewed from the surface plane of the embryo (G-I) and magnified images of CGs (B, E) show that CPG-2, a cargo protein that should be in the lumen of the vesicle, appears to be surrounded by separase signal, which is likely associated with the vesicle membrane. Scale Bars, 10 μm.
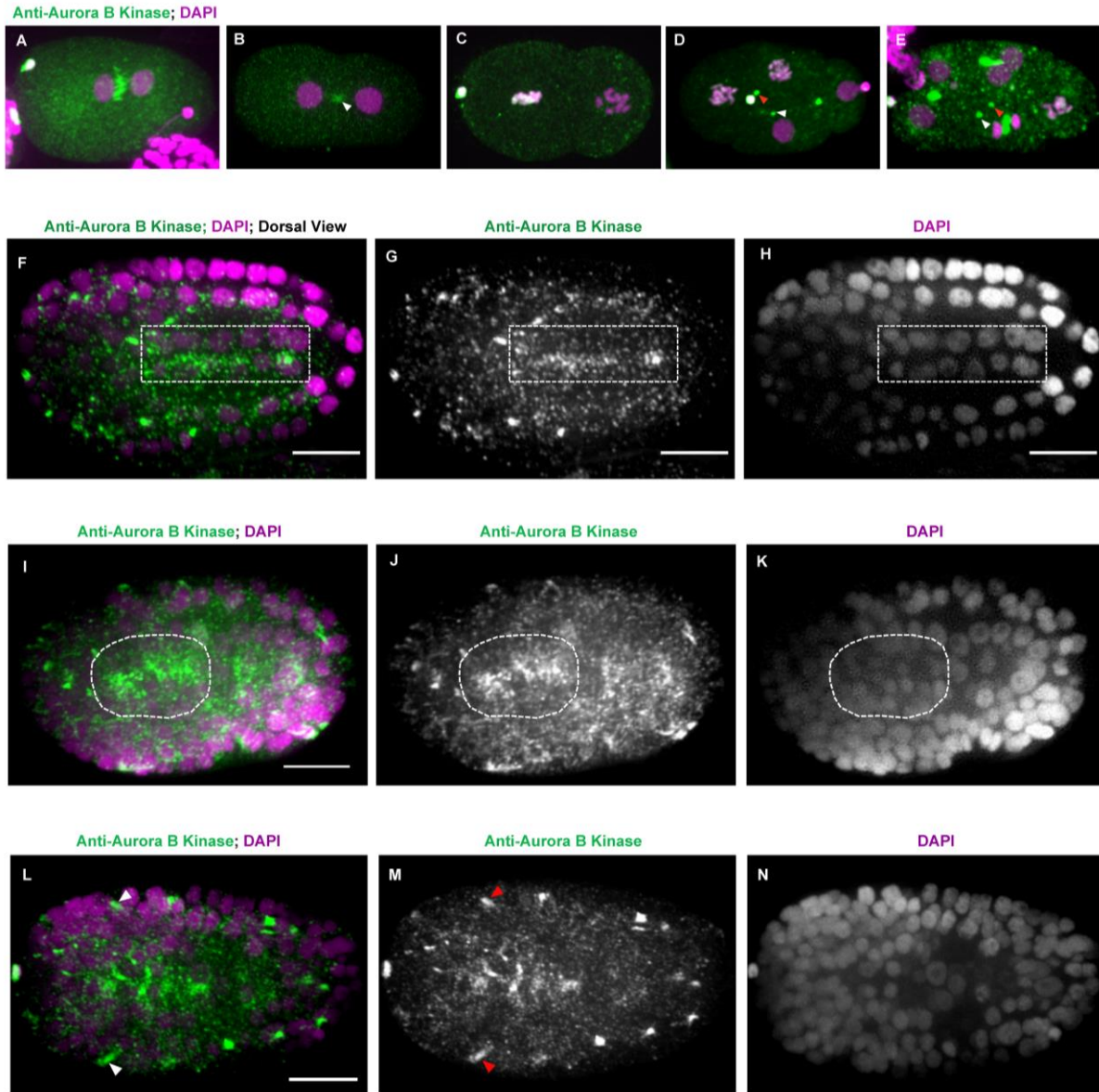
Figure A. 5 Immunostaining of endogenous Aurora B kinase in *C.elegans* embryos.

Immunostaining of Aurora B kinase (green) with DAPI (magenta) staining in wildtype shows the same localization pattern of AIR-2 at central spindle and midbodies during the early cell divisions (A-E) as well as apical surfaces of intestine (F-H, rectangle), pharynx (I-K, dotted circle) and sensilla (L-N, arrowheads). Scale Bar, 10 µm.
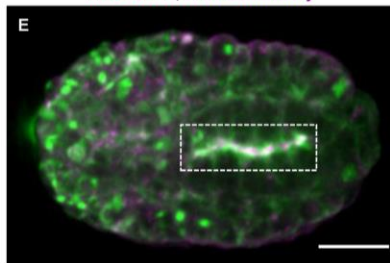
Figure A. 6 Cytokinesis in the intestine epithelia

Cytokinesis in the E8-E16 division. (A-C) Cytokinesis at the E8-E16 division. Midbody ring marker ZEN-4::GFP (green) with tubulin TBB-1::mCherry migrates with midbodies (labeled as 1-8) to midline and persists well after polarization is complete (rectangle box). Time in a minute: second indicated on the left bottom. (D) Kymograph of the single E8 cell division showing the midbody formation and migration to apical. The E8 cell labeled with ZEN-4::GFP (green) and TBB-1::mCherry (magenta). Time in minutes indicated below. (E-G) Apical structure marker PAR-6::mCherry (magenta) and AIR-2::GFP (green) colocalized at apical midline (rectangle). (H-I) RAB-11::mCherry (green) and AIR-2::GFP (magenta) migrate with midbodies (labeled as 1-8) to midline and persists well after polarization is complete (rectangle). Time in a minute: second indicated on the left bottom. (K-M) Terminal E16-E20 division, four midbodies (labeled as 1-4) follow the apical migration pattern like E8-E16 and AIR-2::GFP persist post-migration process. Scale Bar, 10 µm.
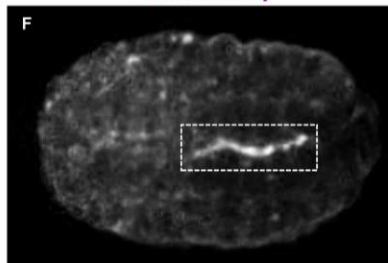
ZEN-4::GFP; TBB-1::mCherry

A 00:00   B 30:00   C 59:00

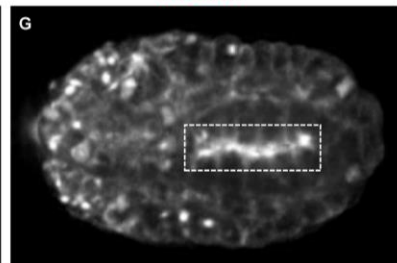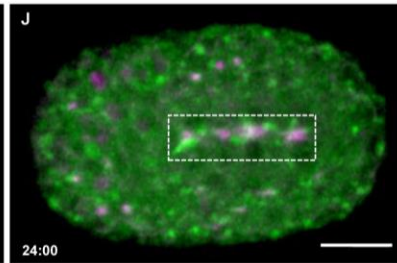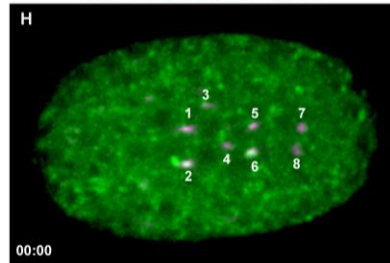1 3 5
2 4 6 7
8

D

Time (Minutes) 0   10   20   28
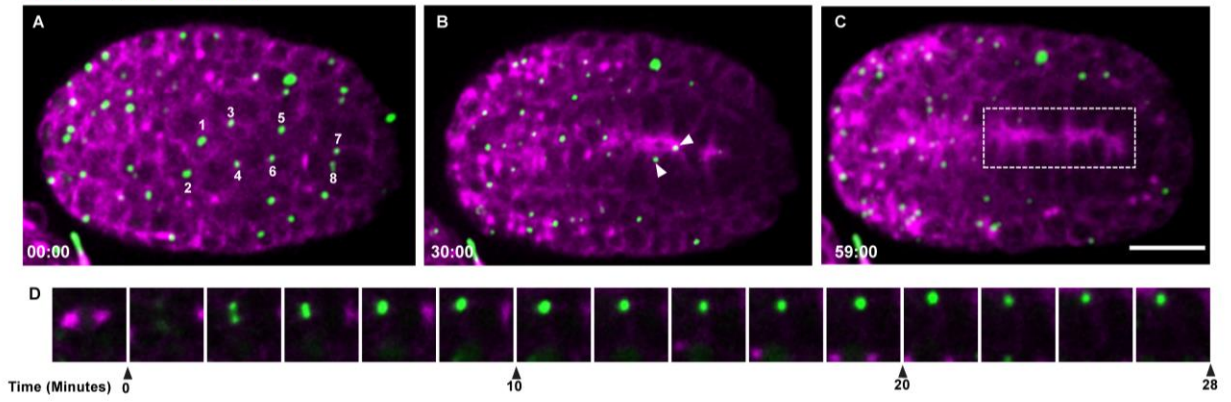
AIR-2::GFP; PAR-6::mCherry   PAR-6::mCherry   AIR-2::GFP
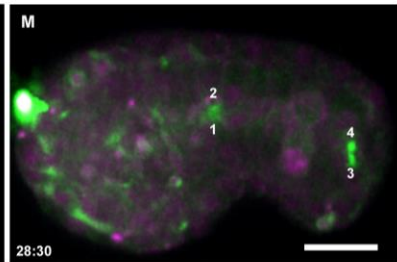
E   F   G

RAB-11::mCherry; AIR-2::GFP

H 00:00   I 15:00   J 24:00

3
1 5 7
2 4 6 8
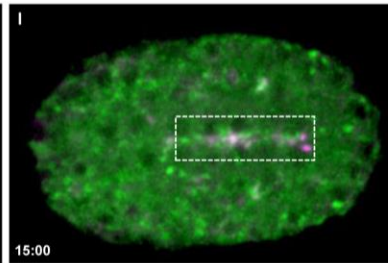
AIR-2::GFP; H2B::mCherry; Dorsal View

K 00:00   L 13:30   M 28:30
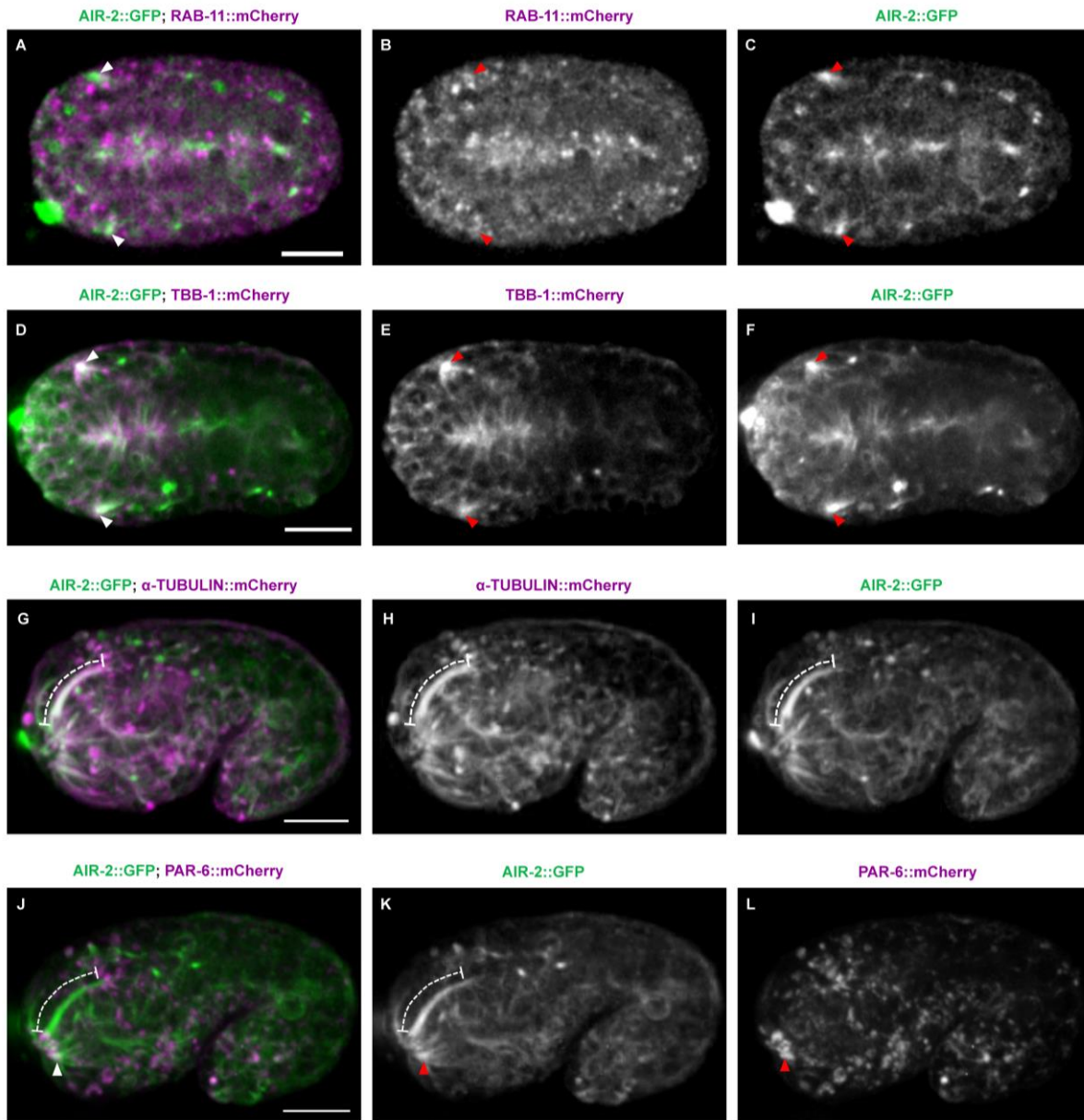
2   2   2
1   1   1   4
       3   3
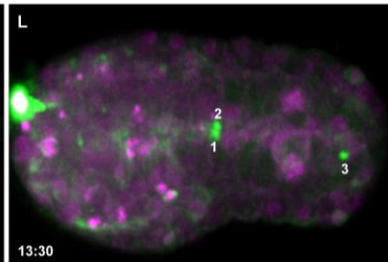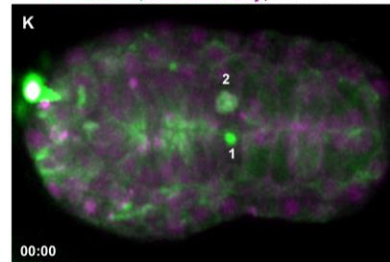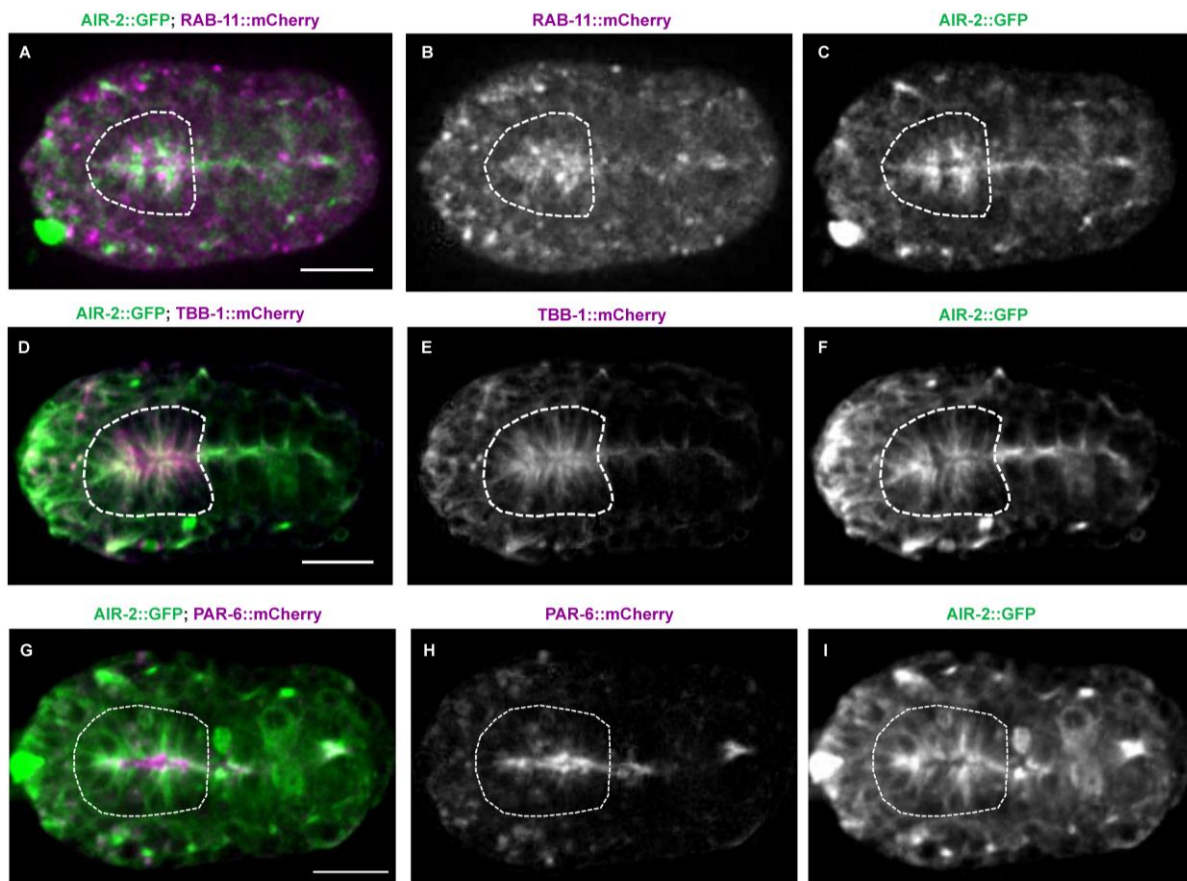
Figure A. 7 Cytokinesis in Pharynx

(A-C) RAB-11::mCherry (magenta) and (D-F) tubulin TBB-1::mCherry (magenta) remain co-localized with AIR-2::GFP (green) to apical surface and appears to remain at pharyngeal bulk throughout the life of the animal (dotted circle). (G-I) AIR-2::GFP (green) also partially co-localized with PPCs apical surface marker PAR-6::mCherry (magenta) at pharyngeal bulk (dotted circle). Scale Bar, 10 µm.
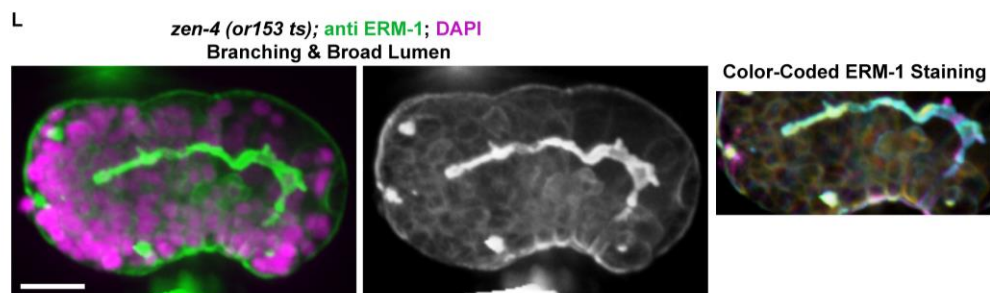
Figure A. 8 Midbody components label dendrites of sensilla neurons

(A-C) RAB-11::mCherry (magenta) and (D-F) tubulin TBB-1::mCherry (magenta) remain co-localized with AIR-2::GFP (green) at the forming sensilla neurons (dotted circle). (G-I) a focus of AIR-2::GFP (green) extends anteriorly until sensilla dendrite extension anchors at the tip of the animal, where co-localized with tubulin TBA-1::mCherry (magenta) (dot line). (J-L) After the dendrite extension to the tip of animal, PAR-6::mCherry (magenta) (arrowhead)was observed to localize at the anchor of the dendrite and partially overlaps with AIR-2::GFP (green). Scale Bar, 10 μm.

Figure A. 9 Cytokinesis mutants have disrupted intestinal and pharyngeal tubulogenesis

(A-C) The immunostaining to apical marker ERM-1 (green) showed that in wild-type (A) embryos at comma stage, ERM-1 enriched at the apical cell cortex of the hypodermis and at the midline of pharyngeal-intestinal primordium. (B) There were various defects, including a broad lumen, branches and discontinuous lumen in intestinal and pharyngeal tubulogenesis in *air-2 (or207 ts)* embryos. (C) Images of the color-coding depth of ERM-1 and nuclei show the detailed z-depth distribution of intestine-pharyngeal primordium. (D-I) The immunostaining to apical marker PAR-3 showed that in wild-type embryos, PAR-3 (green) enriched at the apical cell cortex of intestine, and pharynx primordium. (G-I) various defects were observed in intestinal and pharyngeal tubulogenesis in *air-2 (or 207 ts)* embryos, including discontinuous lumen (G), broad lumen (H), branches (I) and abnormal positioning (G-I). (J-L) There were various defects, including a broad lumen, branches and discontinuous lumen in intestinal and pharyngeal tubulogenesis in *zen-4 (or153 ts)* embryos. Right inserts show the images of the color-coding depth of ERM-1 and nuclei. Scale Bar, 10 µm.

A N2; anti EMR-1; DAPI

B *air-2 (or207 ts);* anti ERM-1; DAPI
Branching & Discontinuity

C Color-Coded ERM-1 Staining
WT (N2)
air-2 (or207 ts)

D WT; anti PAR-3; DAPI; E16 Polarization

E Bean Stage

F Comma Stage

G *air-2 (or207 ts);* anti ERM-1; DAPI
Mispositioning & Discontinuity

H *air-2 (or207 ts);* anti ERM-1; DAPI
Mispositioning & Broad Lumen

I *air-2 (or207 ts);* anti ERM-1; DAPI
Mispositioning & Branching

J *zen-4 (or153 ts);* anti ERM-1; DAPI
Mispositioning & Branching
Color-Coded ERM-1
Intestine Nuclear

K *zen-4 (or153 ts);* anti ERM-1; DAPI
Mispositioning & Broad Lumen
Color-Coded ERM-1
Intestine Nuclear

L *zen-4 (or153 ts);* anti ERM-1; DAPI
Branching & Broad Lumen
Color-Coded ERM-1 Staining

160

Figure A. 10 Cytokinesis mutants have disrupted remolding of microtubule structure at the apical surfaces.

(A-H) There are mild positioning defects of tubulin TBA-1::GFP (green) at intestinal and pharyngeal lumen in *air-2 (or207 ts)* (E-H) compared with wild-type (A-D). (I-J) TBA-1::GFP localized at the flank region of central spindle and midbody during migration to apical surface. (K-L) TBA-1::GFP persists prominently at the intestinal apical surface post cell division. However, the localization of tubulin TBA-1::GFP (green) disappeared at a flank region near midbody in *air-2 (or207 ts)* embryos at the restrictive temperature (M-N). However, the absence of tubulin at flank region did not affect the persistence of tubulin at intestinal primordium post division (O-P). Scale Bar, 10 μm.
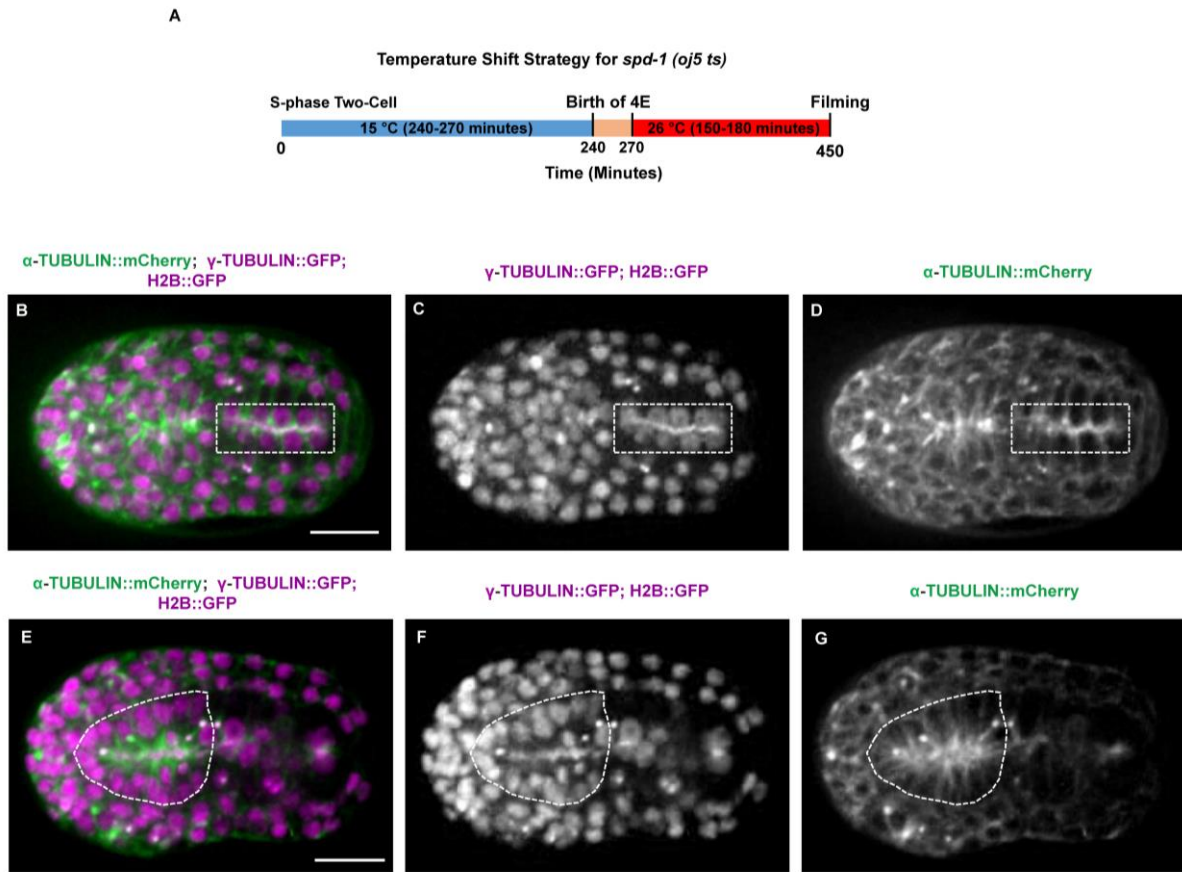
Figure A. 11 Multiple microtubule-based organelles contribute to morphogenesis

(A) Illustration of the temperature shift strategy of the *spd-1 (oj5 ts)* mutants. (B-D) Centrosome marker γ-tubulin::GFP (green) and α-tubulin::mCherry (magenta) colocalized at intestinal primordium (rectangle) and (E-G) pharyngeal primordium (dotted circle). Scale Bar, 10 μm.

Strain	Condition	Total	E2 (~30 Cells)	E2 Prophase	E2 Metaphase	E2 Anaphase	E4	Cytokinesis Failure	< 20 Cells
N2	15 C 4.5 hours, DAPI	20	2	2	2	1	13		
WH12	15 C 4.5 hours, DAPI	31	1	0	1	1	28		
EU630	15 C 4.5 hours, DAPI	31	11	1	7	1	5	4	2

Strain	Condition	Total	E4 (~50 Cells)	E4 Prophase	E4 Metaphase	E4 Anaphase	E8	Cytokinesis Failure
N2	15 C 5.0 hours, DAPI	47	9	6	10	7	14	
WH12	15 C 5.0 hours, DAPI	16	13	0	3	0	0	
EU630	15 C 5.0 hours, DAPI	38	22	11	4	0	0	1

Strain	Condition	Total	E4 (~50 Cells)	E4 Prophase	E4 Metaphase	E4 Anaphase	E8
N2	15 C 5.5 hours, DAPI	39	6	9	9	2	13
WH12	15 C 5.5 hours, DAPI	27	5	3	9	1	9
EU630	15 C 5.5 hours, DAPI	36	20	2	0	1	13

Strain	Condition	Total	E4 (~50 Cells)	E4 Prophase	E4 Metaphase	E4 Anaphase	E8
N2	15 C 6.0 hours, DAPI	30	4	0	3	2	21
WH12	15 C 6.0 hours, DAPI	43	3	4	4	5	27
EU630	15 C 6.0 hours, DAPI	29	7	4	4	0	14

Strain	Condition	Total	E16	Ventral Enclosure (Intestine Asymmetry)
N2	15 C 6.0 hours, 26 C 3 hours DAPI	30	30	16

Figure A. 12 Quantification of DAPI staining assay of embryonic development.

Details quantification of developmental stages under the different temperature shift conditions in wildtype (N2), EU630 *air-2 (or 207 ts)*, and WH12 *spd-1 (oj5 ts)* mutant embryos.

Table A1. Strains used in this study.

Strain	Genotype
N2	Bristol (wild-type)
WH416	*unc-119(ed3) iii; ojis58[sep-1::gfp; unc119(+)]*
WH520	*unc-119(ed3) iii; ojis71[sep-1(pd)::gfp; unc119(+)]*
WH521	*unc-119(ed3) iii; ojis72[sep-1(pd)::gfp; unc119(+)]*
WH522	*unc-119(ed3) iii; ojis73[sep-1(pd)::gfp; unc119(+)]*
WH523	*unc-119(ed3) iii; ojis74[sep-1(pd)::gfp; unc119(+)]*
WH524	*unc-119(ed3) iii; ojis75[gfp::sep-1(pd); unc119(+)]*
WH525	*unc-119(ed3) iii; ojex87[sep-1(pd)::gfp; unc119(+)]*
RQ372	*unc-119(ed3) iii; ojis58[sep-1::gfp; unc119(+)]; itis37 [ppie-1::mcherry::his-58 (paa64); unc-119(+)] iv*
JAB18	*unc-119(ed3) iii; ojis71[sep-1(pd)::gfp; unc119(+)]; itis37 [ppie-1::mcherry::his-58 (paa64); unc-119(+)]*
OD366	*unc-119(ed3) iii; itis151[pso33; pcpg-2::cpg-1sigseq::mcherry-tev-stag::cpg-2; unc-119(+)]*
EKM41	*unc-119(ed3) iii; ltis44 [pie-1p-mcherry::ph(plc1delta1); unc-119(+)] v*
JAB156	*unc-119(ed3) iii; ojis71[sep-1(pd)::gfp; unc119(+)]; ltis44 [pie-1p-mcherry::ph(plc1delta1); unc-119(+)] v*
JAB145	*unc-119(ed3) iii; ojis58[sep-1::gfp; unc119(+)]; ltis44 [pie-1p-mcherry::ph(plc1delta1); unc-119(+)] v*
JAB20	*unc-119(ed3) iii; ojis58[sep-1::gfp unc119(+)]; itis151 [pso33; pcpg-2::cpg-1sigseq::mcherry-tev-stag::cpg-2; unc-119(+)]; ltis37 [paa64; pie-1p::mcherry::his-58; unc-119 (+)]*
JAB174	*unc-119(ed3) iii; ojis58[sep-1::gfp; unc119(+)]; bssi15 [pko109: spd-2p-spd-2-mcherry-spd-2 3'-utr; unc-119(+)] i*
JAB175	*unc-119(ed3) iii; ojis71[sep-1(pd)::gfp; unc119(+)]; bssi15 [pko109: spd-2p-spd-2-mcherry-spd-2 3'-utr; unc-119(+)] i*
WH408	*sep- 1(e2406ts)/ht2[qis48]*
OD56	*unc-119(ed3) iii; ltis37 [pie-1p::mcherry::his-58 (paa64); unc-119(+)]*

Table A1. Continued

Strain	Genotype
N2	Bristol (wild-type)
EKM48	*unc-119(ed3) iii; ojIs51 [Ppie-1::GFP::air-2; unc-119(+)]*
EKM50	*unc-119(ed3) iii; ojIs51 [Ppie-1::GFP::air-2; unc-119(+)]; ltIs37 [Ppie-1::mCherry::his-58 (pAA64); unc-119(+)] iv; ltIs44 [Ppie-1::mCherry::PH (PLC1delta1); unc-119(+)]v*
EKM51	*unc-119(ed3) iii; ojIs51 [Ppie-1::GFP::air-2; unc-119(+)]; ltIs37 [Ppie-1::mCherry::his-58 (pAA64); unc-119(+)] iv*
EKM52	*unc-119(ed3) iii; ojIs51 [Ppie-1::GFP::air-2; unc-119(+)]; ltIs44 [Ppie-1::mCherry::PH (PLC1delta1); unc-119(+)] v*
JAB23	*unc-119(ed3) iii; ojIs51 [Ppie-1::GFP::air-2; unc-119(+)]; weIs21 [pJA138 (pie-1::mCherry::tub)]*
JAB60	*unc-119(ed3) iii; ojIs51 [Ppie-1::GFP::air-2; unc-119(+)]; pwIs476 [Ppie-1::mCherry::rab-11]*
JAB116	*unc-119(ed3) iii; weIs21 [pJA138 (Ppie-1::mCherry::tub)]; unc-119(+)]; zuIs45 [nmy-2::NMY-2::GFP; unc-119(+)] v*
NWG002	*unc-119(ed3) iii; ltIs44 [Ppie-1::mCherry::PH (PLC1delta1); unc-119(+)]v; zuIs45 [nmy-2::NMY-2::GFP; unc-119(+)] v*
JAB24	*zen-4(or153ts) iv; xsEx6 [zen-4::GFP; rol-6 (su1006)]; unc-119(ed3) iii; weIs21 [pJA138 (pie-1::mCherry::tub)]*
JAB34	*zen-4(or153) iv; xsEx6 [zen-4::GFP; rol-6 (su1006)]; unc-119(ed3) iii; ltIs44 [Ppie-1::mCherry::PH (PLC1delta1); unc-119(+)] v*
JAB32	*unc-119(ed3) iii; ddIs26 [Ppie-1::mCherry::T26E3.3; unc-119(+)]v; ojIs51 [Ppie-1::GFP::air-2; unc-119(+)]*
EU630	*air-2(or207) i.*
EU716	*zen-4(or153) iv.*
WH12	*spd-1 (oj5) i*
WH421	*unc-119(ed3) iii; ojIs51 [Ppie-1::GFP::air-2; unc-119(+)];spd-1 (oj5) i.*
JAB52	*unc-119(ed3) iii; ruIs32III;dd156[tbg-1::GFP;unc-119(+)]; ruIs32[Ppi-1::GFP::His-58; unc-119(ed3); weIs21 [pJA138 (pie-1::mCherry::tub)]*

VITA

Xiaofei Bai grew up in Mongolian pasture near Hohhot, the capital city of Inner Mongolia, China. He was drawn to Inner Mongolia Agricultural University at home town, Hohhot for his undergraduate studies, enrolling in the Fall of 2005 with strong passion to be a molecular biologist. After four years' study in Bioengineering major, he graduated from college in 2009 and began his graduate work in Dr. Guojing Li's lab to study the plant stress-resistance signaling pathway in *Arabidopsis* and soybean. In 2012, he graduated from Department of Life Science at the Inner Mongolia Agricultural University with the master degree. He decided to work for Chinese Academy of Agricultural Science as a research assistant, and joined the lab of Dr. Tianfu Han in October, 2012, where he worked on the safety detection of transgenic soybean. In 2013, he began his Ph.D. study at the University of Tennessee, Knoxville and followed his mentor Dr. Joshua N. Bembenek to investigate the mechanisms of cytokinesis in *C. elegans*.